UNIVERSITÀ DI CAPE TOWN
UNIVERSITÀ DEGLI STUDI DI PARMA

DIPARTIMENTO DI SCIENZE CHIMICHE, DELLA VITA E DELLA SOSTENIBILITÀ AMBIENTALE

CORSO DI LAUREA MAGISTRALE IN CHIMICA

SINTESI, STRUTTURA E PROPRIETÀ DI NUOVI METAL-ORGANIC FRAMEWORKS A BASE DI Cu(II)

Relatrici:

Prof.ssa **Alessia Bacchi**

Prof.ssa **Susan Bourne**

Correlatrice:

Dott.ssa **Savannah Zacharias**

Laureando:
Marco Bardini

A.A. 2017/2018

UNIVERSITY OF CAPE TOWN
UNIVERSITY OF PARMA

DEPARTMENT OF CHEMISTRY

MASTER'S DEGREE IN CHEMISTRY

SYNTHESIS, STRUCTURE AND PROPERTIES OF NOVEL Cu(II)-BASED METAL-ORGANIC FRAMEWORKS

Supervisors:

Prof. **Alessia Bacchi**

Prof. **Susan Bourne**

Co-Supervisor:

Dr. **Savannah Zacharias**

Candidate:
Marco Bardini

A.Y. 2017/2018

Riassunto

I materiali cristallini porosi sono noti alla comunità scientifica principalmente per il grande numero di applicazioni derivanti dalla loro porosità, in sensoristica,[1] rilascio di farmaci a livello cellulare,[2] catalisi in stato solido[3] e assorbimento e rilascio controllato di liquidi, gas e piccole molecole in soluzione.[4,5]

All'interno di questa definizione generale, una classe di materiali che ha visto la propria importanza crescere esponenzialmente nelle ultime due decadi è quella dei Framework Metallo-Organici, o MOFs (dall'inglese Metal-Organic Frameworks). Questi materiali hanno mostrato di avere grandi potenzialità, specialmente in tecnologie finalizzate alla rimozione di gas serra (come CO_2 o CH_4) dall'atmosfera[6] o in serbatoi per automobili alimentate a idrogeno.[7] Le caratteristiche che permettono ai MOFs di essere utilizzati in questi contesti sono il loro enorme rapporto tra superficie interna e volume, la stabilità termica relativamente elevata e la possibilità di regolare in maniera molto precisa la struttura di un singolo MOF per renderla ottimale per svolgere un particolare compito.[8]

Un'altra caratteristica propria di alcuni MOFs, specialmente se sintetizzati a partire da leganti organici semiflessibili,[9] è la capacità di cambiare forma, e quindi la dimensione dei loro pori e la loro superficie interna, in risposta a uno stimolo esterno.[2,10] Questa tendenza è di speciale interesse in sistemi che possono essere modificato per assorbire e successivamente rilasciare piccole molecole in modo controllato.[11,12]

Quest'ultima proprietà è quella che avevo programmato di esplorare nel mio lavoro di tesi, partendo da complessi molecolari precedentemente sintetizzati nei laboratori di University of Cape Town (UCT) e variando le condizioni sperimentali per ottenere MOF chimicamente simili a tali sistemi.

Questo elaborato, quindi, sarà dedicato principalmente a descrivere le nuove strutture cristalline ottenute durante il mio periodo di ricerca. Ogni capitolo, inoltre, conterrà una sezione in cui verranno discusse le proprietà spettroscopiche e termiche basilari dei materiali ivi descritti.

Di questi cristalli, due sono nuovi polimeri di coordinazione, chiamati 1-MBUCT e 2-MBUCT, sintetizzati a partire da sali di Cu(II) e caratterizzati da modalità di coordinazione inusuali e altri particolari interessanti, incluse alcune cavità piene di solvente all'interno della loro struttura cristallina, cosa che li rende molto promettenti in quanto materiali che potrebbero soddisfare i requisiti per poter essere considerati MOFs. Dopo aver esplorate la sintesi e la struttura di questi materiali, il testo sarà principalmente dedicato a capire se le cavità all'interno di 1-MBUCT e 2-MBUCT siano accessibili ad altri composti, senza modificare la morfologia generale del materiale. Per fare questo I cristalli sono stati sottoposti a esperimenti di scambio di solvente che, pur non portando a risultati

definitivi, suggeriscono che ogni materiale ha effettivamente mantenuto costante la sua struttura, riuscendo al contempo ad accogliere molecole di solvente dentro ai loro pori, ed essendo quindi idonei ad essere definiti MOFs.

Tutte le altre strutture trattate sono sottoprodotti delle reazioni di sintesi dei MOFs, e sono a loro volta esempi di classi di composti inusuali.

Il primo tra questi solidi è costituito da un composto ciclico di tipo [12]crown-6 a base di Cu(II), in cui due ioni monometilsolfuro per ogni ione di rame fungono da leganti a ponte per costruire la struttura ad anello della molecola, mentre il secondo composto è un complesso molecolare formato da due molecole di acido 2,6-piridindicarbossilico che agiscono da chelanti su uno ione Cu(II). Il terzo sottoprodotto, invece, non è tanto di interesse dal punto di vista strutturale, quanto piuttosto perché tutti i gruppi carbossilici delle molecole di acido 3,5-piridindicarbossilico incluse nel complesso sono stati sottoposti a una reazione di esterificazione. Tale reazione era inattesa, poiché le componenti del sistema in esame non corrispondevano a quelle di nessun'altra reazione di esterificazione reperibile nella letteratura che coinvolgesse l'acido 3,5-piridindicarbossilico.

Summary

Porous crystalline materials are known to be useful for a number of applications, including sensing,[1] drug delivery,[2] solid state catalysis[3] and controlled absorption and release of liquids, gases and small molecules in solution.[4,5]

Within this general definition, a class of materials that has seen its importance grow exponentially in the past two decades has been that of the Metal-Organic Frameworks, or MOFs. These materials have shown a lot of potential, especially in devices aimed at sequestering greenhouse gases (such as CO_2 and CH_4) from the atmosphere,[6] as well as in fuel tanks for hydrogen-powered cars.[7] The characteristics that allow MOFs to be used for such purposes are their high internal surface area to volume ratio, their relatively high thermal stability and the possibility to fine-tune their structure to optimize a given MOF for a given application.[8]

Another feature of some MOFs, especially those built with semiflexible organic linkers[9] between metallic nodes, is that they can change their conformation and therefore their pore size and internal surface area, in response to an external stimulus.[2,10] This behavior is especially interesting for systems which can be engineered to absorb and then release small molecules in a controlled manner.[11,12]

This last property is one that I set out to exploit in my thesis work, starting from Cu(II) molecular complexes previously synthesized in the University of Cape Town (UCT) laboratories and varying experimental conditions in order to get MOFs of similar systems.

Thus, this work will mainly describe the several novel crystal structures I obtained during my research. Each chapter will also discuss the basic spectroscopic and thermal properties of the material explored therein.

Of these crystals, two are novel Cu(II)-based coordination polymers, which were named 1-MBUCT and 2-MBUCT, with seldom-seen coordination characteristics and other interesting features, including solvent-filled cavities within their crystal structure, which makes them promising candidates to be fully considered MOFs. After exploring the synthesis and structure of the materials, this work will mainly focus on determining whether the cavities inside 1-MBUCT and 2-MBUCT are accessible to other guests, without disrupting the overall morphology of the material. This was done through solvent exchange experiments, which were inconclusive but nonetheless suggested that these materials did indeed retain their shape, while allowing guest molecules inside their pores, thus being worthy of being described as MOFs.

All other structures are byproducts obtained during various attempts to optimize the synthesis of these MOFs, and are often examples of unusual compound classes in their own right.

The first of these compounds is a Cu-based [12]crown-6 cyclical compound in which two monomethyl sulfide anions for every copper ion act as bridging ligands within the ring-like structure of the molecule, while the second is a discrete molecular complex formed by two 2,6-pyridinedicarboxylic acid molecules chelating a Cu(II) ion. The main point of interest of the last byproduct, instead, is not its structure, but rather the fact that all the carboxylic acid groups of the 3,5-pyridinedicarboxylic acid molecules included in the complex were subject to an esterification reaction. Such a reaction was unexpected, as the components of this system did not correspond to those found in any reported esterification reaction performed on 3,5-pyridinedicarboxylic acid.

Index

1. Introduction

1.1. Crystal Engineering

"Crystal engineering is the understanding of intermolecular interactions in the context of crystal packing and the utilization of such understanding in the design of new solids with desired physical and chemical properties".[13] This is the sentence with which Desiraju and his colleagues chose to open their invaluable book "Crystal Engineering: a textbook", because they held the opinion that there is no better place to start discussion on a topic than to define the topic itself. Definitions are an extremely useful way to start an argument, because elaborating on the definition of a topic is a good way to give context on research performed within the field and highlight some specifics features of the research itself.

In my research, I started from the compounds discussed in Section 3 of this work, which had previously been synthesized starting from copper nitrate and 2,6-pyridinedicarboxylic acid (Figure 1.1.1) in the UCT laboratories, and which were replicated at the start of this project using copper sulfate. The "desired physical and chemical properties" they displayed were relatively high thermal stability and the ability to vary their cell parameters to accommodate different guests within their crystal structures during solvent exchange experiments. These complexes were also well-defined molecular complexes which did not form a network, and that was by design; the ligand used to synthesize them had intermolecular interactions that were unsuited to form links with metals (in this case Cu(II) ions) in multiple directions. Such ligands are sometimes called "capping agents".

Figure 1.1.1 Comparison of the likeliest coordination models for chemically similar ligands, 3,5-pyridinedicarboxylic acid (3,5 PDA) on the left, 2,6-pyridinedicarboxylic acid (capping agent, 2,6 PDA) on the right

Thus, the project started with an attempt to see what would happen if I tried to develop crystals with components that were chemically very similar, with the only difference being the substitution of the "capping agent" with a ligand able to coordinate three metal ions in three different directions. For this purpose, 3,5-pyridinedicarboxylic acid (Figure 1.1.1) was selected. I hoped the resulting solid would display similar properties to the one synthesized previously, but while it was indeed possible to synthesize crystalline networks by changing reagents their structure and properties were quite unusual

and different from what was expected. It is an example of how the scientific community can sometimes still be lacking in its "understanding of intermolecular interactions" and how it is crucial to examine the data that can be obtained from an experiment without any preconceived notions that might lead to wrong conclusions.

1.2. Metal-Organic Frameworks

The crystalline solids described within this work belong to a specific class of materials: metal-organic frameworks. Metal organic frameworks (usually abbreviated with MOFs) are a sub-class of coordination networks which contain organic ligands and potential void space, whereas a generic coordination network is defined[14] as "A coordination compound extending, through repeating coordination entities, in 1 dimension, but with cross-links between two or more chains, loops or spiro-links, or a coordination compound extending through repeating coordination entities in 2 or 3 dimensions". It should be noted that these definitions do not imply that all MOFs or indeed all coordination networks are crystalline, but all MOFs discussed within this work are, in fact, crystalline solids.[14]

Research on 3D porous materials was initially focused on materials that had already been observed in nature, such as zeolites, and presented a covalent structure that made such materials quite robust and useful for applications such as ion exchange. The presence of covalent bonds, however, also means that these materials are quite rigid, and introducing weaker interactions such as coordination bonds, hydrogen bonds or π-π interactions enables the framework structure to be flexible. These two different types of materials are described as second and third generation networks by Kitagawa et al.[15] Among porous compounds, those constituted by metal "nodes" and organic linkers, coordination polymers, are particularly attractive because they offer endless possibilities to rationally design infinite networks that can respond dynamically and in a reversible manner to external stimuli. All these characteristics mean that such materials are highly tunable and can be engineered to perform specific functions on command. MOFs are categorized as a separate class of materials because of their porosity, and of the consequences that this characteristic has when developing these materials for practical applications.

The volume of research done on MOFs has been steadily climbing over the past two decades, mainly due to the wide range of applications that MOFs can be useful for; this class of materials is noteworthy because it is possible to tune their properties to be suitable for a significant number of applications.

The high thermal stability and extremely high porosity of MOFs are characteristics that make them ideal for applications such as gas storage and release of hydrogen in fuel cells or in sequestration of greenhouse gases such as methane or carbon dioxide. The high porosity is also useful when one wants to incorporate small molecules into the framework for various purposes: catalysis of reactions within the framework, drug delivery, selective adsorption of liquids and other various uses.[16]

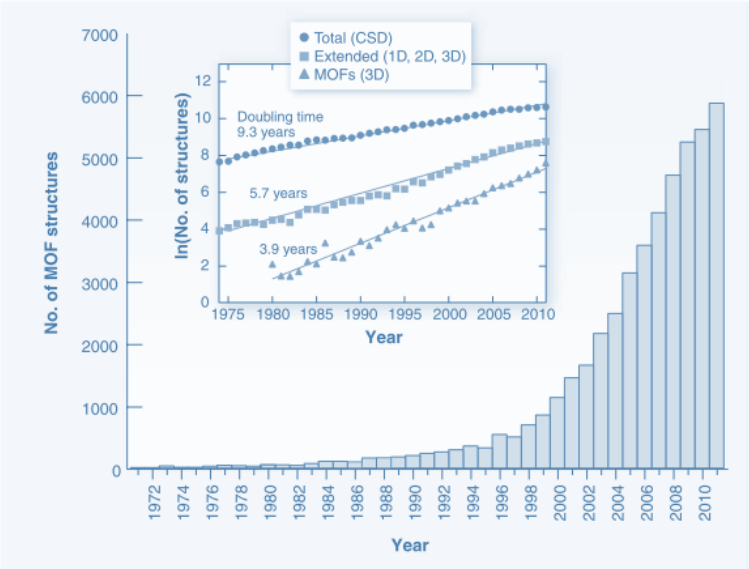

Figure 1.2.1 Graphical representation of year to year growth in porous materials' crystal structures

The explosion in interest over MOFs that occurred within the scientific community after the initial description of the so-called MOF-5 by Yaghi et al. in 1999[17] meant that research into the synthesis, tuning, post-synthetic modification and characterization of these materials have proceeded at a blistering pace during the past two decades, as exemplified in Figure 1.2.1, slightly modified from one displayed by Furukawa et. al.[16] Initially most research in synthesis was focused on obtaining new MOFs that were more stable to moisture, variable temperature and other factors than MOF-5. One of the results of such research was HKUST-1,[18] a copper-based network whose properties made it worthwhile to start thinking about how to synthesize these materials on an industrial scale, and in forms more suited to industrial applications, such as pellets. Another objective of researchers was to make the synthesis of large quantities of any MOF more efficient, both in the quantity of reagents utilized and in the quantity of solvents involved, not only because of economic concerns, but also because of the high environmental costs of using certain solvents in synthetic processes.

At present, MOFs are mainly synthesized by employing five different methods, all of which have inherent advantages and disadvantages. This work details materials synthesized through a traditional solvothermal method, so that will be the synthetic procedure explained in more detail within this section, after a brief introduction to the possibilities available to researchers who try to assemble MOFs.[19,20]

Electrochemical Synthesis: The synthesis is performed within an electrochemical cell, which allows the metal ions necessary for the formation of the network to diffuse into the solution from a metallic anode. The reaction medium is generally a protic solvent (to avoid metal deposition on cathode) in which the organic linkers and a conducting salt are dissolved. The advantages of such a method are

the lack of a metal salt as a source of cations, and therefore the lack of anions which could interfere with the reaction, the possibility to run a continuous process and exceed quantities of product typically produced with batches of reagents and the possibility to tune various parameters such as solution conductivity or intensity of the electrical current in order to improve yield or tune characteristics such as morphology of the material. It should be remarked that this method is quite inefficient, as the ohmic drop within the solution causes a significant expenditure in energy to obtain even modest yields of product.[21]

Microwave-assisted Synthesis: This method is very similar to normal solvothermal synthesis (see later) in that it uses mostly Teflon-lined vessels containing the solvent and reagents, which then get inserted into a microwave oven. The microwave system utilizes an oscillating electric field that induces rapid molecular movement within the medium, quickly heating the system. The ability to modulate power within the microwave equipment allows to sharply decrease synthesis time, at the cost of yield.[22]

Sonochemical Synthesis: Sonochemical synthesis uses a horn-type Pyrex reactor fitted to a sonicator, and uses the device to cause cavitation bubbles within the reaction medium, which means that upon collapse of the bubbles the area around them heats incredibly quickly to 5000 K and then cools down, which creates very small crystallites at a much faster rate than other methods.[23]

Microfluidic Synthesis: This system was developed as a response to the need to develop a continuous synthesis process for industrial purposes. It essentially relies on the preparation of two solutions, an aqueous one with a copper salt and an organic one with the desired linkers in a solvent such as 1-octanol. The two solutions are then continuously mixed in a T-junction, which makes the system evolve into small bubbles of aqueous solution within the organic solvent, with crystals growing at the liquid-liquid interface.[24]

Dry-Gel Conversion Synthesis: This method is particularly useful for the synthesis of zeolites. It consists in the preparation of a dry amorphous aluminosilicate gel through very well-known sol-gel synthesis techniques. The gel is subsequently converted into a MOF through its exposure to vapors of the desired organic ligand.[25]

Mechanochemical Synthesis: It is the most environmentally conscious method of synthesizing MOFs, because it requires little to no solvent and very low temperatures to function. This system is based on grinding the starting materials either without solvent or with the addition of a small amount of liquid (LAG, or liquid-assisted grinding) either in a mortar-pestle or in a ball-mill containing agate spheres. Mechanochemical synthesis is only suitable for specific types of MOFs, a group that has been recently expanded with networks that are obtainable via LAG by using the liquid as a structure-

directing factor or by inserting ions into the mixture so that they act as a templating agent for network formation. The main limitation of this technique is the limited array of available substrates.[26]

Conventional Solvothermal Synthesis: This method is not the first used to obtain MOFs, but it is one of the most straightforward and widely used. Several well-known networks such as MOF-5 or IRMOF-3 can be synthesized starting from zinc salts heated in closed vessels to temperatures around 100ºC in solvents such as DEF (N,N-diethylformamide) or DMF (N,N-dimethylformamide). This method has been shown to be extremely versatile due to the variety of solvents that can be employed, be they organic solvents or ionic liquids (ILs), and the variety of experimental conditions that can be utilized.

While performing reactions in a given solvent, and assuming that the metal salt, organic linkers and their mole ratios are kept consistent from experiment to experiment, there is a significant number of variables that affect solvothermal synthesis. The first and most obvious of these is the concentration of the reagents in solution, which can be increased to obtain smaller crystallites, increase yield and reduce the quantity of solvent that needs to be used for each batch of reagents. In most cases, however, the reaction is performed in a dilute solution, which is ideally suited to produce bigger crystals in order to ensure that their dimensions and quality are suitable for structure determination. Another extremely important variable is reaction temperature, which is heavily dependent on the vessel the reaction is performed in, as well as the heating mechanism and, most importantly, the solvent or mixture of solvents used in the reaction; usually most solvothermal methods require temperatures in the 90ºC to 150ºC range.

If one wants to obtain a less polydisperse distribution of crystallite size and obtain smaller crystals overall one could consider stirring the mixture during the reaction, keeping in mind that the specific stirring rate exerts a significant influence on the final product. Finally, the last important variable that should be taken into account is reaction time, which normally varies from a few hours to a few days. Longer reaction times allow for synthesis of less product, but can have a number of benefits, such as an increase in the purity of the product and a decrease in the number and quantity of other byproducts that are produced in the reaction, since a metastable phase that is kinetically favored might persist for a few hours, but an increase in reaction time to a few days is in some cases enough to only obtain the more thermodynamically stable product. In addition, giving more time to the self-assembly process can increase the conversion rate from reagents to product, and thus reduce the amount of unreacted material within the vessel.

When trying to produce crystals through solvothermal synthesis there is another variable, cooling rate, that is not strictly tied to other synthetic conditions, but that can nonetheless have a profound

effect on parameters such as crystal size and the quantity of byproducts. Cooling the system quickly might prevent the formation of crystals big enough to be used in single crystal X-ray diffraction experiments, while cooling too slowly might sometimes be impractical.

1.3.Porosity

The defining characteristic of a MOF is the presence of pores within the material, which is a feature that is as highly sought after as it is rare, at least in its purest form.

Porosity as a concept has been a topic of debate for at least the past two decades in Supramolecular Chemistry, with the strictest definition of the term being attributed to Kitagawa et al.[15], a definition that requires a successful gas sorption experiment on a candidate material for it to be considered porous. In other words, a material is potentially porous when its structure contains voids, cavities or channels filled with guest molecules, where the latter term is defined as cavities that are unbroken throughout the material. This feature is in no way sufficient to declare the material porous, however, as it is necessary that the overall structure of the material remains constant when all guest molecules are removed, as well as when new molecules are inserted into the voids.[27]

It is also important to keep in mind that when examining the presence of voids in a material the volume occupied by individual atoms needs to be taken into account. This is particularly important when using ball-and-stick models to represent crystals, because while this model is very good for highlighting molecular connectivity, it is quite misleading when employed to evaluate porosity.

This, alongside the definition of MOF outlined earlier, means that the materials outlined in this work are coordination polymers which are potentially porous and can therefore be defined as MOFs. Indeed, part of the objective of this work is to ascertain whether these materials meet some of the standards to be fully regarded as porous.

1.4. Serendipity

The process of scientific discovery usually involves making predictions about a given phenomenon based on the information already available to a researcher, then testing that prediction through a suitable experiment to check whether the system behaves in a way that is in accordance with the initial hypothesis. Sometimes, however, experiments end up producing results that do not answer the initial question posed by the scientist and can, at first glance, be quite puzzling, and it is important to be able to adapt to those circumstances by analyzing the data with an open mind.

A number of breakthroughs have been made by scientists throughout history by taking advantage of unexpected, if interesting, results, of which perhaps the most famous among chemists is the observation of chirality made by Louis Pasteur while studying crystals of tartaric acid both in its

racemic and optically pure form. The great French scientist noticed that the crystals of the two substances, which at the time were thought to be identical, differed in their response when exposed to polarized light. Pasteur could not have known that what he was observing was a conglomerate, or one of the few chiral molecules which can spontaneously solidify in a optically pure crystals of only one of its enantiomers. Furthermore, that phenomenon can occur only within a specific range of temperature, which coincidentally happened to include the temperature of the night air in which Pasteur left his crystals to cool.[28]

While this is not a work of the same relevance, I still had to be similarly curious about unforeseen developments in my research.

2. Methods and Equipment

2.1. Synthetic Methods and Reagents

Purity and sources of the reagents used in this work are detailed in Table 2.1.1. The final column, titled "Further Treatment" details whether or not it was deemed necessary to purify or in any way manipulate the reagent before inserting it into the reaction vessel.

Table 2.1.1 Information on sourcing and purity of reagents

Chemical	Purity (%)	Provider	Further Treatment
4,4-PBA	>95	CGeneTech, Inc.	No
2,6-PDA	>99	Sigma-Aldrich	No
3,5-PDA	>98	Sigma-Aldrich	No
DMSO	>99	Merck	Molecular Sieves
DMF	>99	Sigma-Aldrich	Molecular Sieves
Ethanol	>99.9	Kimix Chemical and Lab Supplies	No

In this work, DMF and DMSO were used in a mixture of 3/1 DMF/DMSO by volume, and said mixture was put in a container with molecular sieves for at least 24h before using it as a solvent in solvothermal synthesis processes. The DMSO used for the mixture was freshly purchased and DMF was already present in the host laboratory, stored in a container with molecular sieves.

Of the synthetic methods listed in Section 1.2, the one used for the reactions examined in this work was conventional solvothermal synthesis. In this specific instance, solid samples were weighed in separate containers, the solvent was inserted into each reaction vessel and solid reagents were then dissolved into the mixture at room temperature. Each reaction vessel was a TEFLON-lined autoclave. The autoclaves were put in an oven heated to 105ºC for varying timeframes depending on the specific reaction, then cooled either at room temperature, or by lowering the temperature of the oven by 10ºC/h for 8h and subsequently by cooling at room temperature. No stirring mechanism was employed.

2.2.Structure Solution

Single crystals of adequate quality, size and optical uniformity were removed from the mother liquor and immersed in a small pool of Paratone oil.[29] They were subsequently mounted on a nylon cryoloop connected to a rigid mounting.

The first of the following instruments was used to check the unit cell dimensions, while the second was used for full intensity data-collections. The unit cell dimension checks were performed on a Nonius KappaCCD single crystal X-ray diffractometer at 298K, using graphite-monochromated MoKα radiation (λ = 0.71073 Å) generated by a Nonius FR590 generator operated at 50 kV and 30 mA. The unit cell was indexed using DENZO[30] from the first twenty frames recorded with width ranging from 1 to 1.5° in ϕ or ω (with κ≠0).

The data-collections were recorded on a Bruker KAPPA APEX II DUO single crystal X-ray diffractometer using MoKα radiation (λ = 0.71073 Å) generated by a Bruker K780 generator operated at 50 kV and 30 mA.[31] All the samples were maintained at low temperature during the data-collection (usually 173 K and in some cases 100 K) by cooling with a constant flow of N_2 gas (rate of flow 20 cm^3 min^{-1}). The cryostream cooler was an Oxford Cryostream, UK. The unit cell refinement and data reduction were performed with the program SAINT.[32] SADABS[33] was used to correct for Lorentz-polarization and absorption effects.

The input file for the structure solution was elaborated using the program XPREP.[34] All the crystal structures were solved by direct methods using SHELXS-97[35] and refined by full-matrix least-squares using SHELXL-97.[35] These programs were implemented with the X-Seed 4.0[36] interface. Some crystal structures required further refinement due to the disordered solvent found in their channels, which was dealt with by using the "Mask" function on the Olex2-1.2 interface.[37] All non-hydrogen atoms were refined anisotropically. The Fourier difference map was used to locate the hydrogen atoms which were placed in idealized positions in a riding model and refined isotropically with assigned temperature factors 1.2 or 1.5 times that of their parent atoms.

It should be noted that all structures in which ellipsoids are pictured represent ellipsoids at 50% probability.

2.3.PXRD

The powder X-ray diffraction instrument used for the measurements was a BRUKER D8 Advance X-ray diffractometer, equipped with a Linkeye Detector. The instrument used a CuKα-radiation source (λ = 1.5406 Å), all the samples were placed on a zero-background sample holder (rotating at 10 rpm) and scanned over the 2θ-range 4° – 40°, with a step size of 0.02° per second. The X-ray

generator settings were 30 kV and 40 mA. All patterns were recorded at 298 K, a receiving slit of 0.6mm and primary and secondary slits of 2.5mm were used. Every sample was lightly ground to a fine powder prior to the measurement. After grinding, each sample was briefly deposited on a sheet of filter paper and subsequently placed on a zero-background sample holder prior to the start of the measurement without being dispersed in a liquid phase.

All PXRD patterns derived from solved SCXRD structures were calculated using the Mercury-3.10.3 tool provided by the Cambridge Crystallographic Structural Database (CCDC), with the following parameters: no preferential orientation, diffraction angle between 4° and 40°, steps of 0.02° and λ = 1.54056 Å. Mercury was also the program used to obtain drawings of the asymmetric unit of the compounds discussed in this work.[38]

2.4. TG/DSC

Thermogravimetric analysis (TGA) exposes a solid sample to heating, cooling or fixed temperature programs. The instrument measures the change in mass of sample as a function of temperature. Differential scanning calorimetry (DSC) measures the difference in energy as a function of temperature between a sample pan and a reference pan. During the analysis it is possible to observe both endothermic and exothermic peaks that are directly correlated to solvent loss, melting, phase transitions or decomposition.

A TA-G500 Thermogravimetric Analyzer with Universal Analysis 2000 software (v4.5A, TA Instruments-Waters LLC) was used. It was operated with a dry nitrogen purge gas flow rate of 60 $cm^3\ min^{-1}$ and samples were heated at a rate of 10 K min^{-1}. The samples, in a mass range of 1-2 mg, were removed from their mother liquor, dried on filter paper and placed in an open crucible.

Differential scanning calorimetry (DSC) was performed on a DSC-25 Discovery Differential Scanning Calorimeter (TA instruments) with TRIOS software (v4.1.0.3179, TA Instruments-Waters LLC). It was operated using a dry nitrogen purge gas flow rate of 40 ml min^{-1} and samples were heated at a rate of 10 K min^{-1} while in vented aluminum pans. Samples, with mass range 1-3 mg were removed from the mother liquor, dried on filter paper and placed inside a closed, vented aluminum pan.

It should be noted that the TGA instrument is calibrated to be accurate on mass loss measurements only to the first decimal digit, therefore all reported measurements will be rounded accordingly within the written portion of this work.

2.5.HSM and Microscopy

Hot Stage Microscopy (HSM) was used as a preliminary test to evaluate the behavior of a crystal at elevated temperatures. Bubbling, color changes or change of opacity of crystals indicates a thermal event that may be correlated to TGA or DSC traces. Samples were placed on a cover slip with a small drop of silicone oil and monitored using a Nikon SMZ-10 stereoscopic microscope fitted with a Linkam THMS600 hot stage and a Linkam TP92 temperature control unit. The images were captured with a real-time Sony Digital Hyper HAD color video camera and viewed using analySIS (the Soft Imaging System program).[39]

Some photographs were taken with an Axiocam 105 color camera attached to a Zeiss SteREO Discovery V8 microscope and processed using the ZEN (blue edition) program (Carl Zeiss Microscopy GmbH, 2011).

2.6. SEM

SEM was performed on samples which were sputter coated with gold/palladium. Either a Leo 1450 LaB6 scanning electron microscope or a Nova Nanosem 230 SEM were used. Energy dispersive spectroscopy (EDS) on the SEM was performed on selected parts of the sample. This analytical technique uses the unique electromagnetic emission spectrum resulting from the atomic structure to identify elements.

2.7. FTIR

The instrument used for data collection was a Perkin Elmer FT-IR Spectrum Two spectrometer fitted with a Universal ATR accessory. Samples were scanned over the 4000 cm^{-1} to 400 cm^{-1} range at a rate of 4 s cm^{-1}. The spectra were saved as text files and rendered by using Microsoft Excel.

3. Starting Molecular Complexes

3.1. IC-1

Section 3 is dedicated to the three compounds that constitute the starting point for this research. All of these compounds had previously been prepared by my co-supervisor, Dr. Zacharias, and the synthesis was repeated before adding variations to the system to independently register their structure, as well as to become more familiar with the synthetic process. The first of these complexes (Figure 3.1.2) was synthesized inserting approximately 0.1 mmol of $Cu(NO_3)_2 \cdot 2.5H_2O$ and 0.4 mmol of 2,6-pyridinedicarboxylic acid (2,6-PDA) and 4-pyridin-4-yl-benzoic acid (4,4-PBA) in ethanol, adding the resulting mixture to a TEFLON-lined autoclave, which was subsequently sealed and heated to 105ºC in an oven for 24h. The reagents are shown in Figure 3.1.1.

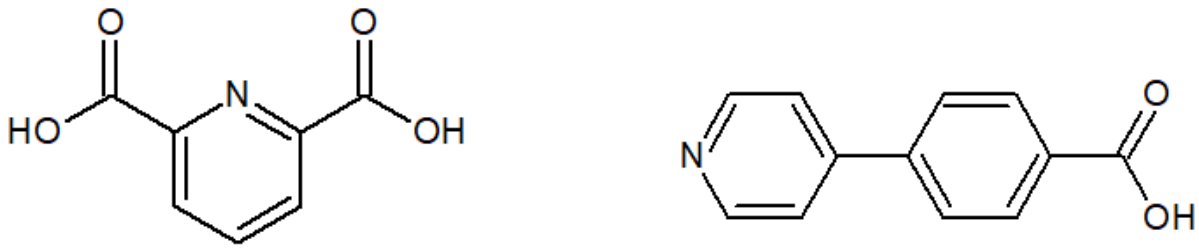

Figure 3.1.1 Reagents utilized in Section 3, on the left 2,6-pyridinedicarboxylic acid (2,6-PDA), on the right 4-pyridin-4-yl-benzoic acid (4,4-PBA).

The resulting complex does not include 4,4-PBA or ethanol in its internal structure, instead, it is characterized by a 2,6-PDA molecule chelating a Cu(II) ion, which is also coordinated by two water molecules. As shown in the unit cell of the complex, the sixth coordinating position on each copper ion appears to have been filled by electrons from one of the chelating oxygen in an adjacent complex molecule. This feature, as shown on the right side of Figure 3.1.2, implies that the material consists of columns with complex to complex connections within each column, but not between columns. All relevant information for the solution of the crystal structure are shown in Table 3.1.1.

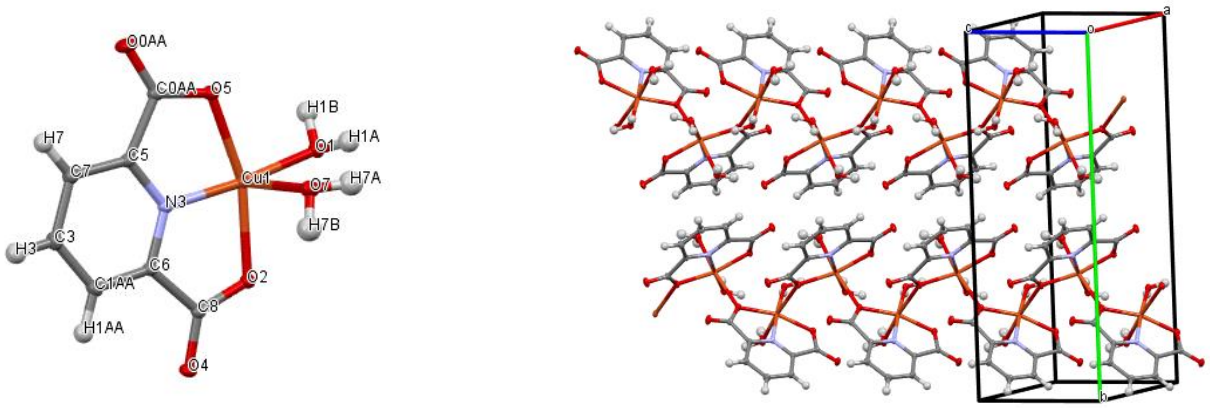

Figure 3.1.2 Single crystal structure of IC-1, synthesized from copper nitrate, 2,6-pyridinedicarboxylic acid, 4-pyridine-4-yl benzoic acid in ethanol.

Table 3.1.1 Relevant information on single crystal structure solution of IC-1

Identification code	IC-1
Empirical formula	$C_7H_7CuNO_6$
Formula weight	264.68
Temperature (K)	173.11
Crystal system	monoclinic
Space group	$P2_1/c$

a (Å)	7.1997(3)
b (Å)	18.9211(8)
c (Å)	6.4234(3)
α (°)	90
β (°)	107.0810(10)
γ (°)	90
Volume ($Å^3$)	836.44(6)
Z	4
ρ_{calc} (g/cm^3)	2.102
μ (mm^{-1})	2.620
F(000)	532.0
Crystal size (mm^3)	0.36 × 0.32 × 0.22
Radiation	MoKα (λ = 0.71073 Å)
2Θ range for data collection (°)	4.306 to 70.164
Index ranges	$-11 \leq h \leq 11$, $-28 \leq k \leq 29$, $-9 \leq l \leq 10$
Reflections collected	18187
Independent reflections	3477 [R_{int} = 0.0249, R_{sigma} = 0.0181]
Data/restraints/parameters	3477/0/165
Goodness-of-fit on F^2	1.063
Final R indexes [I>=2σ (I)]	R_1 = 0.0233, wR_2 = 0.0589
Final R indexes [all data]	R_1 = 0.0261, wR_2 = 0.0600
Largest diff. peak/hole (e $Å^{-3}$)	0.54/-0.33

3.2.IC-2

The second compound from which this project has originated was synthesized with the same reagents in the same molar ratios as the complex discussed in Section 3.1, utilizing water as the solvent. The reaction was performed in an oven at 105ºC for 24h.

The structure of the compound is pictured in Figures 3.2.1 and 3.2.2 and is similar to the one described in Section 3.1, given the presence of a chelating molecule of 2,6-PDA. In this instance, however, the Cu(II) ion in the center of the complex is coordinated by the nitrogen atom of the pyridyl ring in 4,4-PBA and a water molecule, while two other water molecules are found in the space around each complex. It is worth noting that, in this instance, no connections were observed between complex

molecules and the crystal is merely a closely packed ordered distribution of such molecules. All relevant information for the solution of the crystal structure are shown in Table 3.2.1.

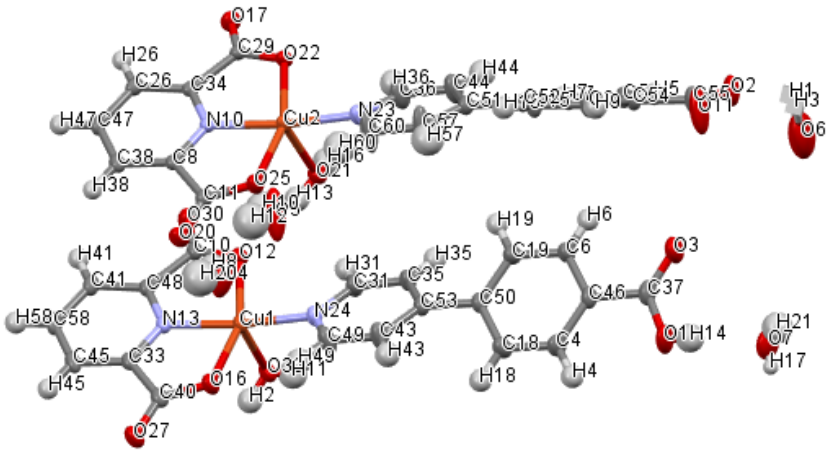

Figure 3.2.1 Single crystal structure of Initial Compound 2, synthesized from copper nitrate, 2,6-pyridinedicarboxylic acid, 4-pyridine-4-yl benzoic acid in water.

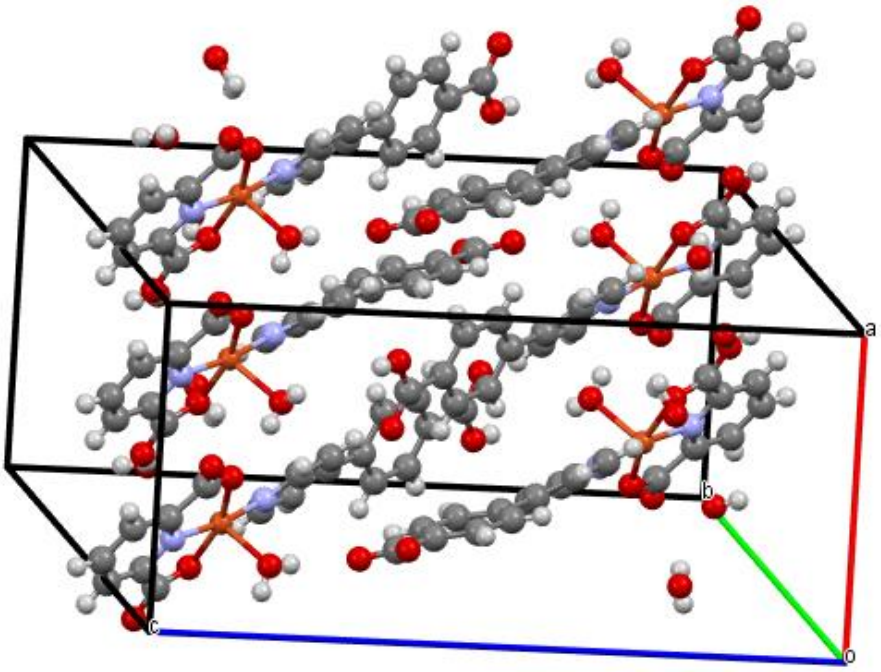

Figure 3.2.2 Single crystal structure of Initial Compound 2, synthesized from copper nitrate, 2,6-pyridinedicarboxylic acid, 4-pyridine-4-yl benzoic acid in water.

Table 3.2.1 Relevant information on single crystal structure solution of IC-1

Identification code	IC-2
Empirical formula	$C_{19}H_{17.5}N_2O_9Cu$
Formula weight	481.26

Temperature (K)	173.15
Crystal system	triclinic
Space group	*P-1*
a (Å)	9.7918(6)
b (Å)	9.9662(7)
c (Å)	22.0376(14)
α (°)	81.490(1)
β (°)	88.986(1)
γ (°)	66.735(1)
Volume ($Å^3$)	1952.0(2)
Z	4
ρ_{calc} (g/cm^3)	1.428
μ (mm^{-1})	1.159
F(000)	986
Crystal Size (mm^3)	0.12 x 0.14 x 0.20
Radiation	MoKα (λ = 0.71073 Å)
2Θ range for data collection (°)	1.87 to 56.96
Index ranges	$-13 \leq h \leq 13$, $-13 \leq k \leq 13$, $-29 \leq l \leq 29$
Reflections collected	56409
Independent reflections	9847 [R_{int} = 0.0402, R_{sigma} = 0.0290]
Data/restraints/parameters	9847/0/611
Goodness-of-fit on F^2	0.925
Final R indexes [I>=2σ (I)]	R_1 = 0.0393, wR_2 = 0.1135
Final R indexes [all data]	R_1 = 0.0666, wR_2 = 0.1393
Largest diff. peak/hole (e $Å^{-3}$)	1.57/-0.61

4. 1-MBUCT

4.1. General Synthetic Conditions

Initially 1-MBUCT was synthesized from the following starting materials: copper sulfate pentahydrate, 3,5 pyridinedicarboxylic acid (3,5-PDA), 4-pyridin-4-yl-benzoic acid (4,4-PBA) and ethanol (solvent). The mole ratio between reagents was 4 moles of each ligand for every mole of salt, and the solution was quite dilute, since the target values set for the experiment were 0.1/0.4/0.4 mmol

for every 5mL of solution, for a molar concentration of approximately 0.08M. For a comprehensive list of the exact masses and moles involved, see Table 4.4.1. The reagents are pictured in Figure 4.1.1.

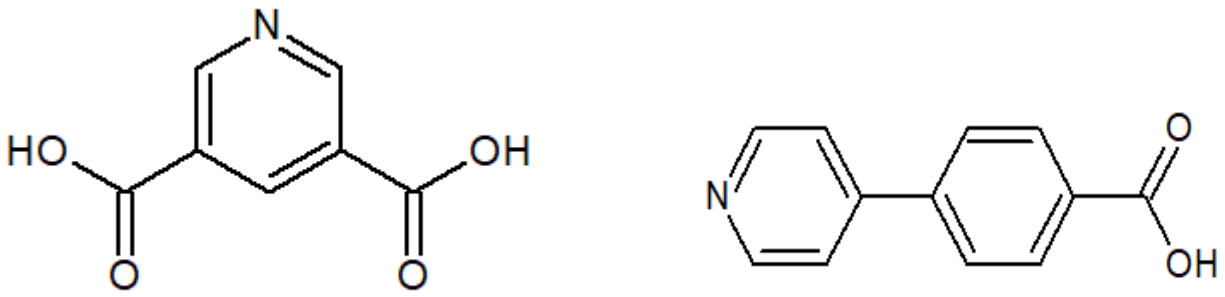

Figure 4.1.1 The two ligands utilized in the synthesis, 3,5-pyridinedicarboxylic acid (3,5-PDA) on the left and 4-pyridin-4-yl-benzoic acid (4,4-PBA) on the right.

The synthesis was initially performed in an oven, within sealed and TEFLON lined autoclaves, for a period of 24h at a temperature of 105ºC; the autoclaves were then removed from the oven and left to cool until they reached room temperature. These synthetic conditions produced 1-MBUCT, but the final mixture was also contaminated by impurities and unreacted starting materials. To solve this problem, the next attempt was carried out in modified conditions by aligning the mole ratios of the reagents with the ones found in the asymmetric unit (ASU) of the crystalline product, or 1 mole of salt for 2 moles of each ligand. The attempt was unsuccessful, as the problem it was meant to solve remained, while the yield and quality of product worsened considerably. The best result obtained with 1/4/4 (Cu(II)/3,5-PCA/4,4-PBA) molar ratios involved extending the reaction time to 72h and implementing a more gradual, controlled cooling protocol, decreasing the temperature in the oven by 10°C every hour for 8 hours and then letting the autoclaves cool at room temperature. These parameters, however, were still not enough to obtain a product pure enough to be utilized for bulk thermogravimetric analysis or powder X-ray diffraction, so further changes needed to be made. Table 4.1.1 and the next paragraphs of this work will detail these changes and the effects they had on the product, while later Sections will explore the consequences of these effects on further experimentation aimed at gaining a broader understanding of this system.

Table 4.1.1 Table on molar ratios and related results in attempts to synthesize 1-MBUCT.

Metal Salt	Salt Mass (mg)	Salt Moles (mmol)	3,5 Ligand Mass (mg)	3,5 Ligand Moles (mmol)	4,4 Ligand Mass (mg)	4,4 Ligand Moles (mmol)	Time (h)	Result
$CuSO_4 \cdot 5H_2O$	26.2	0.105	69.4	0.415			72	Imp.
$CuSO_4 \cdot 5H_2O$	26.4	0.106	69.7	0.417			72	Imp.
$CuSO_4 \cdot 5H_2O$	24	0.10	68	0.41	83	0.42	24	Imp.
$CuSO_4 \cdot 5H_2O$	25	0.10	66	0.39	79	0.40	24	Imp.
$Cu(CH_3COO)_2$	18.5	0.102	66.5	0.398			72	
$Cu(CH_3COO)_2$	17.9	0.0986	67.1	0.402			72	
$Cu(CH_3COO)_2$	18.9	0.104	69.2	0.414	80.5	0.404	72	Imp.
$Cu(CH_3COO)_2$	18.1	0.0997	65.5	0.392	79.7	0.400	72	Imp.
$CuCl_2 \cdot 2H_2O$	16.7	0.0980	66.7	0.399			72	Gel
$CuCl_2 \cdot 2H_2O$	17.0	0.100	66.0	0.395			72	Gel
$CuCl_2 \cdot 2H_2O$	16.3	0.0956	66.3	0.397	80.8	0.406	72	
$CuBr_2$	24.6	0.110	65.9	0.394			72	Imp.
$CuBr_2$	23.0	0.103	68.4	0.409	80.8	0.406	72	Imp.
$CuBr_2$	22.4	0.100	67.4	0.403	81.2	0.408	72	Imp.
$Cu(ClO_4)_2 \cdot 6H_2O$	36.3	0.0980	68	0.407			72	1-A
$Cu(ClO_4)_2 \cdot 6H_2O$	34.6	0.0934	68.1	0.407			72	1-A
$Cu(ClO_4)_2 \cdot 6H_2O$	36.4	0.0983	66.4	0.397	82.5	0.414	72	Imp.
$Cu(ClO_4)_2 \cdot 6H_2O$	36.3	0.0980	67.2	0.402	78.4	0.394	72	Imp.

Table 4.1.1 is a comprehensive representation of various attempts to synthesize 1-MBUCT while varying the experimental conditions of the reaction. The result column of the table highlights which systems produced 1-MBUCT crystals suitable to perform single crystal X-ray diffraction experiments (dark blue colour, Figure 4.1.2), which systems produced a light blue crystalline solid that did not contain crystals big enough for SCXRD (light blue colour) and which system did not produce crystals at all (grey colour). It is also specified whether the products were contaminated by impurities or unreacted starting material (Imp.), whether a gel was produced by separating the mother liquor of the reaction from 1-MBUCT and letting it cool down (Gel) or whether drying out said mother liquor revealed the presence of a byproduct in solution (1-A). All of these features of the system will be explored shortly, by focusing on the impact that each metal salt used for the reaction had on its outcome and characteristics.

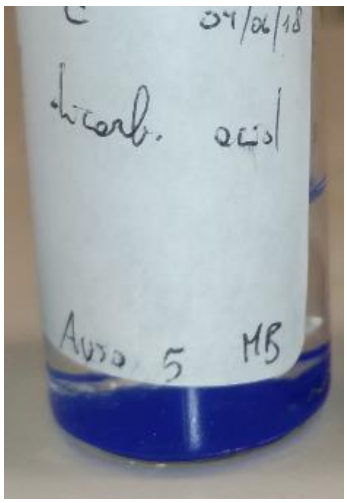

Figure 4.1.2 Picture of bulk 1-MBUCT in fresh ethanol after purification.

$CuSO_4 \cdot 5H_2O$: This metal salt was selected for the initial attempt at synthesizing a MOF with this reaction mainly due to the fact that it is not hygroscopic, it is quite easy to manipulate and is of relatively low toxicity. Furthermore, the sulfate anion is usually not a particularly strong coordinating ligand, which made it likely that the anion would not interfere with MOF formation. As detailed at the start of this Section, the synthesis worked, but it was not possible to totally eliminate impurities from the reaction mixture. For this reason, copper sulfate products were not utilized for bulk analysis beyond some initial attempts and each sample was identified as 1-MBUCT by checking the unit cell of crystals within it. The crystals of product appeared as thin, rhombohedral plates, and this crystal habit remained consistent regardless of the metal salt utilized to synthesize the MOF.

$CuBr_2$: The samples synthesized starting from copper bromide were not utilized for analysis due to the fact that they showed the highest quantity of impurities, as the dark blue crystals of 1-MBUCT were dispersed within a dark green amorphous powder of unknown composition. A similar powder is what appeared when it was attempted to dry out the clear green mother liquor that submerged the final product. For this reason, similarly to the previous reaction, it was necessary to verify whether the dark blue crystals produced by this reaction were indeed the same product as all the other reactions by checking the cell parameters on a single crystal, rather than by comparing PXRD patterns.

It is worth noting that the autoclaves containing copper bromide gave out the same product in reactions where 4,4-PBA was included and in reactions where that same ligand was removed, the same behavior displayed by the system involving copper sulfate.

$Cu(CH_3COO)_2$: The systems involving copper acetate were not particularly interesting because the results obtained from these systems were remarkably consistent and characterized by an almost complete lack of impurities or byproducts, especially in reactions in which 4,4-PBA was not used as a ligand. It was quite easy to remove the small traces of impurities left in each sample by washing it

with fresh solvent. This made it feasible to use copper acetate products to perform some of the bulk analysis on 1-MBUCT.

As with the systems discussed previously, reactions involving copper acetate resulted in the same material being produced whether or not 4,4-PBA was utilized as a ligand, although it should be noted that the addition worsened the quality of the product and resulted in a sizable amount of unreacted starting material persisting in the system.

$CuCl_2 \cdot 2H_2O$: The product described here was synthesized with essentially the same method utilized for all the previously considered systems, with one key difference: the MOF synthesized under these conditions and the byproducts that accompanied it appear to be extremely sensitive to sudden changes in temperature while in the cooling phase of the synthesis process. This behavior was registered in two separate instances, in which an error in the implementation of the cooling protocol meant that batches of the material were cooled at a much faster rate while still being contained within the autoclave. The result of this mistake was a viscous, dark blue solution with a visibly reduced number of 1-MBUCT blue crystals at the bottom of the vial, and, as will be explored in depth in other Sections, the solution quickly turned into a gel.

Upon realizing this feature of the system, the synthesis was repeated several times under more controlled conditions and it was consistently possible to completely purify the product by merely removing its mother liquor and washing the crystals repeatedly in fresh ethanol.

$Cu(ClO_4)_2 \cdot 6H_2O$: The last Cu(II) salt used to synthesize 1-MBUCT was copper perchlorate hexahydrate, and in this instance it is necessary to discuss the product of the reaction that did not involve 4,4-PBA as a ligand separately from the product of the reaction that utilized the ligand, because in this system the two products have markedly different characteristics.

The use of copper perchlorate, in fact, resulted in the system no longer producing the expected blue crystals of 1-MBUCT altogether and the end result of the reaction consisted of a light blue powder and a light blue, clear mother liquor (Figure 4.1.3). Despite several improvements to the reaction that significantly increased the crystallinity of the powdery product, it was not possible to obtain a single crystal big enough to be used for single crystal X-ray diffraction within the time allotted for the experimental portion of this work. It was, however, possible to isolate a second product from the system by slowly evaporating the mother liquor for thirty days, and this second material was constituted of crystals suitable for SCXRD analysis (coded as 1A-MBUCT and described in Section 4.8.1). The resulting structure is useful in understanding this system, as well as the likely role of the perchlorate anion in preventing the formation of 1-MBUCT.

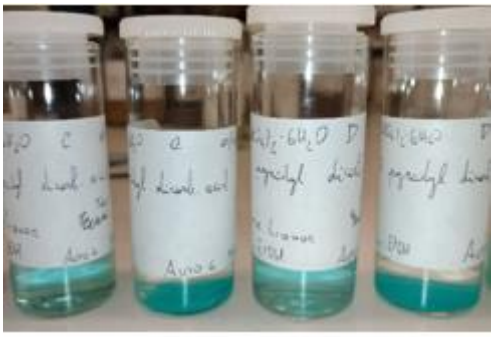

Figure 4.1.3 First and third vial from the left are mother liquor prior to evaporation, while second and fourth are powdery crystalline product.

The first attempt at performing this reaction featured a 48h reaction time and the autoclaves containing the reaction mixtures were left to cool directly at room temperature. With these parameters it was expected that the product would be 1-MBUCT, as was the case with other Cu(II) salts. These conditions, while not ideal, were utilized due to time constraints and should have been enough to obtain a product that could be used to confirm whether the result of the experiment was consistent with previous attempts. What was found, instead, was an azure powder that, under a microscope, appeared to be constituted mainly of very small crystals. A PXRD pattern of the solid was registered and the synthesis experiment was repeated with a reaction time of 72h and the same rigid cooling protocol that had been adopted for all the other samples. These efforts resulted in a seemingly identical result, as the product appeared to be a powder of the same quality and crystallinity as the one synthesized previously, save for a slight increase in the dimension of the crystals.

4.2. Structure

The X-ray diffraction data analyzed in this section was obtained from a single crystal selected from a sample that utilized copper chloride dihydrate as a reagent. As shown in Figure 4.2.1, the morphology of the crystal is a thin, monoclinic plate; this morphology is remarkably consistent within the samples, irrespectively of the size of the crystal one might take into consideration. The deep blue color is typical of Cu(II) complexes in which a metal ion is coordinated by nitrogen or oxygen atoms.

Crystallographic information is shown in Table 4.2.1. The ASU of the system is constituted of a Cu(II) ion coordinated by the two nitrogen atoms in two pyridyl rings belonging to 3,5-PDA molecules. Upon expanding the structure one can obtain the image in Figure 4.2.2. Three out of the four peripheral carboxylate moieties in the ligands are coordinated to copper ions, and that each individual copper ion is coordinated by five heteroatoms, three oxygens and two nitrogens, giving rise to a 3D-MOF with square channels (Figure 4.2.2). Figure 4.2.3 depicts the ASU of the system.

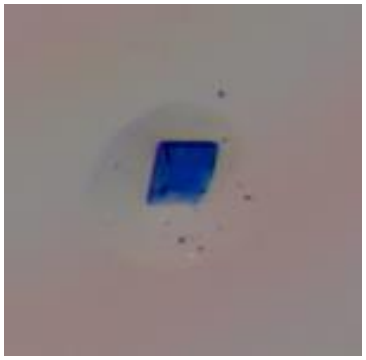

Figure 4.2.1 Picture of a single crystal of 1-MBUCT, obtained from a sample synthesized from copper chloride dihydrate, the edge of the crystal can be measured at approximately 0.41mm.

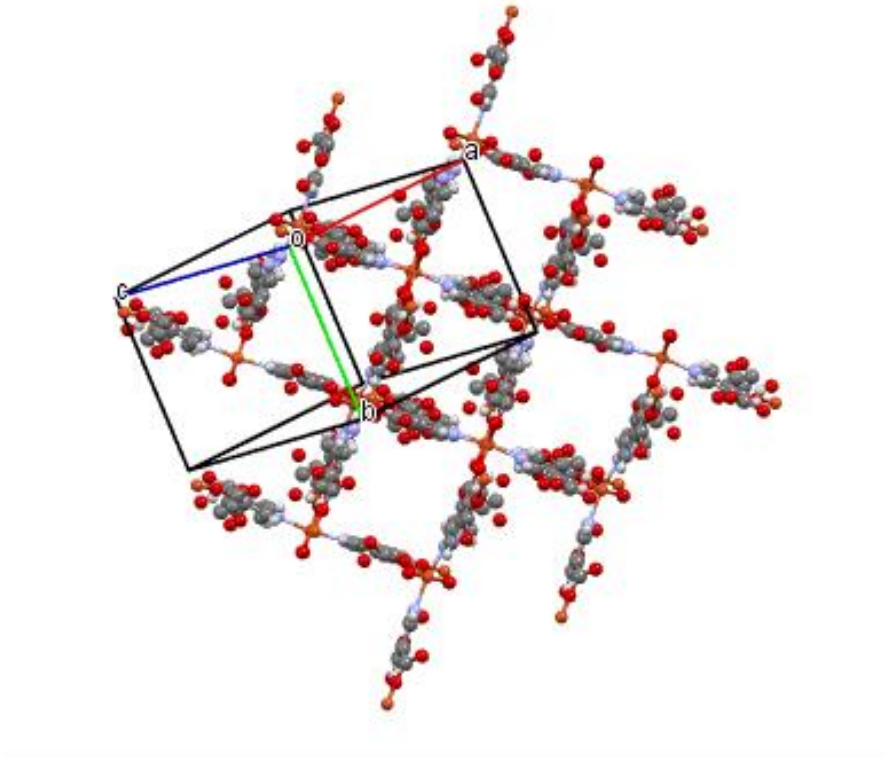

Figure 4.2.2 Structure of 1-MBUCT channels with unit cell axes and channels

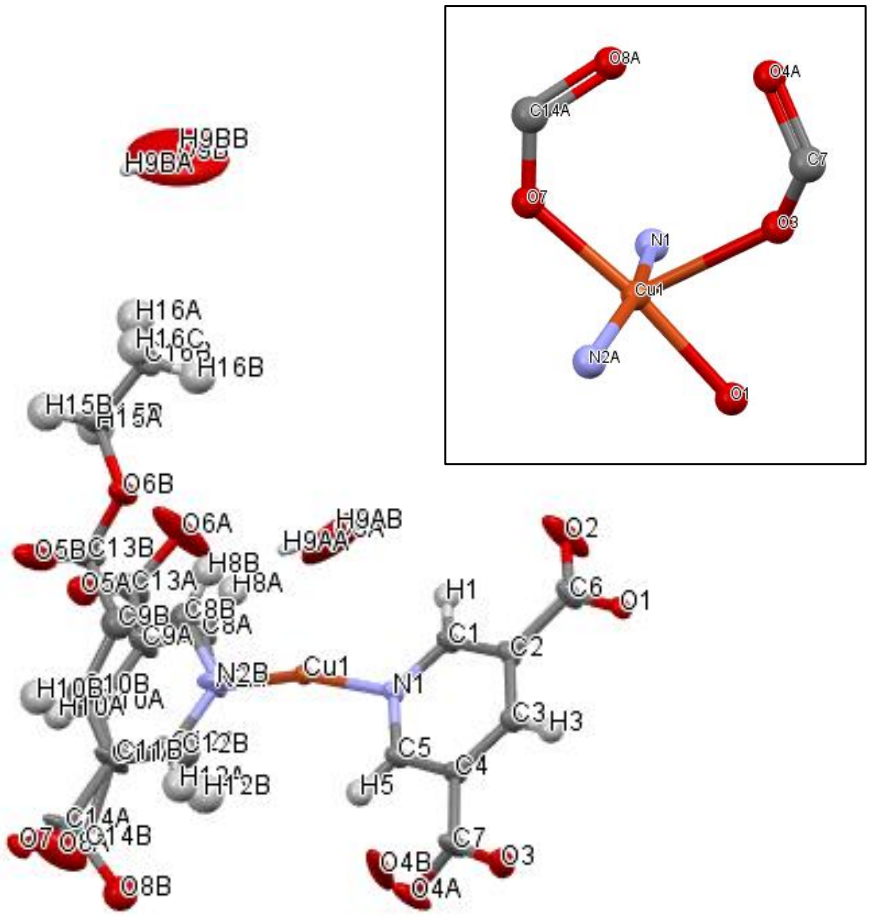

Figure 4.2.3 Structure of the ASU of 1-MBUCT

Table 4.2.1 Relevant information on structure solution of 1-MBUCT

Identification code	1-MBUCT
Empirical formula	$C_{14.4}H_{8.16}CuN_2O_{8.58}$
Formula weight	409.95
Temperature (K)	293(2)
Crystal system	monoclinic
Space group	*P2₁/c*
a (Å)	12.5912(9)
b (Å)	10.2762(8)
c (Å)	15.1970(12)
α (°)	90
β (°)	97.495(2)
γ (°)	90
Volume ($Å^3$)	1949.5(3)
Z	4
ρ_{calc} (g/cm^3)	1.393
μ (mm^{-1})	1.163

F(000)	820.0
Crystal size (mm^3)	0.10 × 0.12 × 0.14
Radiation	MoKα (λ = 0.71073)
2Θ range for data collection (°)	3.262 to 61.352
Index ranges	$-18 \leq h \leq 18$, $-14 \leq k \leq 14$, $-21 \leq l \leq 21$
Reflections collected	68571
Independent reflections	6018 [R_{int} = 0.0883, R_{sigma} = 0.0415]
Data/restraints/parameters	6018/496/307
Goodness-of-fit on F^2	1.073
Final R indexes [I>=2σ (I)]	R_1 = 0.0656, wR_2 = 0.1963
Final R indexes [all data]	R_1 = 0.0854, wR_2 = 0.2161
Largest diff. peak/hole (e $Å^{-3}$)	3.84/-1.52

Researching the unit cell of this crystal in the most recent version of the CSD (Cambridge Structural Database) with a 3% tolerance on cell parameters did not yield any results, it is therefore thought that this structure has so far been unknown. A MOF containing Cu(II) and 3,5-PDA as a ligand, and displaying a square pyramidal coordination geometry has been reported alongside similar cobalt-based compounds by Huang et. al.[40] In their work, these materials could be synthesized via self-assembly by slowly introducing an aqueous solution of a metal salt in a benzene solution containing 3,5-PDA and pyridine, which is the factor that differentiates that reaction from the one discussed here. Other groups studied the topology and tuning[41] of other coordination polymers involving Cu(II) and 3,5-PDA, as well as their properties as light-emitting materials.[42] All of these materials only contain one molecule of 3,5-PDA in their ASU, instead of the two molecules found in 1-MBUCT.

The aforementioned coordination environment means that there is a net charge of -1 on the overall structure, and therefore that the entire network must be negatively charged, which means that somewhere within the structure of the MOF a cation must be found to preserve the electrical neutrality of the material. The most likely candidate for this role would be a hydrogen atom bonded to either of the disordered carboxylate moieties facing each other close to the metal center. In the ASU of Figure 4.2.3. those are the oxygens labeled as O4A/O4B and O5A/O5B, and they are pictured in the close-up view of the metal center in the upper right corner of Figure 4.2.3. Given the disorder inherent in that specific area of the structure it is conceivable that the position of such a hydrogen atom to not be fixed in every unit cell, which, alongside its few electrons, might be why it was not possible to model it in the crystal structure.

Another structural factor supporting these hypotheses is the fact that the Cu-O bonds of the carboxylates coordinating the H atom do not block free rotation around the bond axis, which means that there would be a possibility for the two electron-rich carboxylate moieties to be farther apart while still coordinating the metal center.

All of these considerations are based on evidence that is not conclusive, since the only way to know with certainty whether or not a hydrogen atom is indeed located in that position is to perform a neutron diffraction experiment on the crystals.

One of the ligands within the ASU is visibly disordered, to the point that its heterocyclic ring and most of the functional groups attached to it occupy two separate positions with each one having a different probability of occurring in any given unit cell. The most likely configuration is present in 80% of the unit cells, while the least likely is present in 20% of the unit cells. It is noteworthy that the disordered ligand is the one having only one of its carboxylic moieties coordinated to a Cu(II) ion and that the part of the molecule with the clearest signs of disorder is precisely the free carboxylic group on the ligand. This can be explained examining Figure 4.2.3, in which it can be seen that the disordered carboxylic group has been esterified by the solvent during the synthesis of the material. That picture is, however, slightly deceptive because, as outlined in Figure 4.2.4 and 4.2.5, the esterified carboxylate is present only in one asymmetric unit every five, according to the structure solution model that produced the best results. Thus, the square channels displayed in Figure 4.2.2 are sometimes blocked by the presence of the ester, while in all other configurations they are filled with solvent.

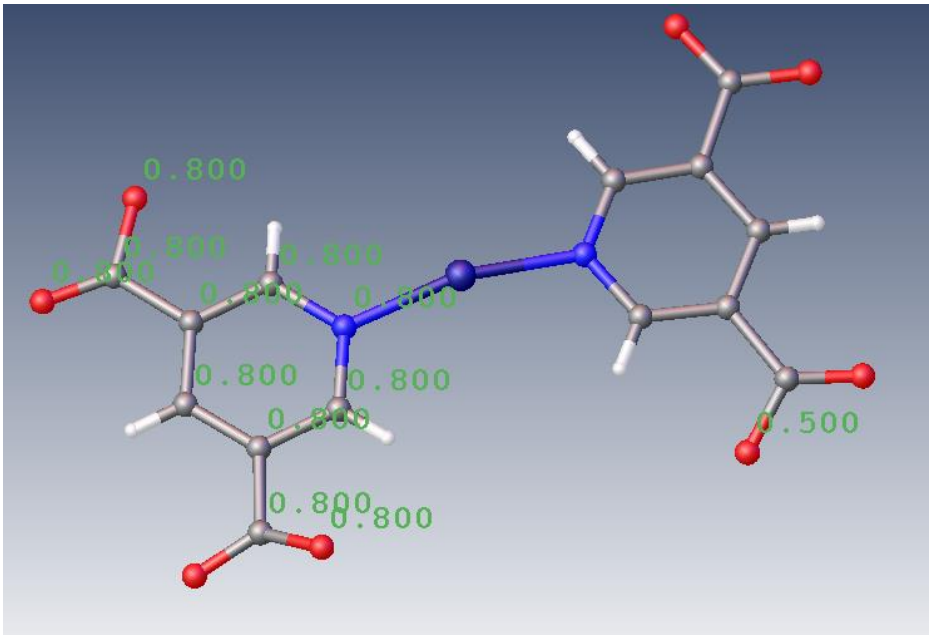

Figure 4.2.4 Structure of 1-MBUCT, partial asymmetric unit with chemical occupancies of disordered atoms

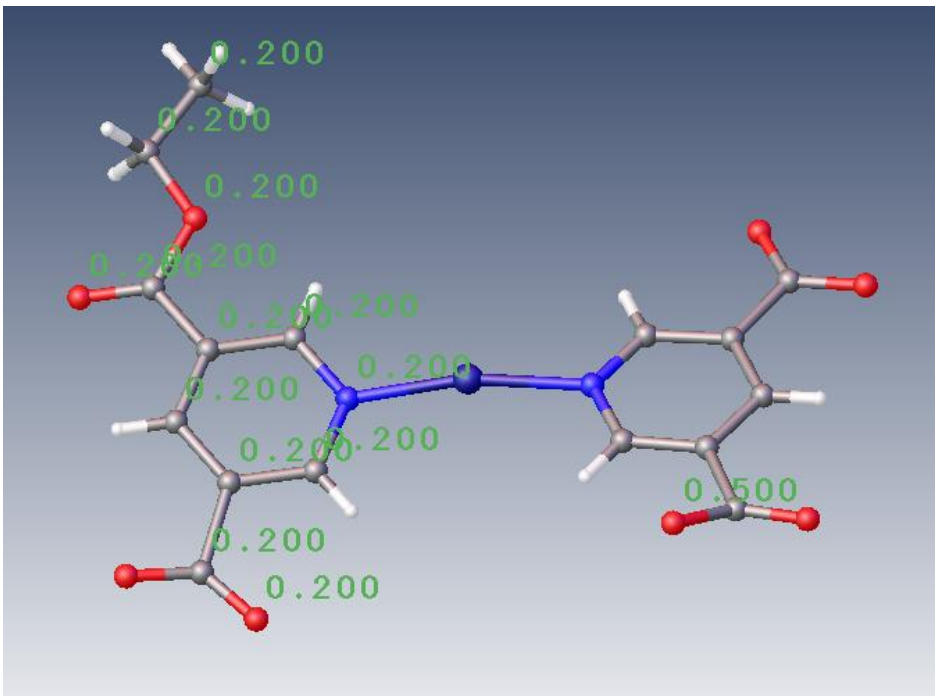

Figure 4.2.5 Structure of 1-MBUCT, partial asymmetric unit with chemical occupancies of disordered atoms

It was necessary to precisely model the disorder on the ligands because the electron density of the solvent could not be modeled. It was therefore necessary to use the "Mask" function in the Olex2 structure solution software in order to ascertain both the volume of the space occupied by the channels within the structure and the total number of electrons present inside the channels themselves. Said function identifies the channels containing unmodeled and disordered molecules of solvent, analyzes the electron density present in the channels and applies a Fourier transform to the functions that identify the electron density. The output of the Fourier transform is then utilized by the software as a mediated expression of the effect of the solvent on the overall structure, thereby allowing the user to improve the refinement of the structure and to know how many electrons were present within the channels. An incorrect or incomplete count of the electron density belonging to the ligands would pose problems when attempting to use the parameters estimated by Olex2 to deduce the content of the channels.

In this instance, each channels within a unit cell of the structure contain 48 electrons, and each unit cell was shown to include two cavities, which meant that there were 96 electrons per unit cell and, given the symmetry of the system, 24 electrons per asymmetric unit (ASU). This information will make it possible to narrow down the range of possibilities that will need to be discussed when analyzing the thermal stability data obtained on this system.

4.3. PXRD Analysis

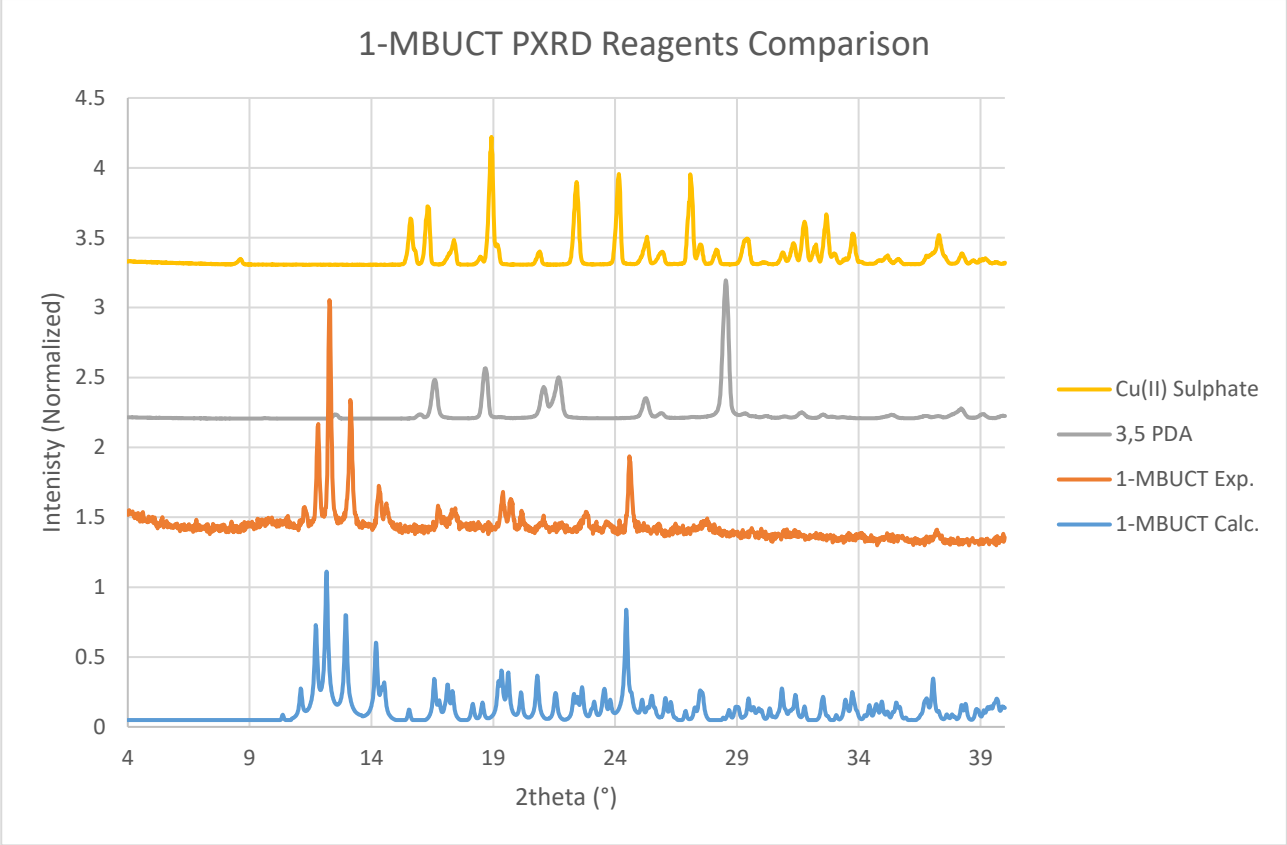

Figure 4.3.1 Picture of PXRD comparison of 1-MBUCT and reagents. The 1-MBUCT Exp. dataset has been scaled to twice the size of the other sets, to highlight its smaller peaks.

Firstly, it is verified that the product is a distinct phase from either of the reagents, and that the bulk product does not have crystalline impurities that might not be visible under a microscope but still influence both the PXRD pattern and any other bulk analysis in a significant way. Allowing for the fact that the experimental pattern will necessarily capture fewer details than the ones extrapolated from the single crystal structure, one can clearly see that there are peaks in the calculated pattern that do not have a corresponding peak in the experimental pattern. In addition, the peaks in the experimental pattern appear to be slightly shifted with respect to the ones in the calculated patter. It is therefore likely that the mechanical stress of grinding the sample might have induced a partial loss of solvent from the cavities within the material and a slight reduction in the dimensions of the unit cell. This conclusion could be verified by performing single crystal or powder diffraction experiments at a temperature higher than the solvent loss peak highlighted in the DSC experiments, but lower than the decomposition peak displayed in DSC. Conversely, there is no peak in the experimental pattern that is unaccounted for in the calculated pattern.

4.4. Thermal Analysis

Thermal stability is an important feature in any material, and it is therefore paramount to evaluate the behavior of 1-MBUCT when exposed to high temperatures. Firstly, the material was examined under a hot stage microscope to look for color changes, bubbling or any other visual sign that might point to internal changes within the crystals. Another benefit of the technique is that it enables the experimenter to set up successive thermogravimetric analysis (TGA) and differential scanning calorimetry (DSC) experiments so as not to damage the machinery with the byproducts of a violent decomposition that can sometimes occur when a sample is heated past a certain threshold.

The first picture displays a few crystals of 1-MBUCT at room temperature, and will be used as reference to detect color changes.

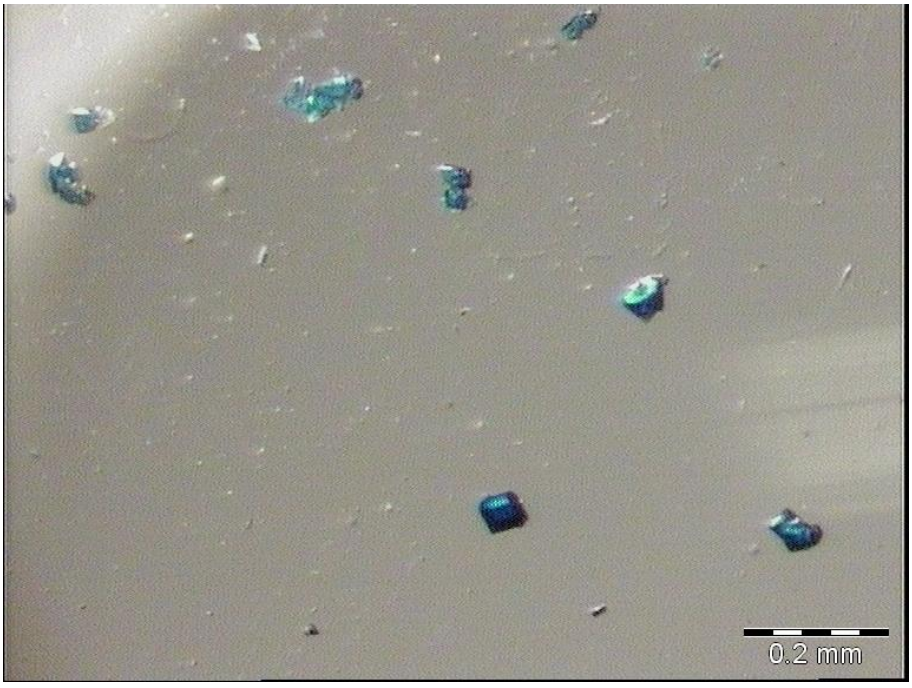

Figure 4.4.1 Picture of hot stage microscopy experiment on 1-MBUCT without solvent exchange, 28.6°C

Figure 4.4.2 shows the end point of a gradual darkening of the crystals that took place throughout the experiment. No bubbling was observed.

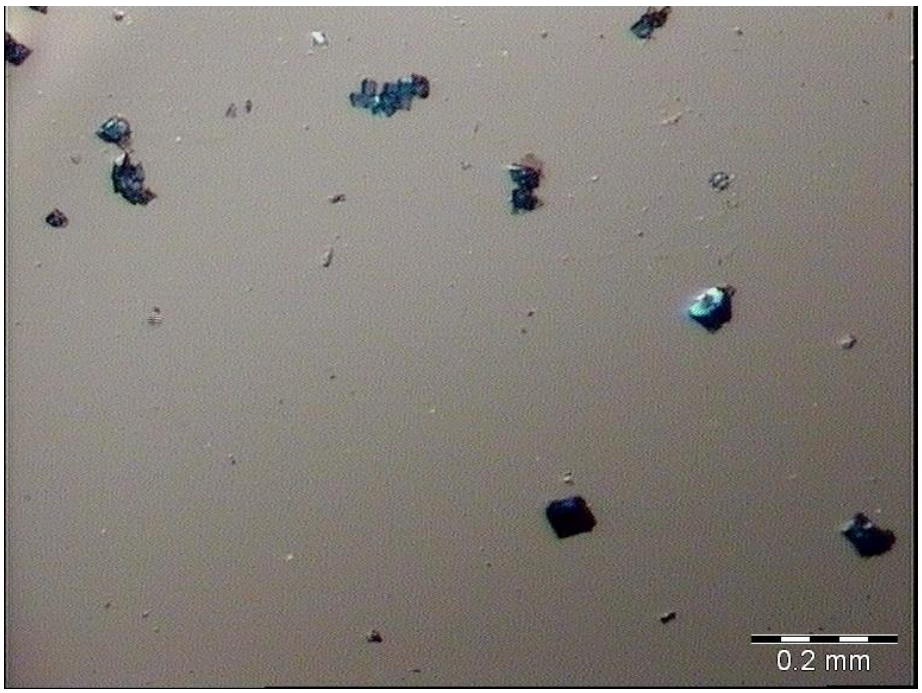

Figure 4.4.2 Picture of hot stage microscopy experiment on 1-MBUCT without solvent exchange, 310.2°C

The bubbles and radical change in color of the crystals shown in the final picture signify the start of the decomposition process for the material.

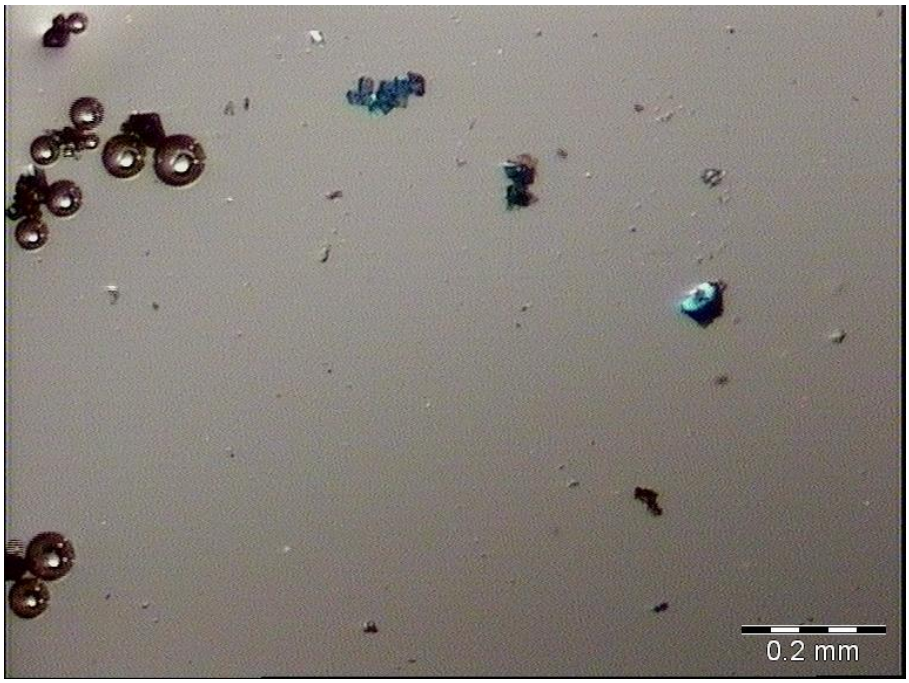

Figure 4.4.3 Picture of hot stage microscopy experiment on 1-MBUCT without solvent exchange, 318.4°C

It is necessary to point out that, due to issues with the glass in the sample holder of the HSM apparatus the outer cover of the holder had to be removed, leading to a temperature within the sample that is not a reliable indicator of the exact temperatures at which the changes in the material have taken place.

To verify whether the deductions on the observations made previously were valid, it was necessary to complement the HSM with multiple replications of TGA and DSC experiments on the sample. The curves displayed below are the observations that were most representative of the average result obtained in the experiments.

DSC is a technique in which it is possible to measure the variations in the energy a given system needs to increase its temperature by a set amount of degrees. In each experiment a control is utilized to account for the specific characteristics of the DSC machine and of the sample holder. The result is a graph in which the sample can show either events that cause it to give out energy to the surrounding environment or events that cause the sample to absorb energy from its surroundings. The latter case is the one that identifies phenomena such as evaporation of solvent out of the channels of a porous material. Knowing the range of temperatures at which these events occur makes it possible to be more accurate when measuring the mass lost during TGA experiments by giving the experimenter a better grasp of the temperature intervals in which the mass loss actually takes place. One of the DSC experiments performed on 1-MBUCT is depicted in Figure 4.4.4.

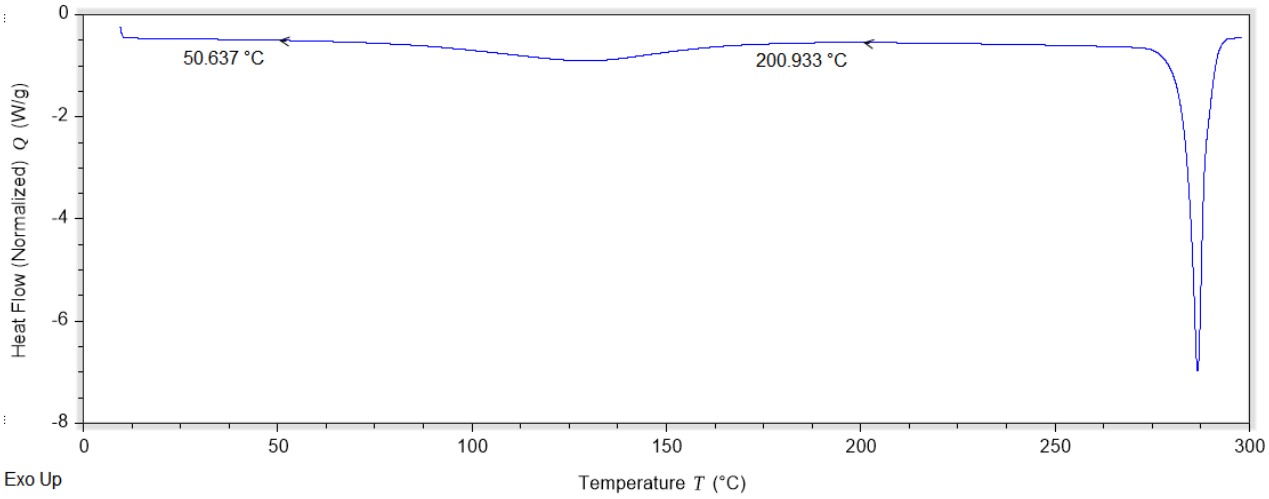

Figure 4.4.4 Thermogram of a DSC experiment on 1-MBUCT

Two main endothermic peaks can be seen, a broad, shallow one from 50ºC to 200ºC, centered around 105°C and a sharper one at 290°C. It can be hypothesized that the broad, shallow peak is the one that signals the loss of solvent from the material and the sharper one indicates the temperature at which the material decomposes. To fully understand what these peaks mean, however, it is necessary to couple these observations with the TGA curve pictured below.

In the TGA graphs the green curve represents the mass loss as a percentage of the total mass of the solid sample, while the blue curve represents the first derivative of the green curve and it was utilized, alongside the DSC patterns, to ascertain the most appropriate temperature ranges in which to measure mass losses in a given system. One of the TGA experiments on 1-MBUCT is depicted in Figure 4.4.5.

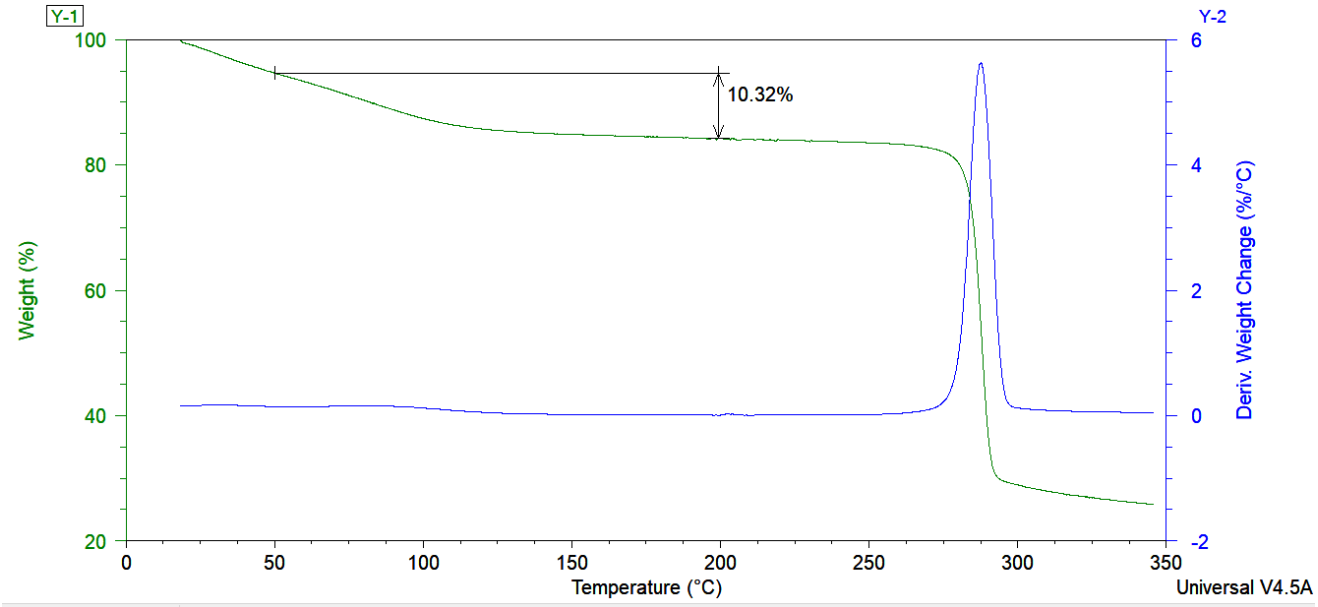

Figure 4.4.5 Graphical representation of a TGA experiment on 1-MBUCT

As predicted by the DSC, the decomposition of the material occurs in correspondence of the enormous mass loss around 290ºC, while the broad, shallow DSC peak corresponds to a 10.32% mass loss between 50ºC and 200ºC. It is safe to assume that this is a loss of solvent from the material, but it is still not enough to understand how many molecules of solvent were in the channels and whether those were ethanol or water molecules.

For the record, it should be specified that the system tended to quickly lose mass, and there were some instances in which issues in handling the sample caused the mass loss to fluctuate, remaining well below the 10% threshold. One example of such an experiment is outlined in Figure 4.4.6.

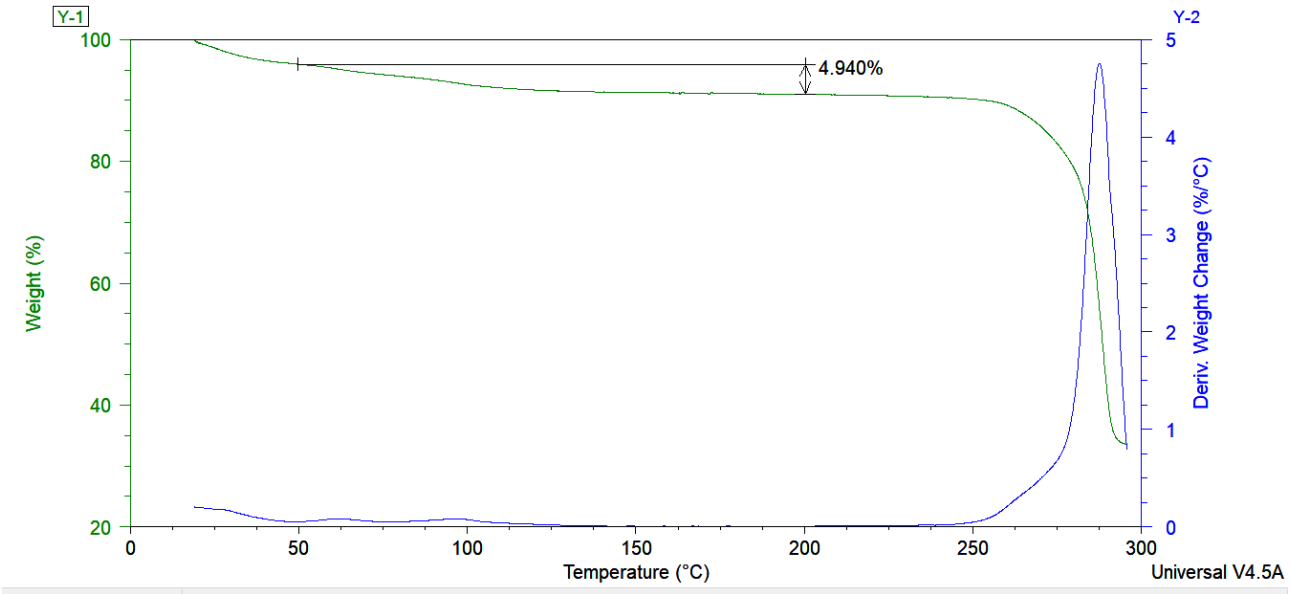

Figure 4.4.6 Graphical representation of a TGA experiment on 1-MBUCT with underestimated mass loss

In Section 3 it was shown that by obtaining the crystalline structure of 1-MBUCT it was possible to estimate the number of electrons present within its channels, and that information is extremely useful when interpreting thermal data. It was discovered that for each asymmetric unit present in the structure of the MOF, its channels contained 24 electrons which, allowing for small errors in the estimate, could mean that either 2.5 molecules of water (25 e^-) or 1 molecule of ethanol (26 e^-) resided alongside each ASU of the MOF structure. This means that it is possible to predict the expected mass loss if all the solvent were to be expelled in each of these two scenarios; this prediction is outlined in Table 4.4.1.

Table 4.4.1 Outline of the correspondence between the predicted and experimental mass losses in 1-MBUCT TGA

Hypothesis	Solvent Mass (g/mol)	ASU Mass (g/mol)	Predicted Electrons (#/ASU)	Exp. Electrons (#/ASU)	Predicted mass loss (%)	Exp. mass loss (%)
Dry	N/A	396	0	24	0	10.32
Ethanol (1 molecule)	46	442	26	24	10.41	10.32
Water (2.5 molecules)	45	441	25	24	10.20	10.32

From these data it is immediately clear that it is impossible to tell whether ethanol or water is the solvent leaving the material, but they confirm that the entirety of the solvent leaves the channels during the TGA experiments. The water molecules uncovered in the unit cell during the solution of the crystal structure seem to indicate that water is the solvent responsible for the mass loss, but the degree of disorder and uncertainty associated with this particular dataset means that further experimentation is required for a conclusive observation.

These data are nonetheless useful as points of comparison between 1-MBUCT samples before and after the solvent exchange experiments, to conclude the process of determining whether the experiments have been successful.

4.5. Gel Analysis

The first attempt to synthesize 1-MBUCT using copper chloride dihydrate could be considered an interesting failure, since shortly after being removed from the autoclave and being put into a glass vial the mother liquor of the system would form a light-blue gel, making it virtually impossible to recover the desired product, the dark blue crystals of MOF at the bottom of the vial. It was, however,

possible to remove the mother liquor from the vial before gelation occurs to isolate the crystalline product and obtain a gel (Figure 4.5.1).

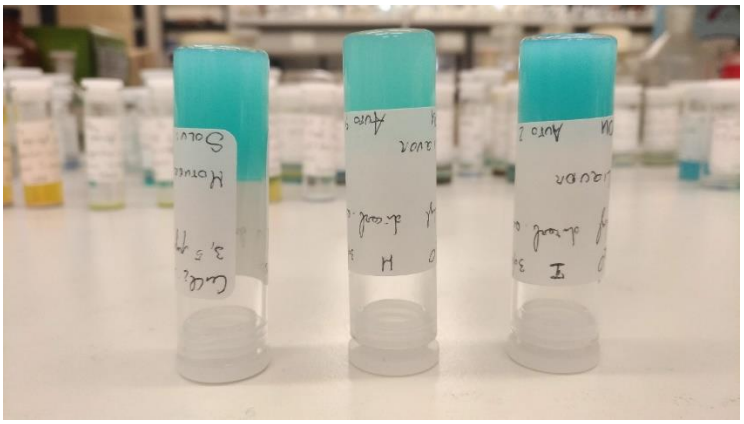

Figure 4.5.1 Picture of three samples of wet gel, from the mother liquor of a reaction involving copper chloride dihydrate

As detailed in Section 4.1, the system exhibits this behavior when heated to 105ºC for 72h and then cooled by 10ºC/hour for 8 hours, and is extremely sensitive to sudden drops in temperature. These conditions influence the system not only by modifying the quantity and quality of product synthesized, but also by changing the color, viscosity and uniformity of the gel that is a byproduct of that synthesis.

Given that no other system among the ones used for these experiments produced a gel, and that the variation that triggered gelation seemed to be the introduction of copper chloride as a starting salt, the experiment was repeated several times to ensure that the result was not the consequence of impurities that had contaminated the system. It was during all these replications that the sensitivity to rapid changes in temperature detailed in Section 4.1 was registered. Interestingly, variations in those parameters also seemed to simultaneously affect the viscosity of the gel and the uniformity of its blue color.

It should be noted that gels containing 3,5-PDA and a number of metal ions have already been obtained with various methodologies and reported by UCT researchers.[43] Furthermore, prior work by Piepenbrock et al.[44] showed that generally Cu(II)-based metallogels tend to have more stable and easily obtainable structures when starting from halogens as counterions in the Cu(II) salt used as a reagent. Those tendencies are maintained in the results described in this work.

Previous research also shows that, given a specific linker and metal salt as reagents, the formation and quality of a gel is heavily influenced by the solvent the reaction is performed in,[45] which is likely part of the reason why in this instance only the system involving ethanol resulted in gel formation.

The color of the gel makes it easy to hypothesize that it must contain copper in some part of its structure, either in solution within the ethanol contained in the pockets created by the gel structure or,

more likely, as a part of the molecular structure of the gel. This is because none of the reagents put into the system should ordinarily produce a covalent gel under the aforementioned experimental conditions, so the gel that was produced is very likely to be based around copper-coordinated synthetic units or other supramolecular interactions[46].

To verify these hypotheses a number of tests were performed on the gel, both in its initial state and after drying it out, a process that reduced its volume by a considerable amount. The most informative of these tests was the one performed on a scanning electron microscope (SEM) with which it was possible to see the microscopic structure of the dry gel, as well as notice the presence of microscopic crystals in certain regions of the material. An important detail to know in order to be able to interpret the information on SEM pictures is that the dry gel could be broadly separated into three areas, a white, soft region put into two vials marked as vial 1 and vial 2, a light blue, relatively hard region that was cut away and put into vials marked vial 3 and vial 4, and a dark blue, extremely hard region that was difficult to cut with metal instruments and which ended up being shattered in jagged fragments, rather than cleanly sliced. The fragments of this last portion of the gel were put into vials marked as vial 5 and vial 6, and this classification was utilized to index the following SEM images to aid in their analysis, as well as an analysis on the percentage of each element within different regions of the material.

This characterization is also useful while examining the IR spectra of both dry and wet gel (from Figure 4.5.3 to Figure 4.5.6). While the latter might not be particularly interesting, given that it replicates the FTIR spectrum of ethanol (Figure 4.5.2) almost exactly, the former can be a useful source of data while trying to ascertain the internal structure of the gel.

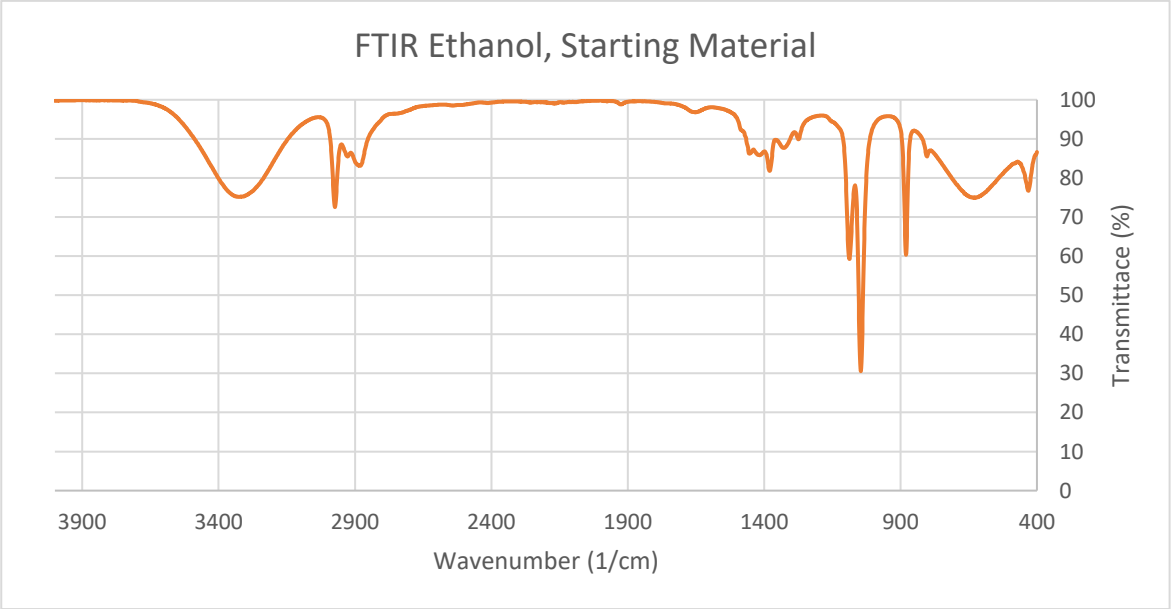

Figure 4.5.2 FTIR spectrum of ethanol, not normalized

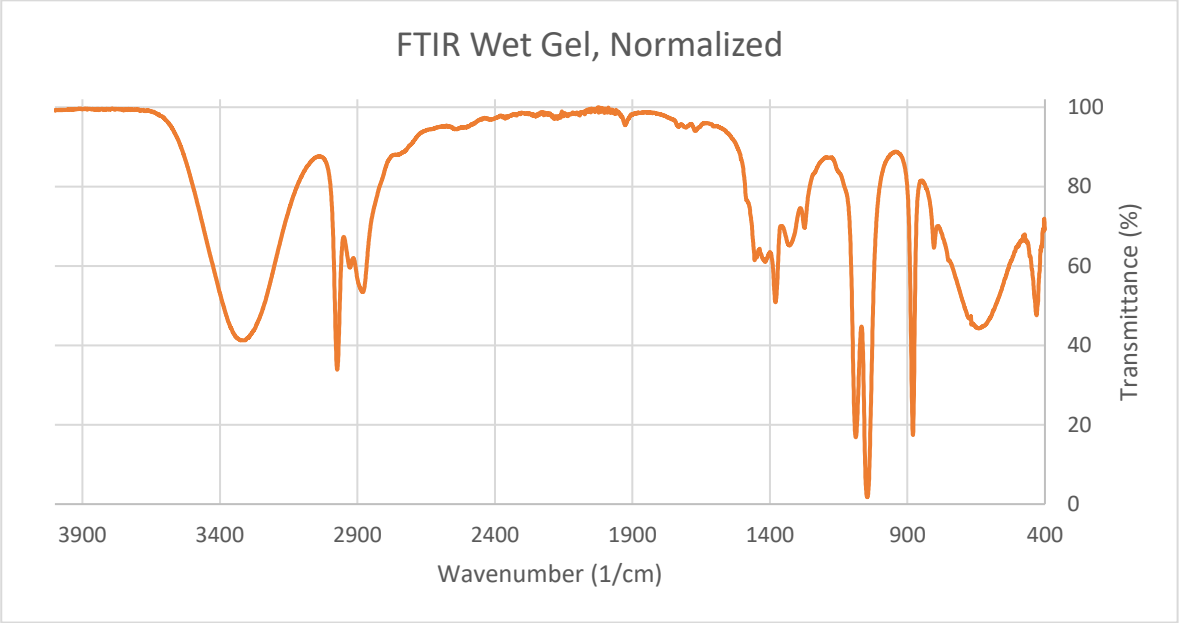

Figure 4.5.3 FTIR spectrum of the wet gel

As previously stated, the two spectra are almost identical, the interesting differences come into play when considering the spectra of different areas of the dried gel, taken from the same sample as the wet gel.

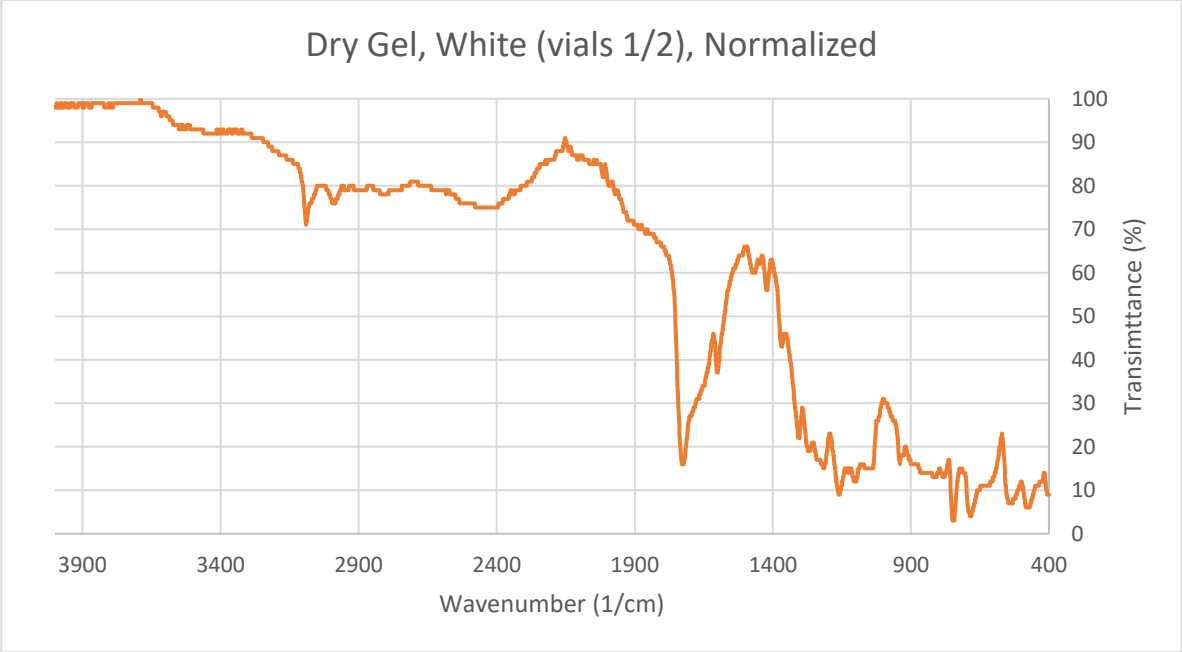

Figure 4.5.4 FTIR spectrum of the dry gel, vials 1 and 2, white region

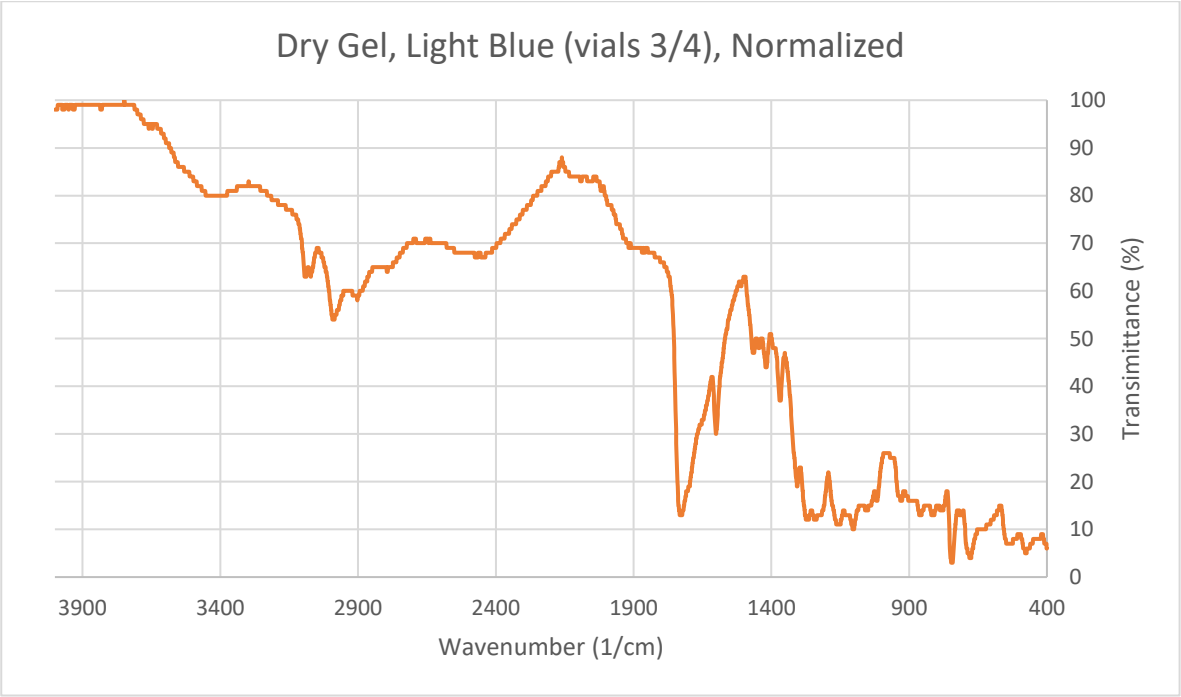

Figure 4.5.5 FTIR spectrum of the dry gel, vials 3 and 4, light blue region.

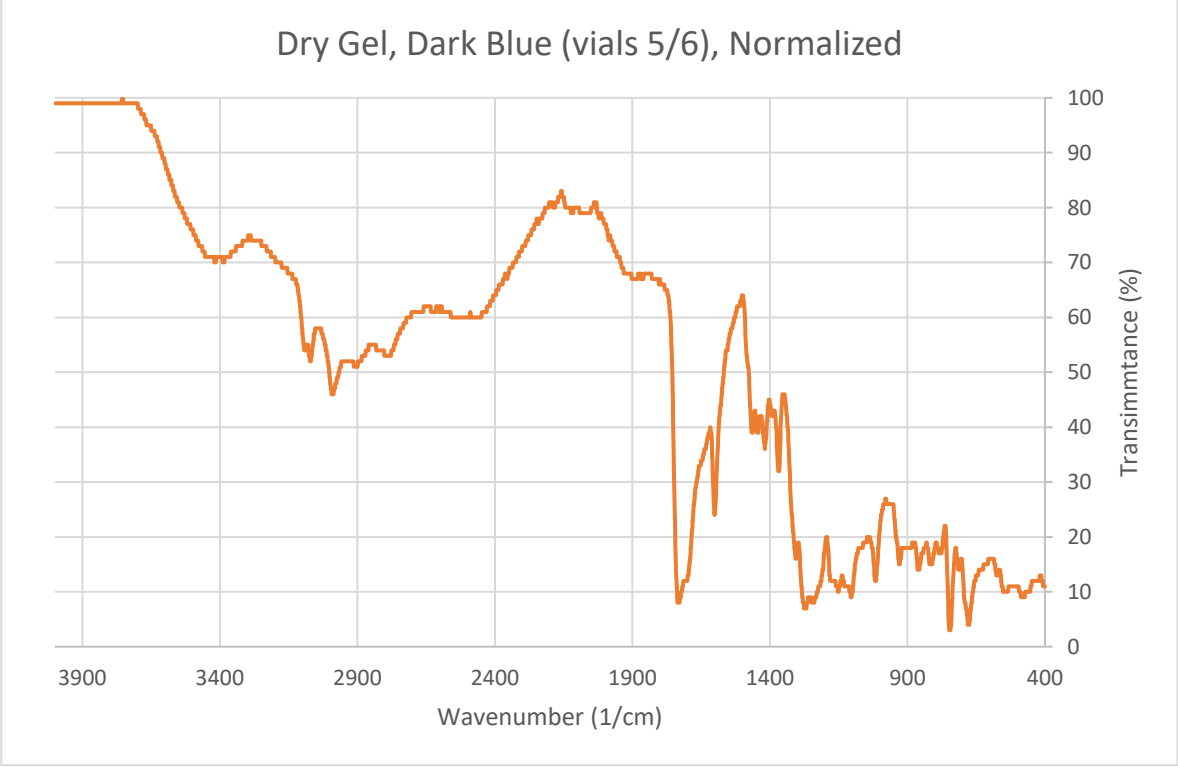

Figure 4.5.6 FTIR spectrum of the dry gel, vials 5 and 6 dark blue region.

The spectra exhibit almost identical signals until around 2200 cm^{-1}, where the dark colored regions of the gel exhibit stronger signals. Unfortunately, the complex nature of the material and the difficulty in interpreting IR spectra of materials makes it very challenging to draw any meaningful conclusions beyond the following: the difference in color between different parts of the gel is either due to a difference in the composition within the material in those specific regions, or due to the presence of

multiple compounds within the structure of the gel that are distributed in differing quantities throughout its structure.

The second hypothesis is corroborated both by the SEM images and the powder patterns of different regions of the gel. Normally, amorphous gels such as this one should not exhibit any sharp peaks when analyzed with an X-ray powder diffraction experiment, which means that, if those peaks can be found, it is certain that a microcrystalline phase is present within the structure of the gel. When broad peaks are present, they could also be caused by the presence of the short-range order that characterizes the gel structure.

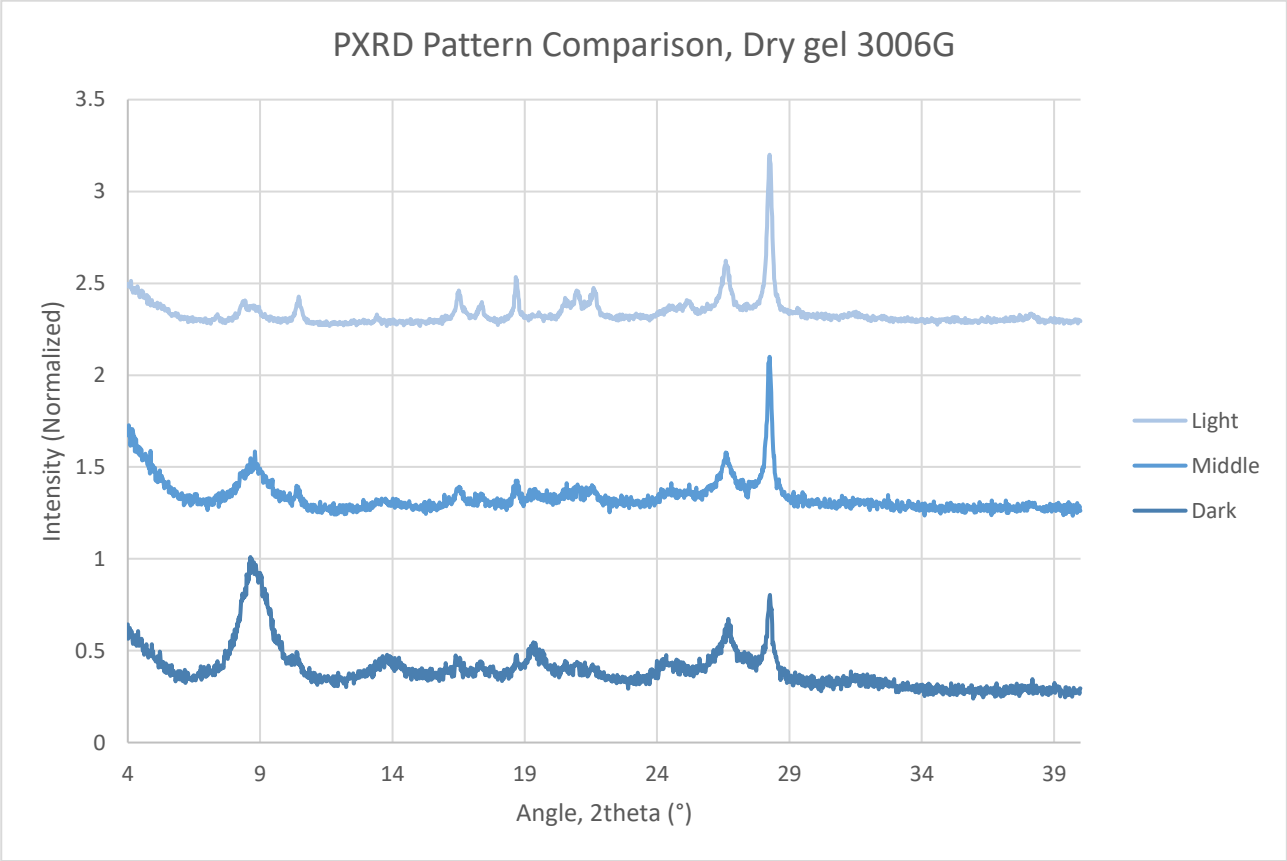

Figure 4.5.7 PXRD patterns of dry gel, sample 3006G, from top to bottom white region (light), light blue region (middle), dark blue region (dark)

Given the shape of the PXRD patterns there appear to be two crystalline phases, present in small quantities throughout the gel, but their distribution is most likely not uniform. SEM pictures partly support this hypothesis, as micron-sized crystals can be observed on the gel surface throughout the material. It should be noted that said crystals are not present on all gel surfaces, but only in some sections of the system. The analysis of the SEM data starts with the dark blue region, to which Figure 4.5.8 and Figure 4.5.9 belong. The images displayed in this section are the most representative of the appearance of the system, but the conclusions reached here also draw upon pictures only displayed in the Appendix.

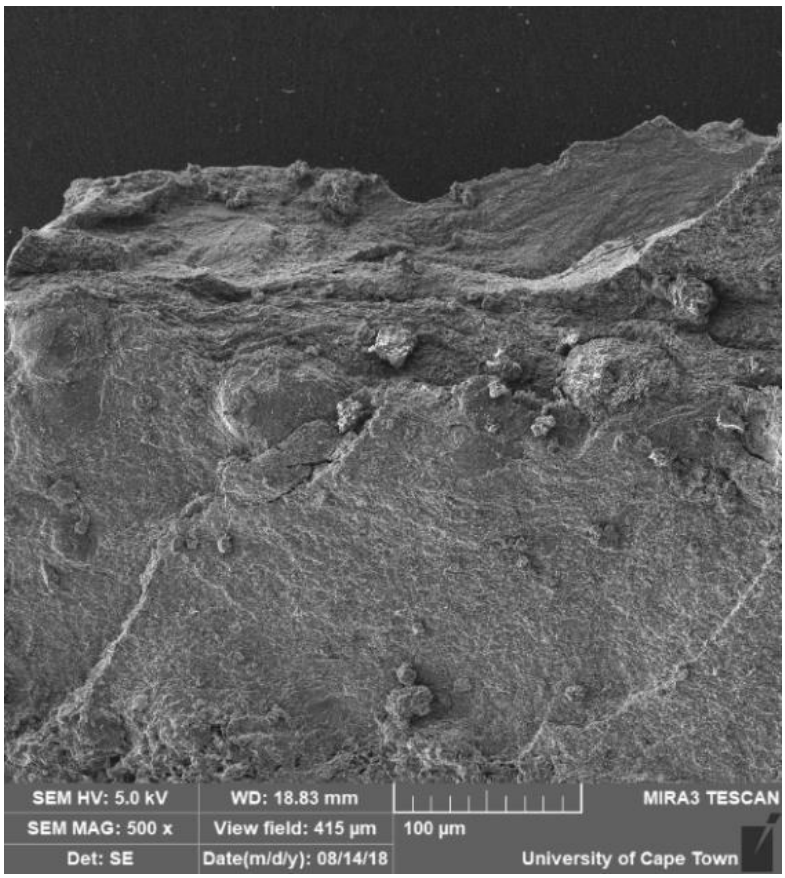

Figure 4.5.8 SEM image 6.1, representing a fragment of the dark blue region of the dried gel, vial 6

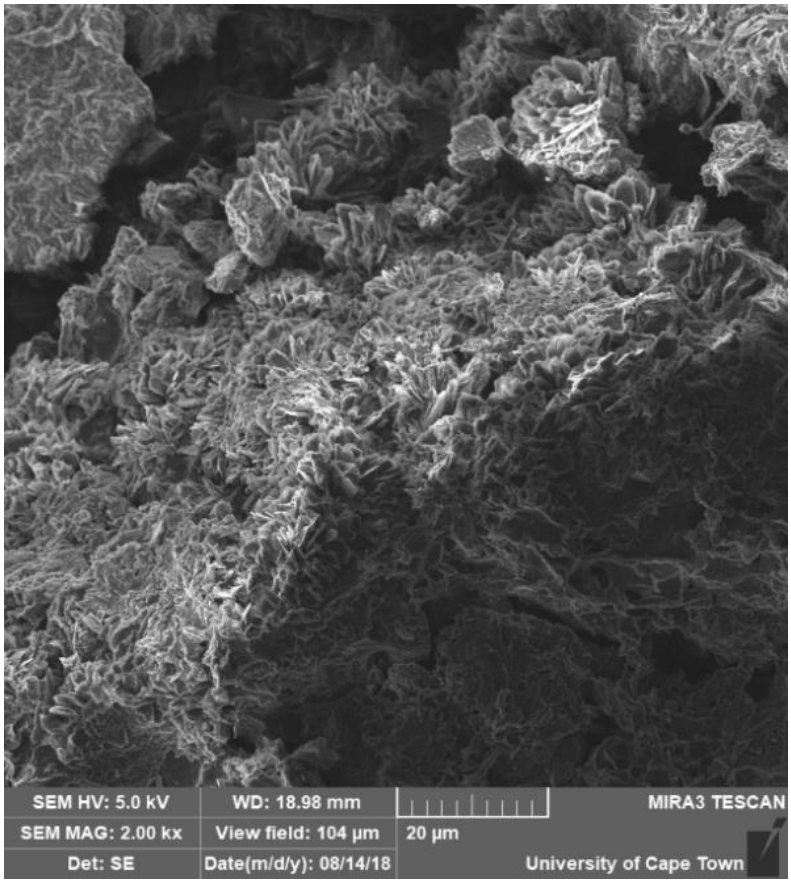

Figure 4.5.9 SEM image 6.7, representing a fragment of the dark blue region of the dried gel, vial 6

The images above, taken from vial 6 of the sample, represent the dark blue section of the dry gel. While wider angle images with x500 magnification show a material with a relatively even surface, a closer look at x2000 magnification reveals that some of the surfaces are indeed even, while others contain what appear to be very small crystals with two distinct morphologies, one thin, plate-like, and another that is more needle-like, with a large excess of the plate-like phase with respect to the needle-like crystals.

From Figure 4.5.10 to Figure 4.5.12 the region of the gel that will be examined is the light blue region, contained in vials 3 and 4.

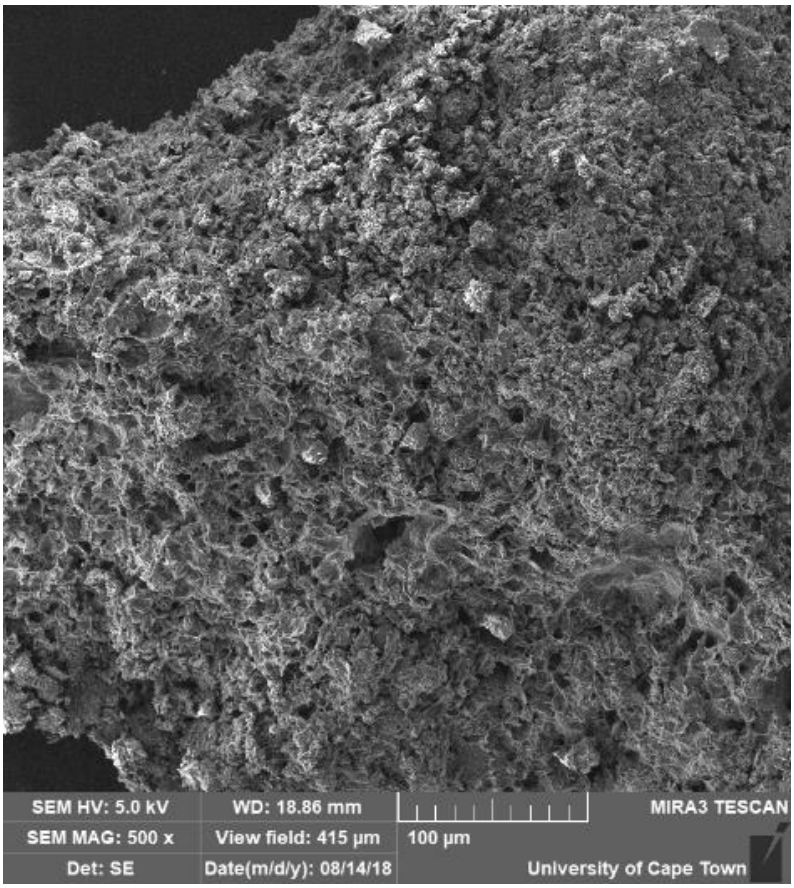

Figure 4.5.10 SEM image 4.1, representing a fragment of the light blue region of the dried gel, vial 4

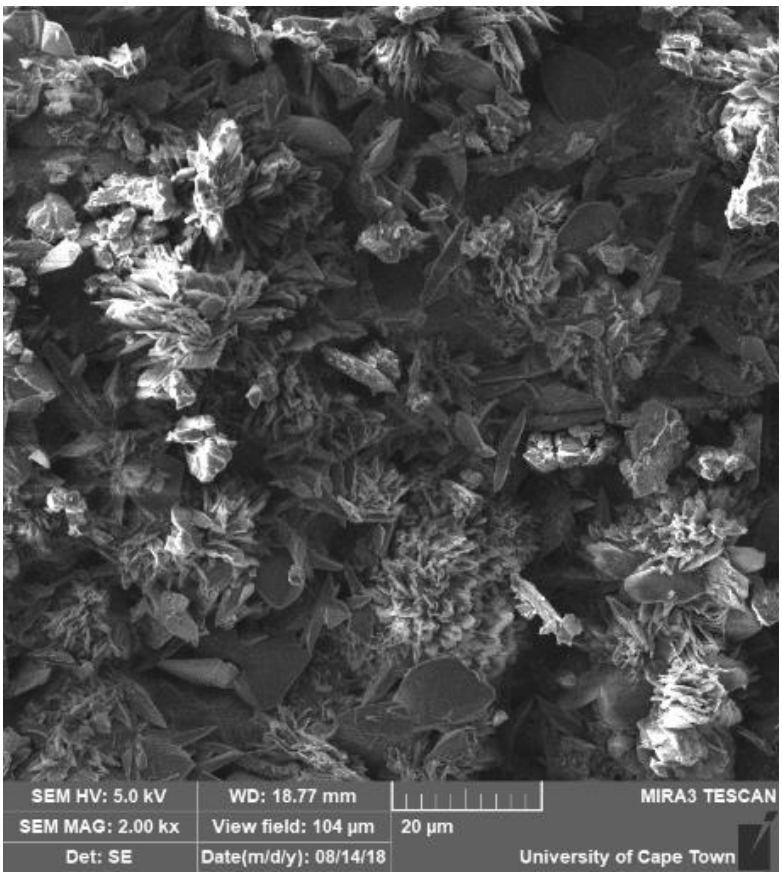

Figure 4.5.11 SEM image 4.4, representing a fragment of the light blue region of the dried gel, vial 4

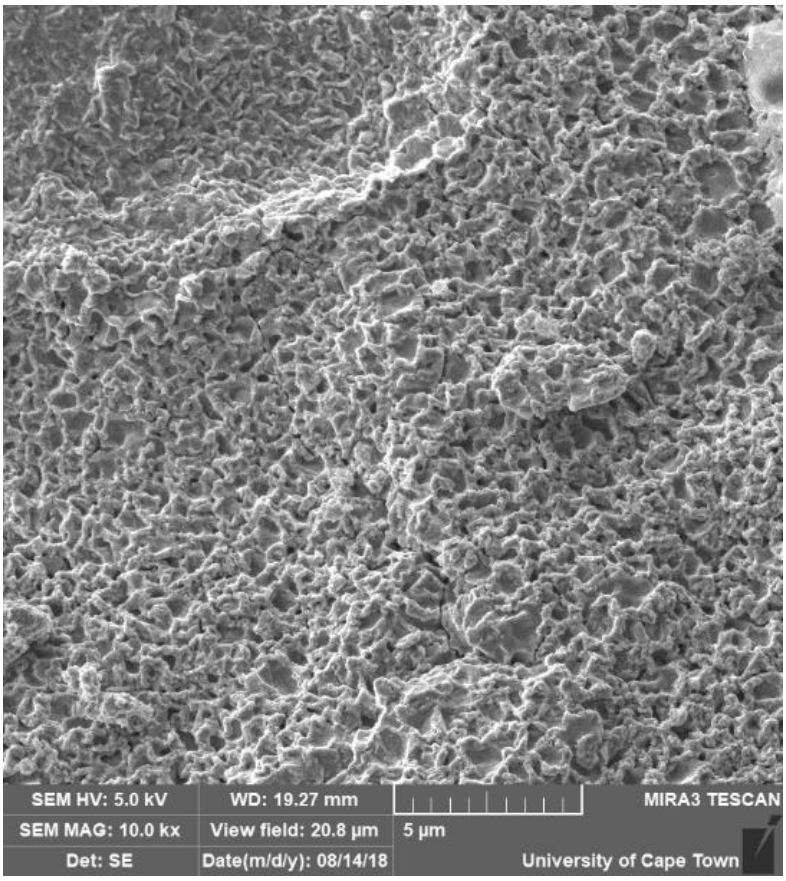

Figure 4.5.12 SEM image 3.7, representing a fragment of the light blue region of the dried gel, vial 3

The images above, taken from vial 3 and 4 of the sample, picture the transition zone of the gel, in which the surface of the material is notably rougher and more varied than what I observed in the dark blue area. Some surfaces still show a presence of the crystalline phases detailed in the previous paragraph, and there appears to be more of an abundance of the needle-like crystals. The last image shown is the only one registered at 10.000x magnification, and it shows that what looks like a flat and even surface when crystals are not present is in fact anything but. Most likely, the small sphere-like indentations on the gel surface are the remains of the pockets of liquid that used to reside within the gel before the solvent evaporated.

Lastly, this Section will examine Figure 4.5.13 and 4.5.14, which belong to the white region of the dry gel.

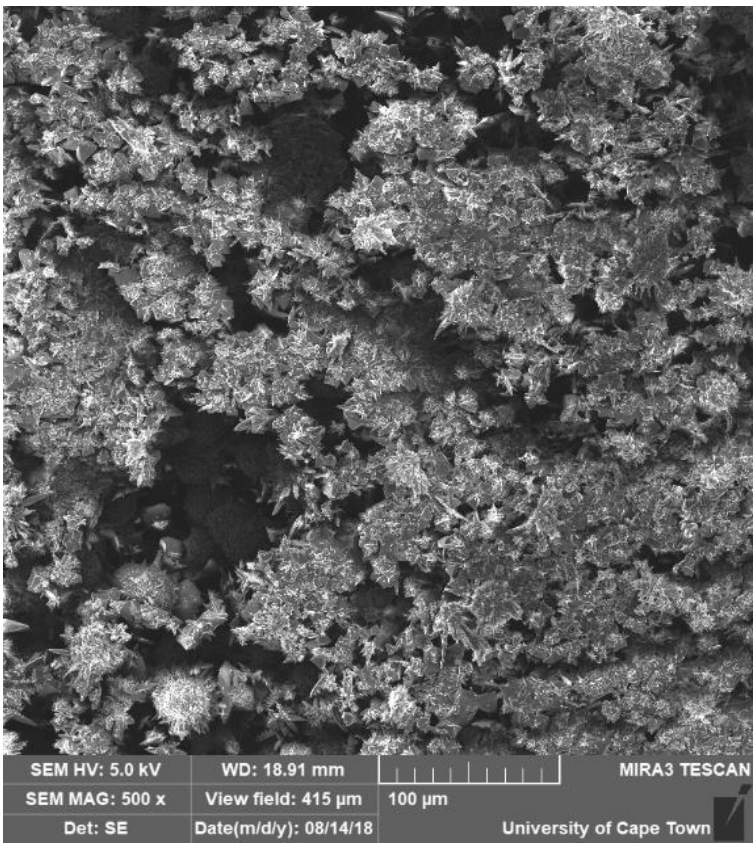

Figure 4.5.13 SEM image 1.1, representing a fragment of the white region of the dried gel, vial 1

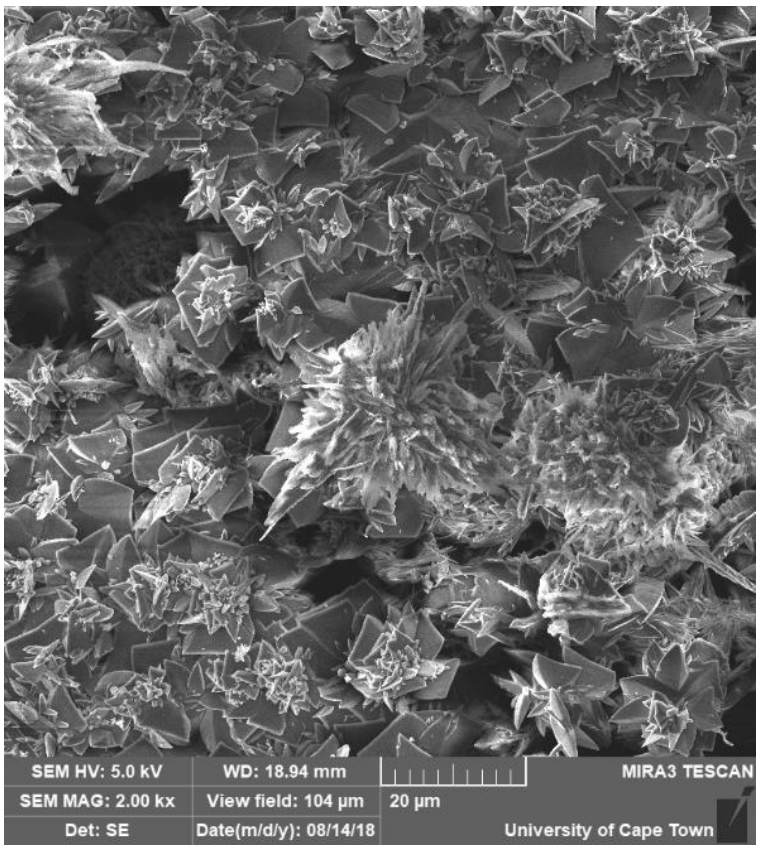

Figure 4.5.14 SEM image 1.2, representing a fragment of the white region of the dried gel, vial 1

This last series of images was taken from vials 1 and 2 of the sample, and represents the white part of the gel. It is immediately apparent from the 500x images that the surface of the gel in this area is much rougher and more irregular than the surface captured in the other samples, and while there is still a significant presence of both crystalline phases the needle-like phase is much more widespread in this region of the material.

All the data outlined so far give very little information on the exact structure and composition of the gel and on the nature of the crystals on the gel surface, which is why a SEM analysis on the composition of the system was also performed. The analysis is performed on portions of pictures taken with the SEM, therefore the results vary depending on which specific portion of the gel is included in a given picture. On average, the two most interesting elements are copper and nitrogen, because within this system nitrogen is only found in the structure of 3,5-PDA, which means that the ratio of nitrogen to copper can be a good estimate of the ratio between metal ions and ligand molecules within the system. The mass percentage of nitrogen stays relatively constant regardless of the gel region that is taken into consideration, while the percentage of copper varies quite significantly. Generally, when the mass of copper increases, there is a corresponding increase in the mass of chloride, a small decrease in the mass of nitrogen and significant decrease in both the mass of oxygen and the mass of carbon. The molar ratio between copper and nitrogen atoms oscillates between 1:5

and 1:30, which denotes an excess of ligand with respect to metal ions, which means that most likely the gel is formed by hydrogen bonds between carboxylate groups of ligands, occasionally interspersed by carboxylate or pyridyl moieties coordinated to copper ions.

These pieces of information, however, do not answer some fundamental questions about this system, regardless of how deeply they are examined. It is still impossible to deduce any details on how or if chloride ions are involved in the structure of the gel, which also means that no conclusions on how or why the presence of chloride ions catalyzes gel formation can be drawn. The data outlined in Table 4.5.1 refer to Figure 4.5.15.

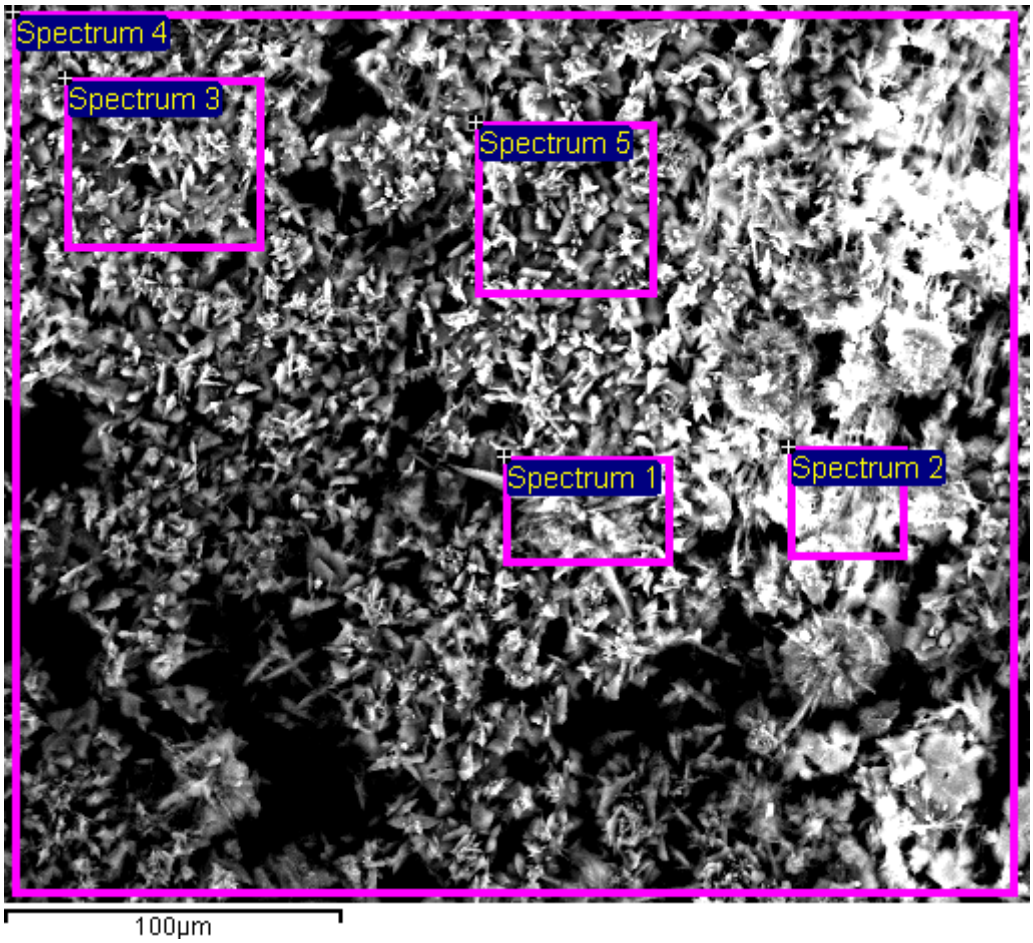

Figure 4.5.15 SEM image on Sample 1, representing a fragment of the white region of the dried gel, vial 1

Table 4.5.1 Example of a table of data harvested from one SEM image, displayed above. All results were given in Weight/Weight %

Spectrum	In stats.	C	N	O	Cl	Cu	Total
Spectrum 1	Yes	54.28	8.54	33.86	1.71	1.61	100
Spectrum 2	Yes	53.71	9.45	32.78	2.27	1.79	100
Spectrum 3	Yes	51.26	8.49	37.7	1.47	1.09	100
Spectrum 4	Yes	55.16	7.61	32.79	2.35	2.09	100
Spectrum 5	Yes	51.67	8.88	37.27	1.21	0.98	100
Mean		53.22	8.59	34.88	1.8	1.51	100
Std. deviation		1.69	0.67	2.42	0.5	0.47	
Max.		55.16	9.45	37.7	2.35	2.09	
Min.		51.26	7.61	32.78	1.21	0.98	

Given the PXRD patterns of the various regions of the dry gel displayed in Figure 4.5.7, it should be possible to glean information on the nature of the crystals present within the gel by comparing the result of those PXRD patterns with the ones obtained from my crystalline starting materials and the main product of the reaction. Those substances are the most likely candidates to be the crystals that could be seen in the SEM images, and it is therefore imperative to verify whether some of them have indeed been trapped into the gel structure. The results of the comparison are outlined in Figure 4.5.16.

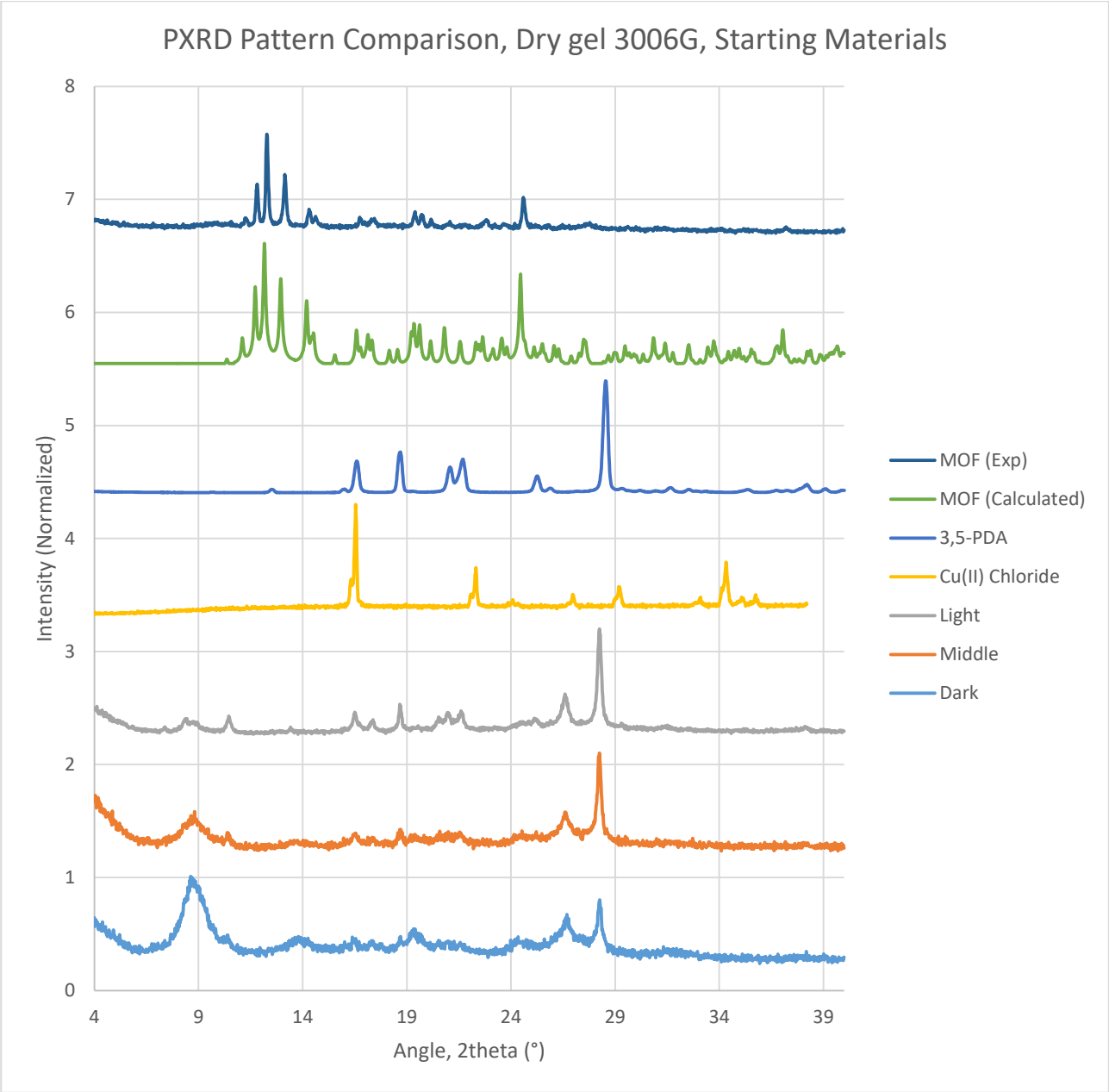

Figure 4.5.16 PXRD patterns of dry gel, from top to bottom white region (light), transition region (middle), dark blue region (dark), compared with PXRD pattern of Cu(II) sulfate pentahydrate, 3,5-PDA and the calculated and experimental spectra of 1-MBUCT.

There are a few conclusions that can be drawn from this comparison: firstly, there is no starting material or product with a significant peak around 9°, while the sharp peak around 28° could be due to a residual amount of 3,5-PDA trapped within the gel structure. Moreover, there is no significant overlap between the X-ray peaks of the product and the X-ray peaks generated by any of the gel regions.

4.6. Solvent Exchange Experiments

The next step in the analysis of this material involved testing whether it could exchange the solvent molecules trapped within its channels with other solvent molecules of varying dimensions and

chemical characteristics. For this reason, various batches of 1-MBUCT were submerged in acetonitrile, DMF, DMSO, a 1/1 mixture of DMF and DMSO and a 3/1 mixture of the same solvents. It was possible to obtain a single crystal structure from the sample submerged in DMF, but the same could not be done for any other system involved in these experiments. Thus, the analysis of any changes these systems might have undergone will mainly be relying on bulk analysis. The goal of this analysis is to build the best possible comparison between the MOF samples before and after they underwent the solvent exchange process.

Before starting to delve deeper into this topic, however, it is important to specify that, while all analysis on samples that were utilized in solvent exchange experiments occurred consistently 24h after each sample was put into the desired solvent, in all systems containing DMSO a colour change was observed in the system after 72h of exposure to the new solvent. This phenomenon was not observed in samples containing only DMF or acetonitrile. The dark blue crystals of 1-MBUCT shifted to an azure hue, which presumably signalled that other changes had occurred within the system. The colour change was not investigated further due to time constraints.

It should also be remarked that a solvent exchange experiment was performed with two other solvents, pyridine and THF, but the initial results of these experiments were such that it would have been very time consuming to research these systems further.

4.6.1. PXRD Analysis

The fastest and most practical method of testing whether a given solvent exchange sample has undergone any structural changes after spending 24h submerged in its solvent of choice is to perform a PXRD experiment. The resulting pattern is then compared to all other experimental PXRD patterns obtained from other samples, as well as the experimental and calculated patterns of the standard 1-MBUCT system (Figure 4.6.1.1).

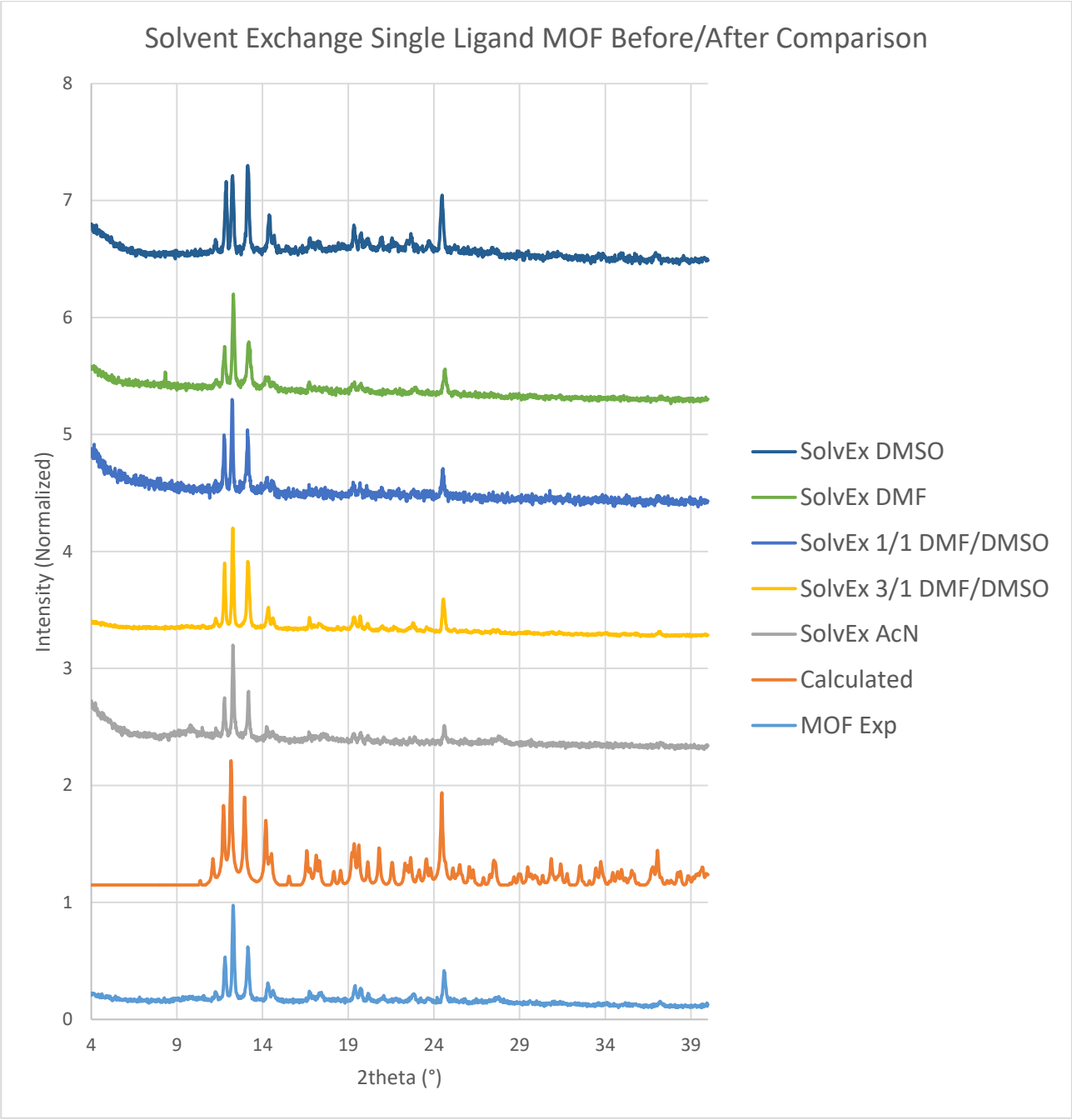

Figure 4.6.1.1 Comparison of PXRD patterns of 1-MBUCT before and after solvent exchange experiments

The PXRD patterns are consistent with each other, there are no major differences in the number and location of visible peaks. This is rather puzzling, given that it was attempted to find a single crystal suitable for a SCXRD experiment within all of these samples and only the batch of material immersed in DMF contained single crystals that diffracted well enough for the measurement to be possible. In every other instance it was possible to find multiple crystals which displayed the required characteristics under a microscope, but when these crystals were irradiated with X-rays the resulting diffraction pattern was not clear enough to provide meaningful structural information. Either way this comparison is quite clearly indicating that the structure of the MOF stays the same regardless of the solvent employed, provided that exposure to said solvent lasts only for 24h.

Given this information, it can be inferred that the available volume within the pores of each of these samples is roughly the same, which will be important when discussing the behavior of these compounds at high temperatures.

4.6.2. FTIR Analysis

Given that solvents such as acetonitrile have very distinctive peaks in IR spectra, if those peaks are displayed in the IR spectrum of 1-MBUCT only after a given solvent exchange experiment has been performed it would corroborate the hypothesis that the new solvent has indeed penetrated into the channels within the material.

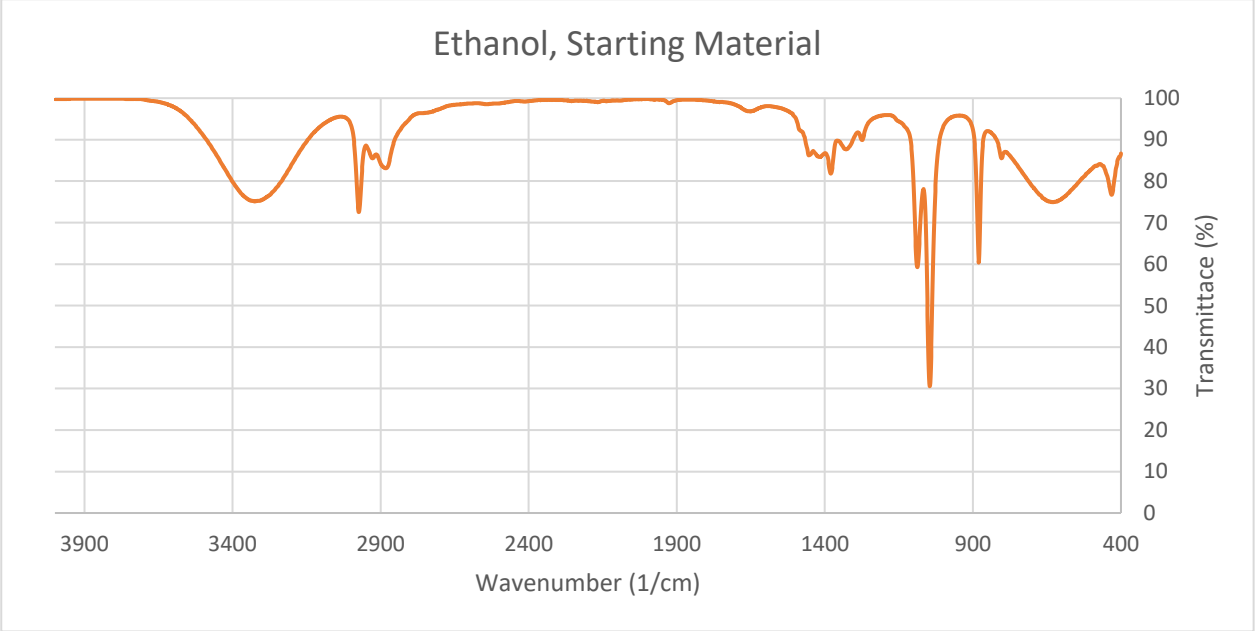

Figure 4.6.2.1 FTIR spectrum of ethanol, not normalized

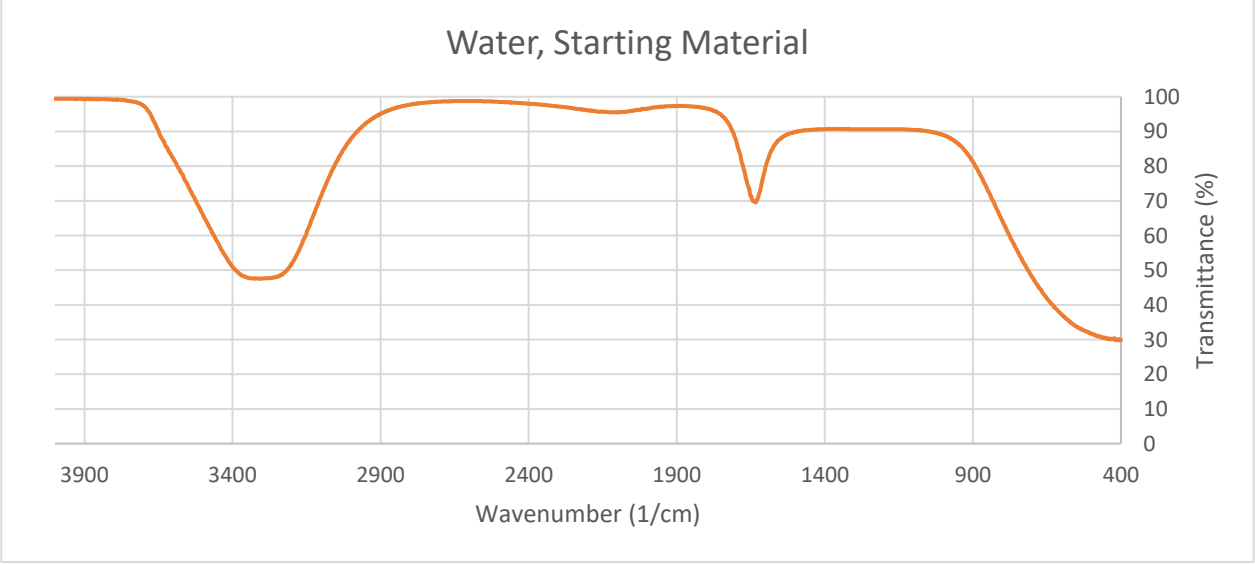

Figure 4.6.2.2 FTIR spectrum of water, not normalized

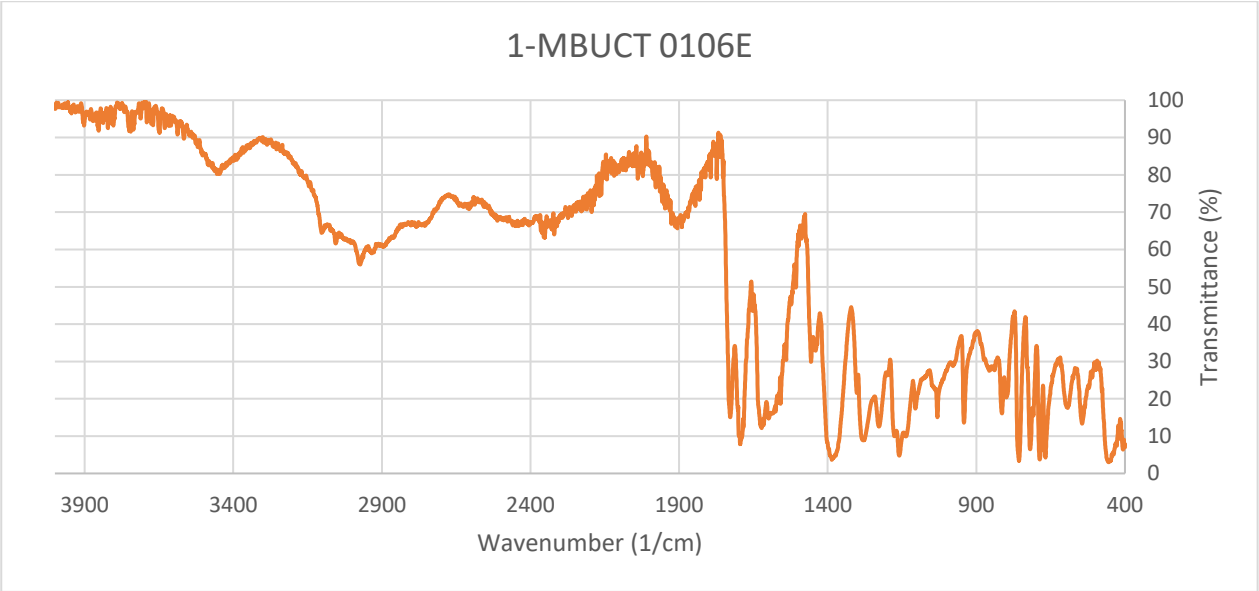

Figure 4.6.2.3 FTIR spectrum of 1-MBUCT

Before delving into the analysis it is worth noting that the typical broad O-H stretching peak that can be clearly seen in the ethanol spectrum is much less prevalent in the MOF spectrum. Moreover, given that a hydrated salt was utilized for the synthesis and that a small fraction of water was most likely present in the ethanol before the reaction, it is likely that water is also present within the channels.

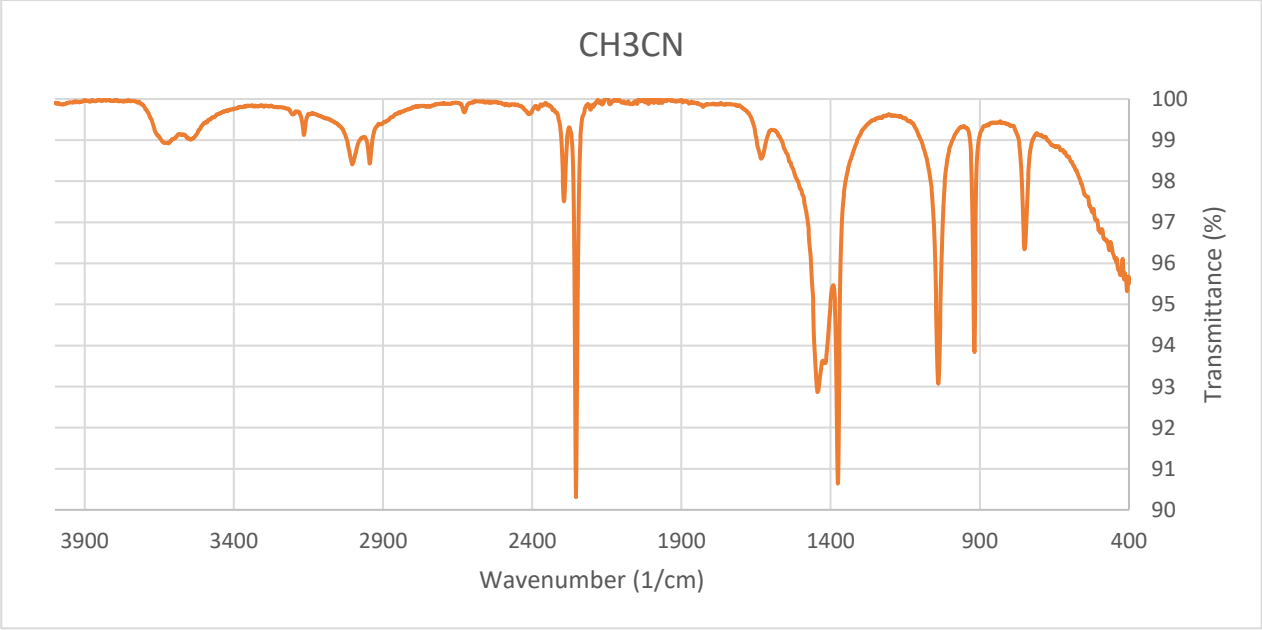

Figure 4.6.2.4 FTIR spectrum of acetonitrile

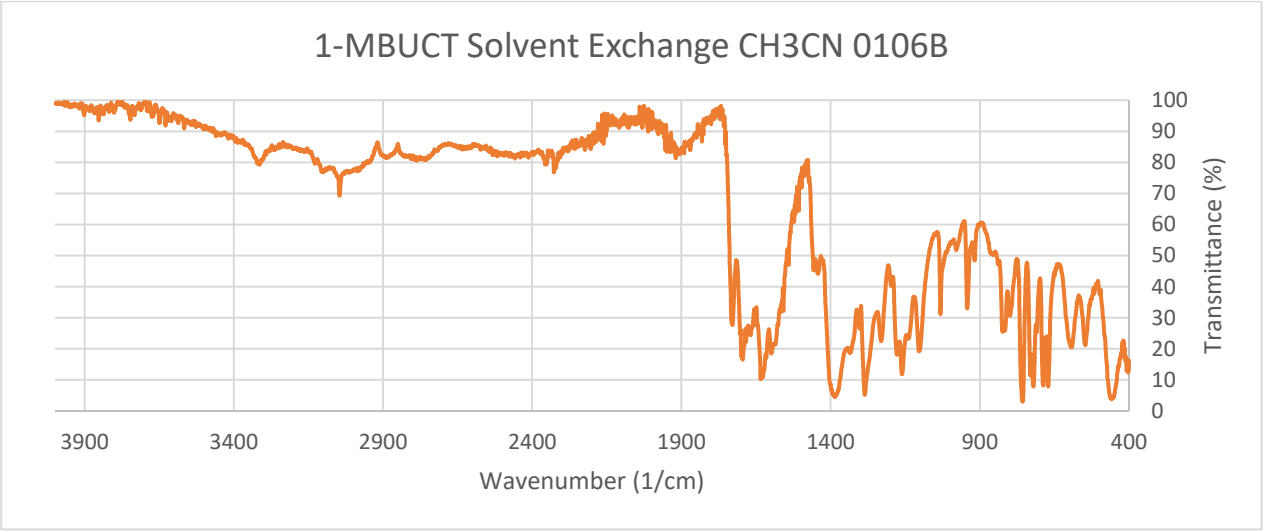

Figure 4.6.2.5 FTIR spectrum of 1-MBUCT after acetonitrile solvent exchange experiment

It is immediately apparent that the spectrum registered after immersion of the sample in acetonitrile does not display the sharp peaks around 2300 cm^{-1} that identify the stretching of the CN triple bond and are the trademark of an acetonitrile spectrum. It is, however, possible to see two small peaks in the same location, which could signify that a small quantity of acetonitrile has indeed been transferred into the channels of 1-MBUCT, but not enough to significantly alter either the crystalline structure of the material or its FTIR spectrum. It also might mean that, in this specific instance, it would have been possible to successfully complete the substitution of the solvent by either prolonging the experiment past 24h or modifying the experimental process altogether.

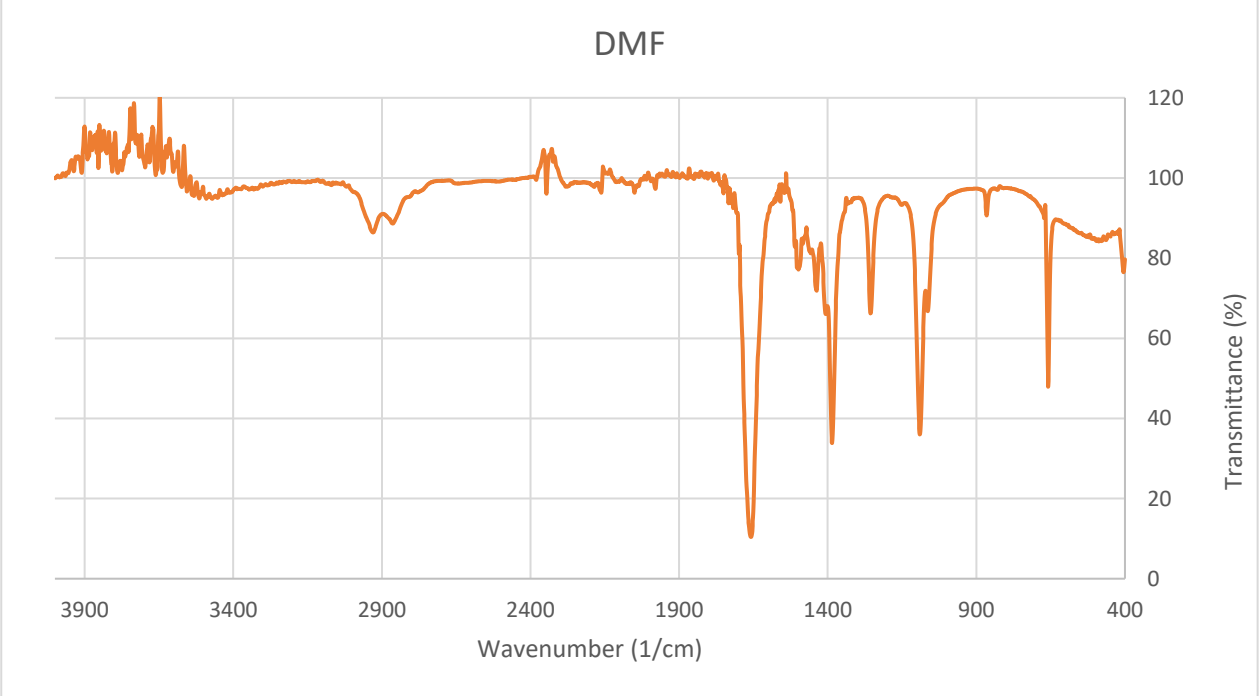

Figure 4.6.2.6 FTIR spectrum of DMF

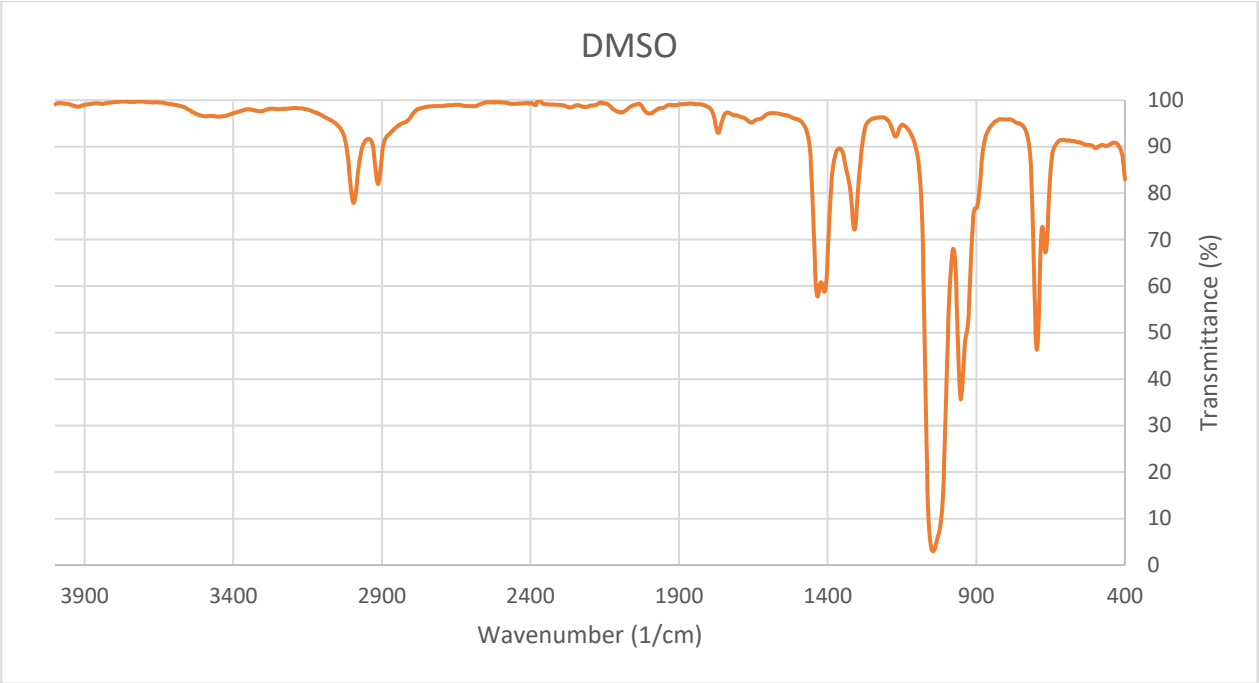

Figure 4.6.2.7 FTIR spectrum of DMSO

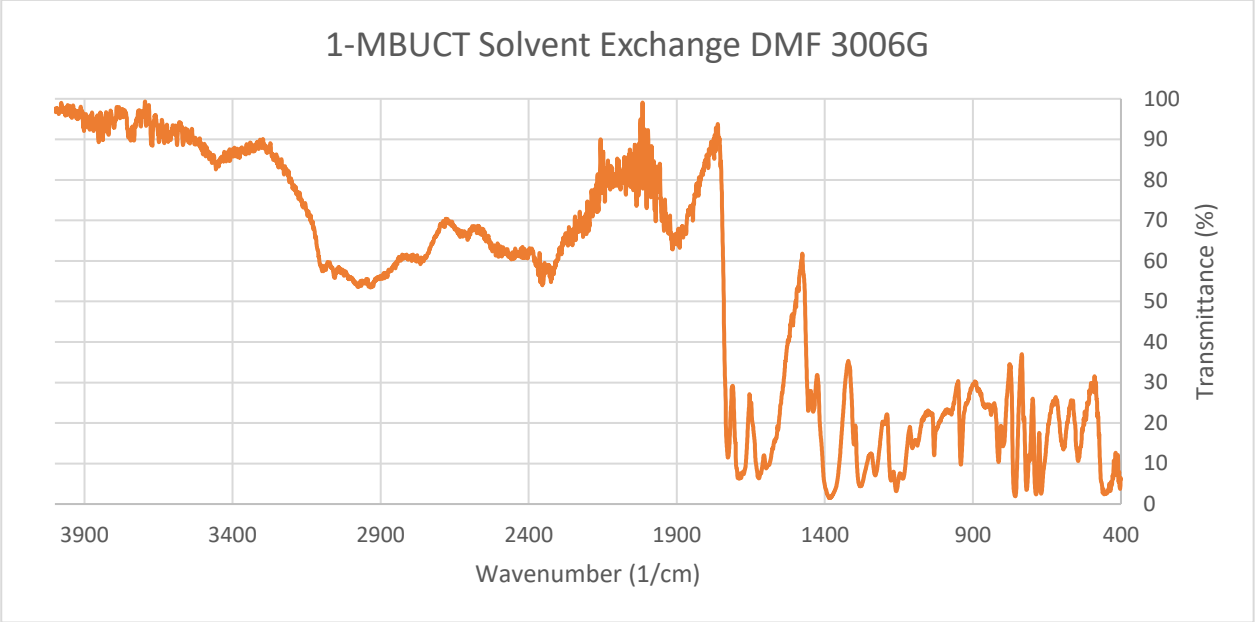

Figure 4.6.2.8 FTIR spectrum of 1-MBUCT after a solvent exchange experiment in DMF

In a system without any other carbonyl moiety the most significant aspect of the FTIR spectrum of DMF is the sharp peak at 1700 cm^{-1} originating from the stretching of the CO double bond, but unfortunately that area of the MOF spectrum is already occupied by other signals. It is therefore quite challenging to draw any meaningful conclusion by comparing the spectrum after immersion in DMF with the original.

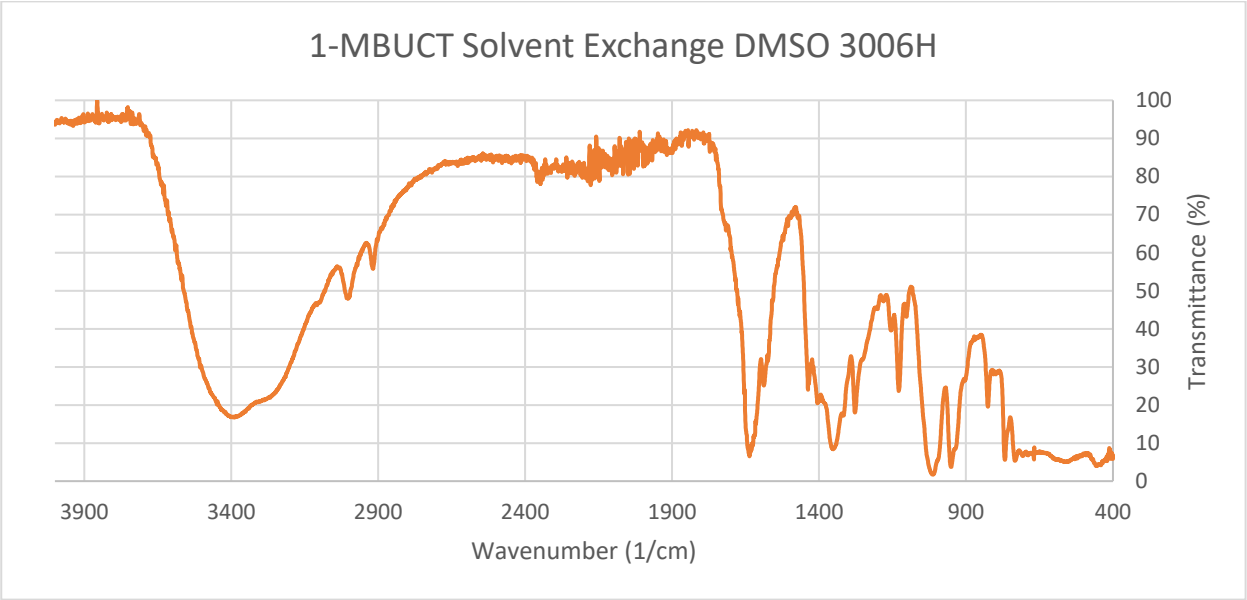

Figure 4.6.2.9 FTIR spectrum of 1-MBUCT after a solvent exchange experiment in DMSO

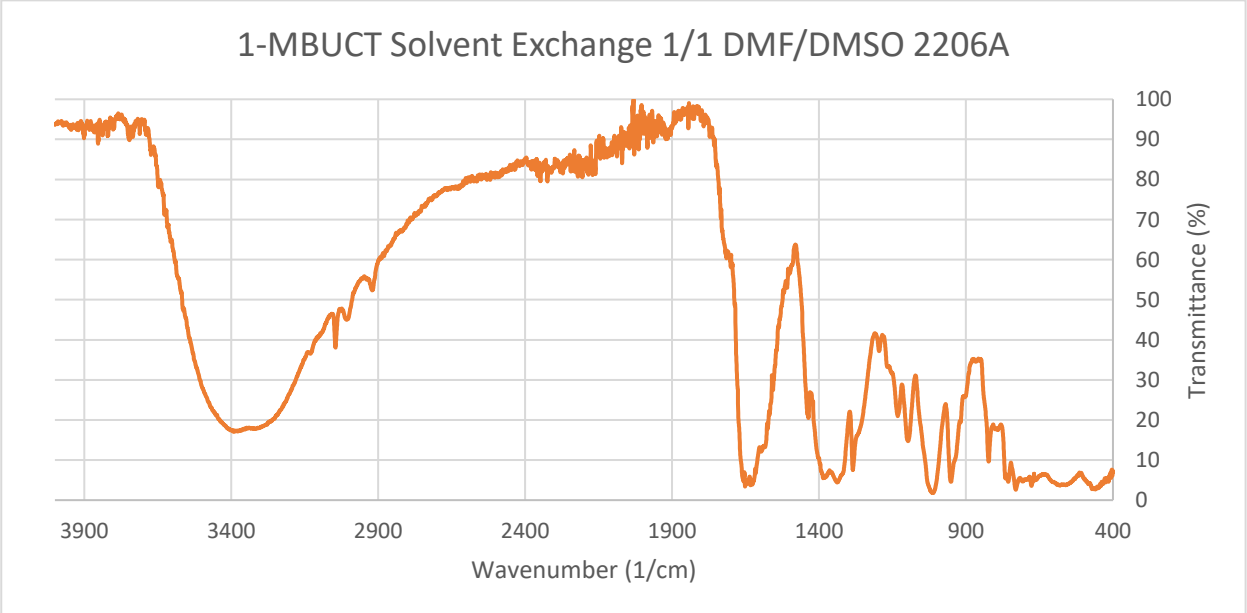

Figure 4.6.2.10 FTIR spectrum of 1-MBUCT after solvent exchange experiment in a 1/1 mixture of DMF/DMSO

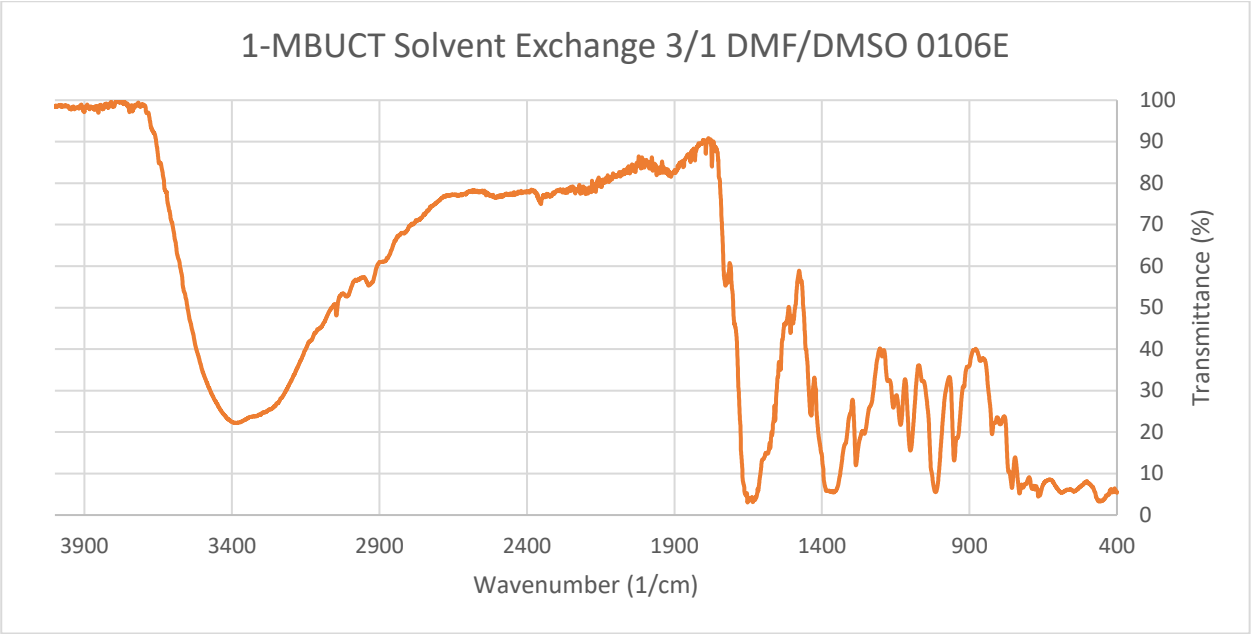

Figure 4.6.2.11 FTIR spectrum of 1-MBUCT after a solvent exchange experiment in a 3/1 mixture of DMF/DMSO

Finally, it appears that any system containing DMSO produced a similar FTIR spectrum, which always contains at least a portion of the two sharpest peaks within the pure DMSO spectrum, located around 1000 cm^{-1}. This feature suggests that DMSO was able to replace ethanol or water within the channels of 1-MBUCT.

The most interesting part of these spectra, however, is the broad peak that appears around 3400 cm^{-1}, because it is completely absent in either the spectrum of DMF or the spectrum of DMSO. Out of any starting material, the one with the spectrum most resembling these is water, which makes explaining this phenomenon rather difficult. One possible explanation might be found in the fact that the signals in the region between 2600 cm^{-1} and 1750 cm^{-1} are much less significant in the presence of DMSO than in the original 1-MBUCT IR spectrum. Given that the molecular vibrations that correspond to FTIR peaks largely coincide with vibrations around specific bonds, it is quite common to observe that, in complex systems, peaks such as the broad O-H stretch found in a liquid water spectrum change shape significantly if the related bonds are strongly affected by their chemical environment. It is the reason why the O-H peak in the water and ethanol spectra are so broad, all the bonds within the liquid vibrate at slightly different energies (and therefore frequencies) depending on how their chemical environment affects them in the form of hydrogen bonding.

The same principle holds true within the channels of a MOF, and it is possible that the variability in nature and strength of these external effects on O-H bonds within the material led to an extreme broadening of the FTIR peak associated with them. The introduction of DMSO within the system might therefore have locked some molecules of water or ethanol into very specific positions within

the material, thereby reducing the possible environments to which these molecules were exposed and aligning their behavior under IR light to the one displayed in the liquid state.

One way to obtain more information in order to prove this theory might be to expose 1-MBUCT to DMSO in the gaseous phase, so as to promote a slower, more controlled uptake of this molecule with the ultimate objective of isolating single crystals suitable for single crystal X-ray diffraction, which would hopefully show the average position of DMSO molecules within the channels of the MOF.

Lastly, it should be noted that DMSO has two peaks associated with stretching of C-H bonds at 2900 cm^{-1} and 3000 cm^{-1} and they are visible in all three FTIR spectra involving solvent mixtures in which DMSO is present. Furthermore, the peaks become less and less pronounced the more the percentage of DMSO in the system is reduced.

4.6.3. Thermal Analysis

Each solvent exchange sample will be described in the same way as a standard 1-MBUCT sample and then compared to that system.

The first solvent exchange sample that will be examined here is the one involving acetonitrile, which has remarkably similar visual signs of changes in the material to the base system. There is a slow and gradual change in the color of the crystals (Figure 4.6.3.1), which darken until around 300ºC (Figure 4.6.3.2) and then decompose at around 330ºC (Figure 4.6.3.3).

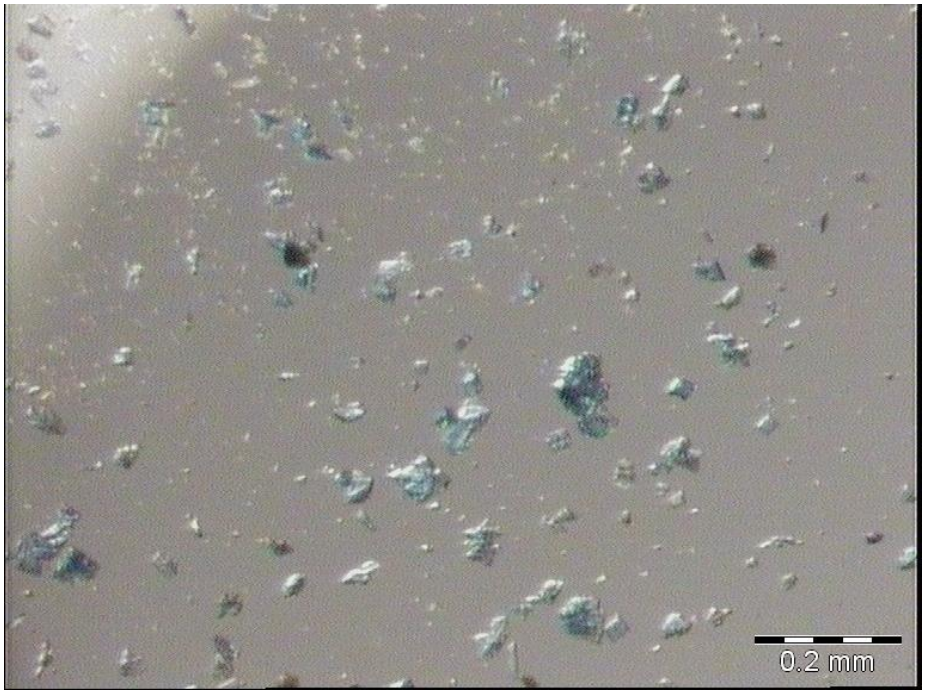

Figure 4.6.3.1 Picture of hot stage microscopy experiment on 1-MBUCT after exposure to acetonitrile, at 26.4ºC

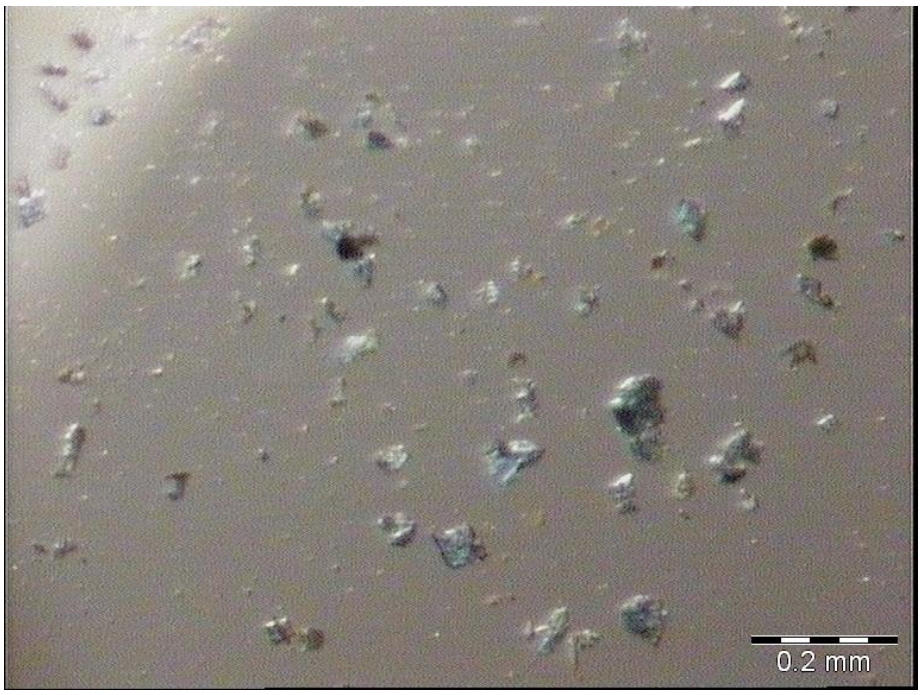

Figure 4.6.3.2 Picture of hot stage microscopy experiment on 1-MBUCT after exposure to acetonitrile, at 290.0°C

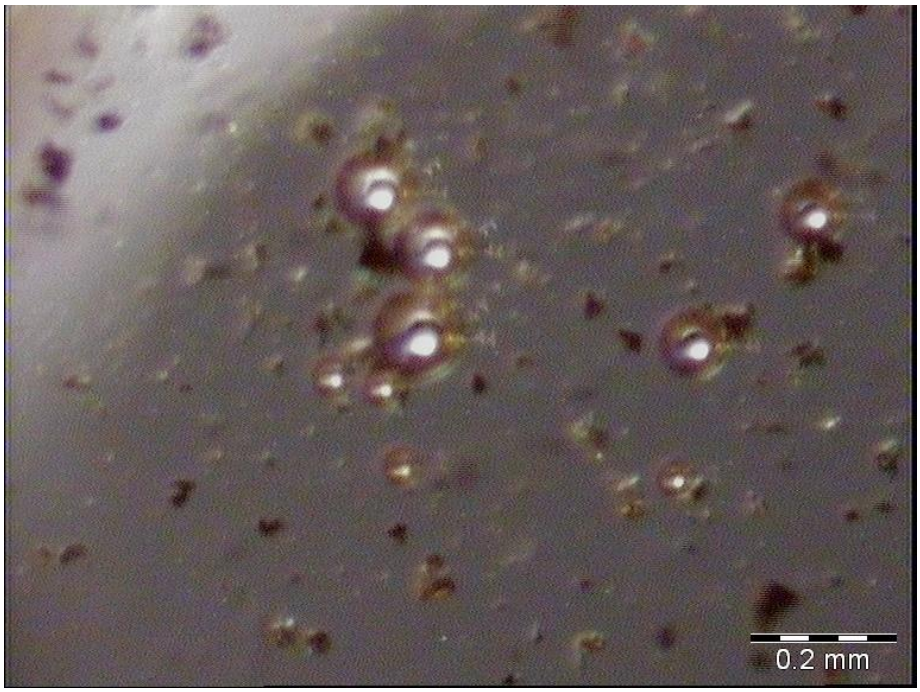

Figure 4.6.3.3 Picture of hot stage microscopy experiment on 1-MBUCT after exposure to acetonitrile, at 333.0°C

The DSC experiments were both consistent and very similar to the ones resulting from the base sample. The only difference is the relative shallowness of the first, broad endothermic peak (Figure 4.6.3.4).

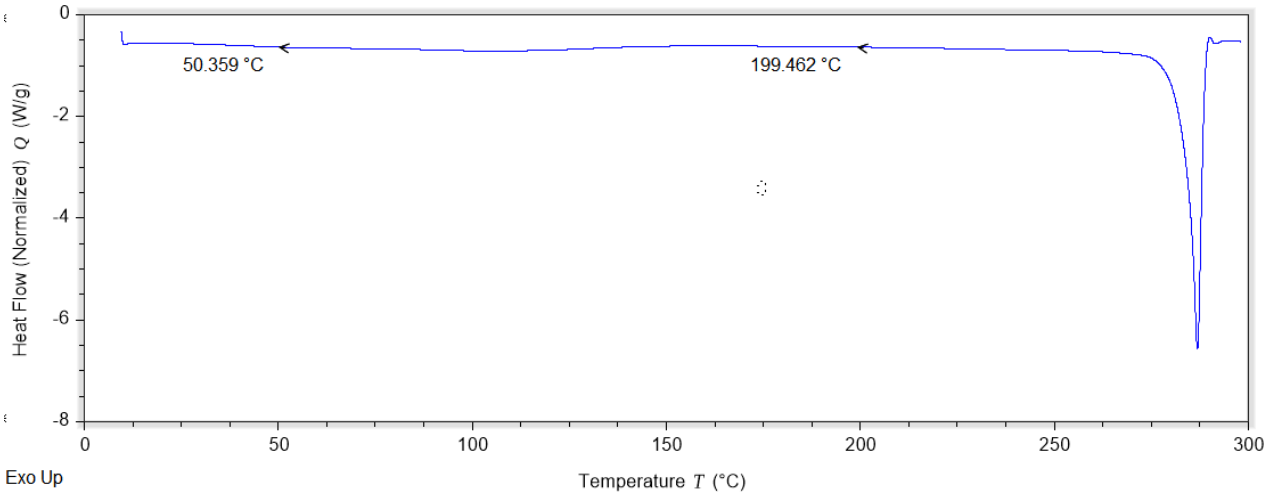

Figure 4.6.3.4 Thermogram of a DSC experiment on 1-MBUCT after exposure to acetonitrile

The TGA mass losses, instead, fluctuated a bit more than the measurements made on the base system, with an average mass loss around 4% (Figure 4.6.3.5).

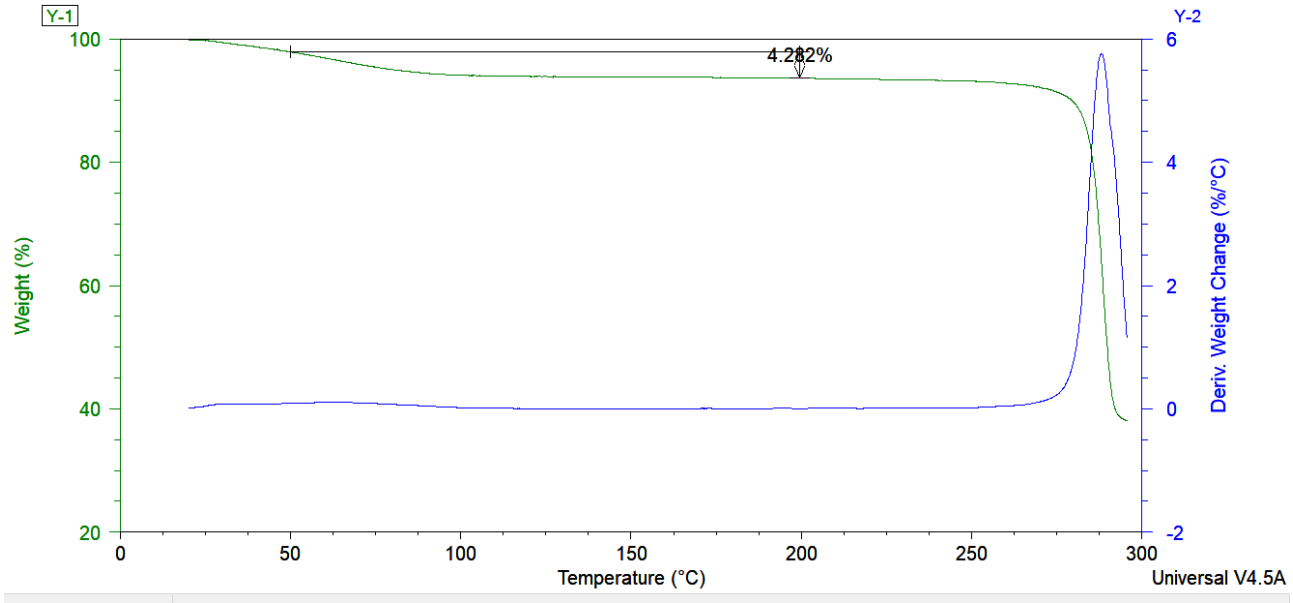

Figure 4.6.3.5 Graphical representation of a TGA experiment on 1-MBUCT after exposure to acetonitrile

It is entirely possible that this number is due to quick loss of solvent from the sample while it was being transferred into the TGA instrument. Indeed, it might be the best explanation for why the mass loss percentage in these experiments is so low. Given the similar size of the ethanol and acetonitrile molecules it is reasonable to assume that if an acetonitrile molecule were to insert itself in the channels of 1-MBUCT it would occupy a similar volume to the one occupied by ethanol in the base system, which would mean that there would likely only be one molecule of acetonitrile for each ASU. If that were the case, the expected mass loss would be around 10%, much higher than the experimental one.

The next sample detailed in this analysis will be the one exposed to liquid DMF, and its behavior during HMS experiments is in line with the expectations set by previous experiments (from Figure 4.6.3.6 to Figure 4.6.3.8).

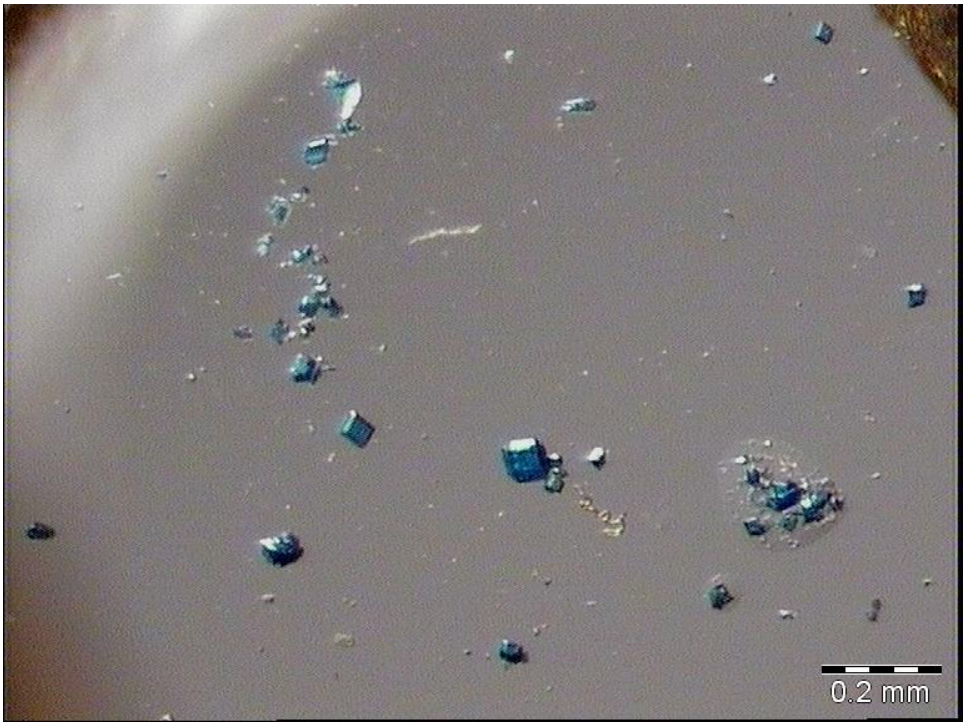

Figure 4.6.3.6 Picture of hot stage microscopy experiment on 1-MBUCT after exposure to DMF, at 27.7°C

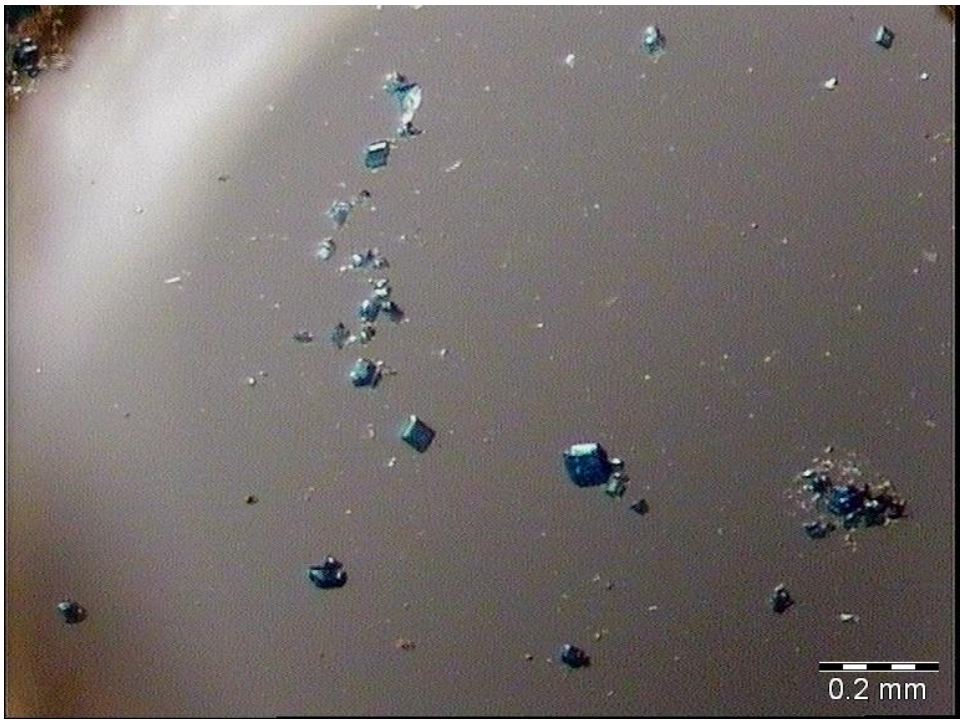

Figure 4.6.3.7 Picture of hot stage microscopy experiment on 1-MBUCT after exposure to DMF, at 300.0°C

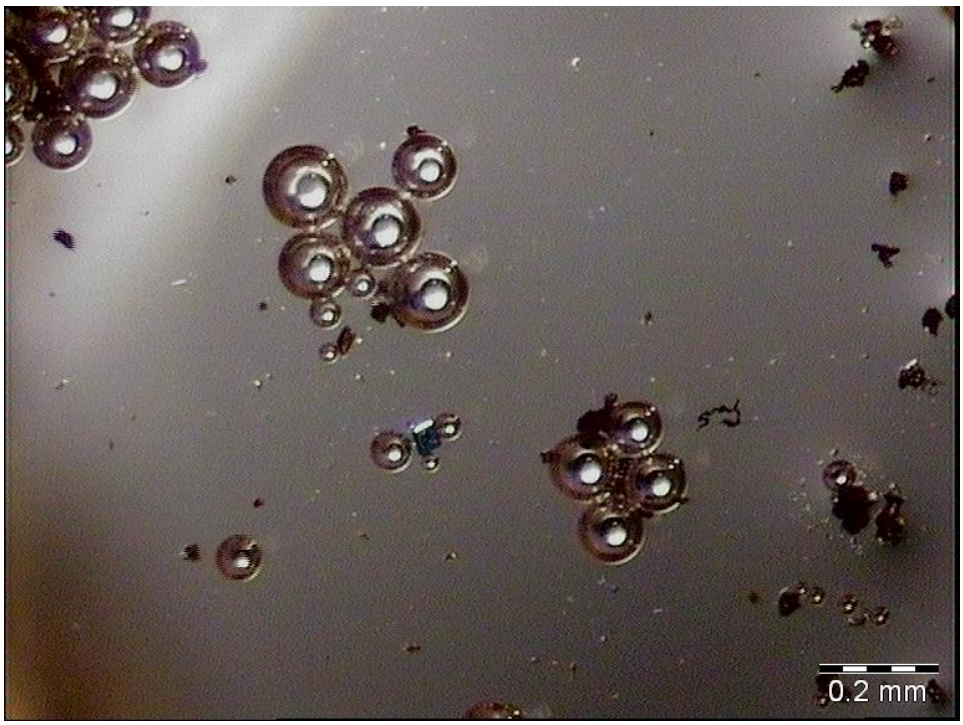

Figure 4.6.3.8 Picture of hot stage microscopy experiment on 1-MBUCT after exposure to DMF, at 325.1ºC

As in other instances, a slow and gradual darkening of the crystals can be observed, up until decomposition starts to occur at around 320ºC.

The DSC experiments in this case were slightly inconsistent with HSM due to impurities in the sample that caused an unexplained DSC peak around 80ºC (Figure 8.2.1, Appendix).

This anomaly, however, was not present in all samples and it was possible to obtain DSC measurements that were consistent with HSM observations. In those instances, the shape of the peaks is quite similar to what was observed in previous systems, a broad peak from 50ºC to 200ºC and a sharp peak corresponding to decomposition (Figure 4.6.3.9).

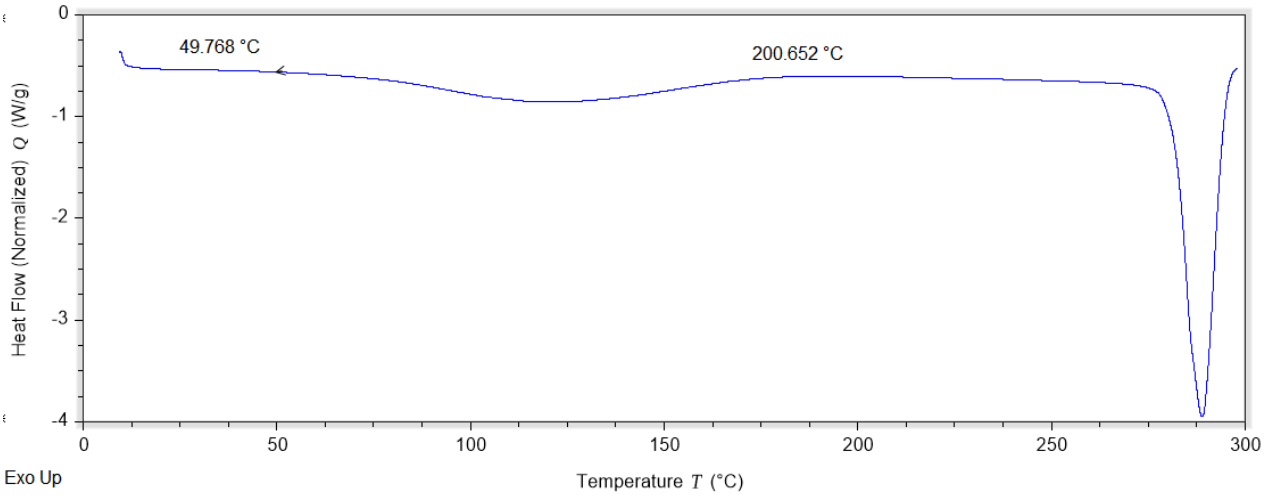

Figure 4.6.3.9 Thermogram of a DSC experiment on 1-MBUCT after exposure to DMF

This system was the first instance in which the mechanical difficulties in drying out the sample before inserting it into the TGA machine led to TGA curves that were quite inconsistent with each other, which meant that it was impossible to accurately compare the experimental data with the estimates derived from the analysis of SCXRD structural data (Figure 4.6.3.10 and Figure 4.6.3.11).

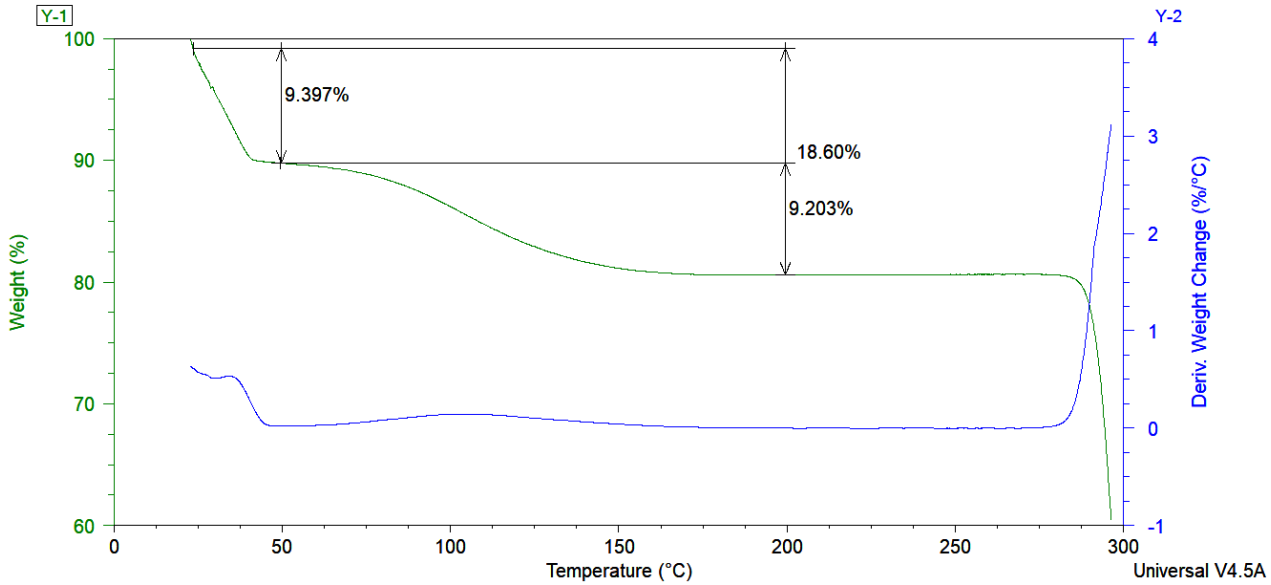

Figure 4.6.3.10 Graphical representation of a TGA experiment on 1-MBUCT after exposure to DMF, minimum value of the first mass loss

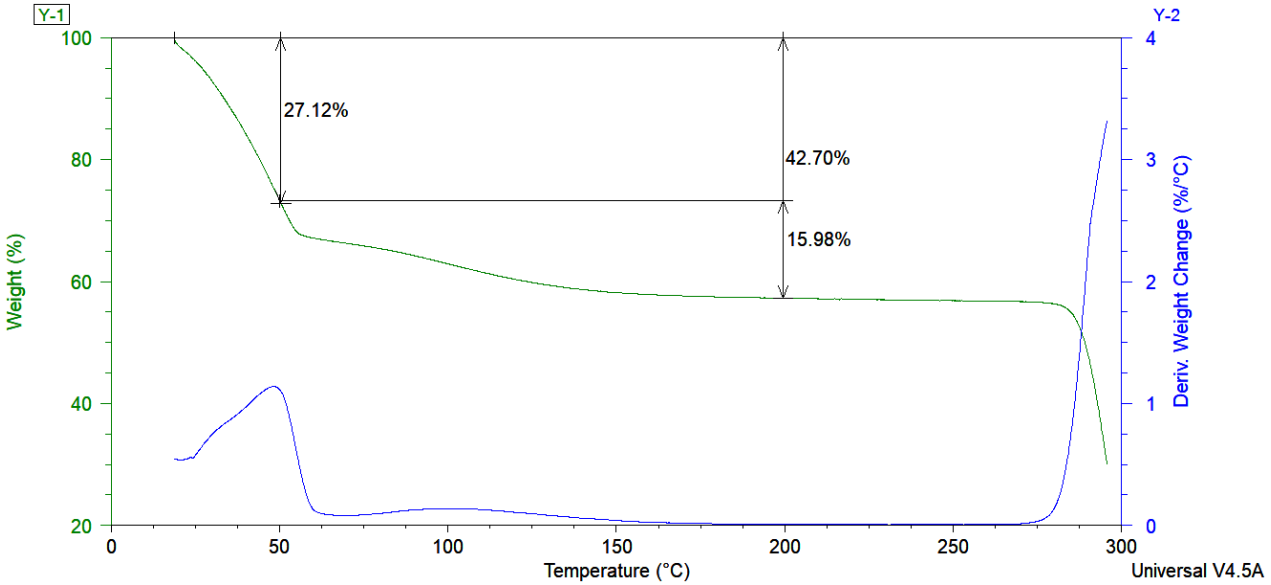

Figure 4.6.3.11 Graphical representation of a TGA experiment on 1-MBUCT after exposure to DMF, maximum value of the first mass loss

After DMF, it is necessary to analyze the samples treated with DMSO and use these results to aid in the interpretation of the data involving mixtures of these two solvents. In this instance there are stark visual signals that the system behaves differently than what was observed in all previous systems.

The material displays a slightly different color than all previous samples at low temperature, with crystals that are not exactly blue, showing a slight green tinge instead. The color of the material then shifts back to blue around 130ºC, a much lower temperature than the one observed for the previous systems. It should be noted once again that the exact temperature of these changes is not indicative of the temperature at which they will occur in TGA and DSC, because it was necessary to remove the cover of the thermal unit in order for the camera to be able to capture the sample (Figure 4.6.3.12).

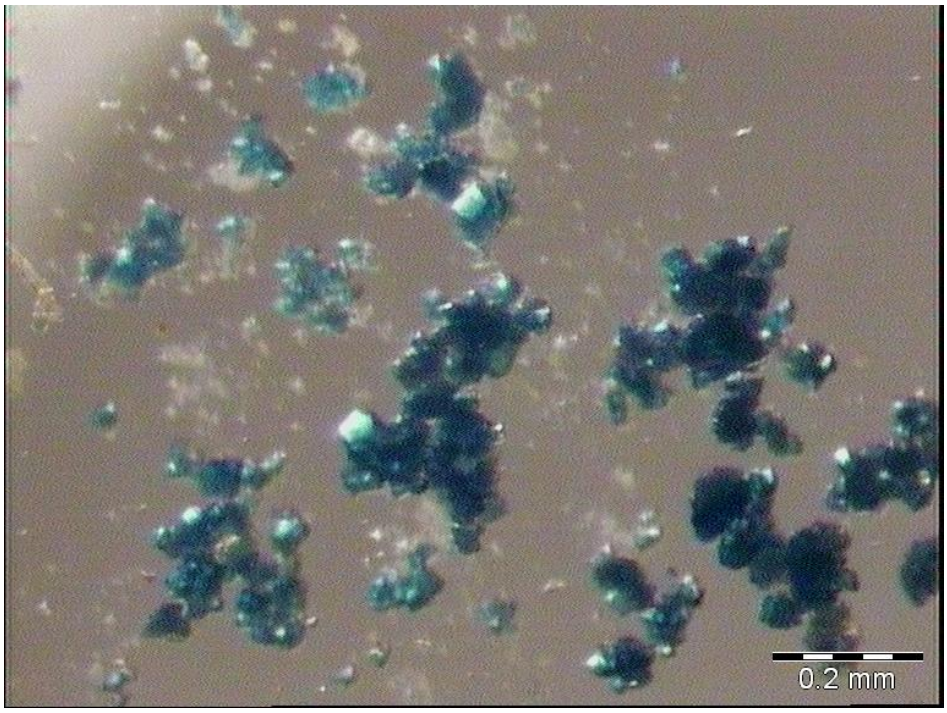

Figure 4.6.3.12 Picture of hot stage microscopy experiment on 1-MBUCT after exposure to DMSO, at 28.4ºC

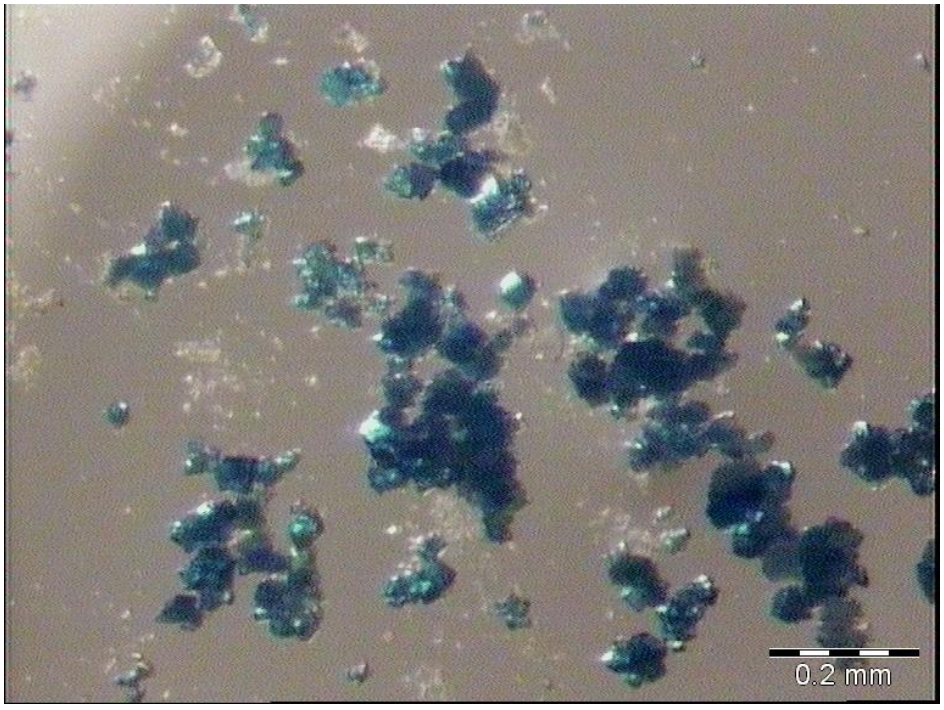

Figure 4.6.3.13 Picture of hot stage microscopy experiment on 1-MBUCT after exposure to DMSO, at 130.1ºC

Soon after regaining its customary blue color, 1-MBUCT quickly darkens, then, in a continuous process, the system gradually changes color again (Figure 4.6.3.14), ending up with dark green crystals until decomposition, which occurred around 275ºC (Figure 4.6.3.15).

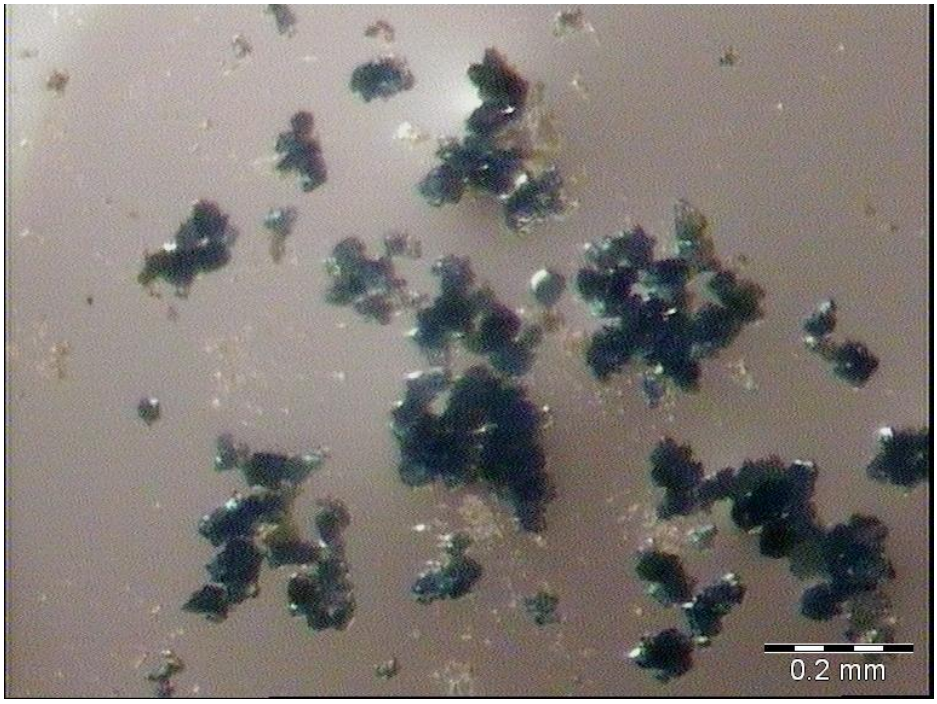

Figure 4.6.3.14 Picture of hot stage microscopy experiment on 1-MBUCT after exposure to DMSO, at 260.0ºC

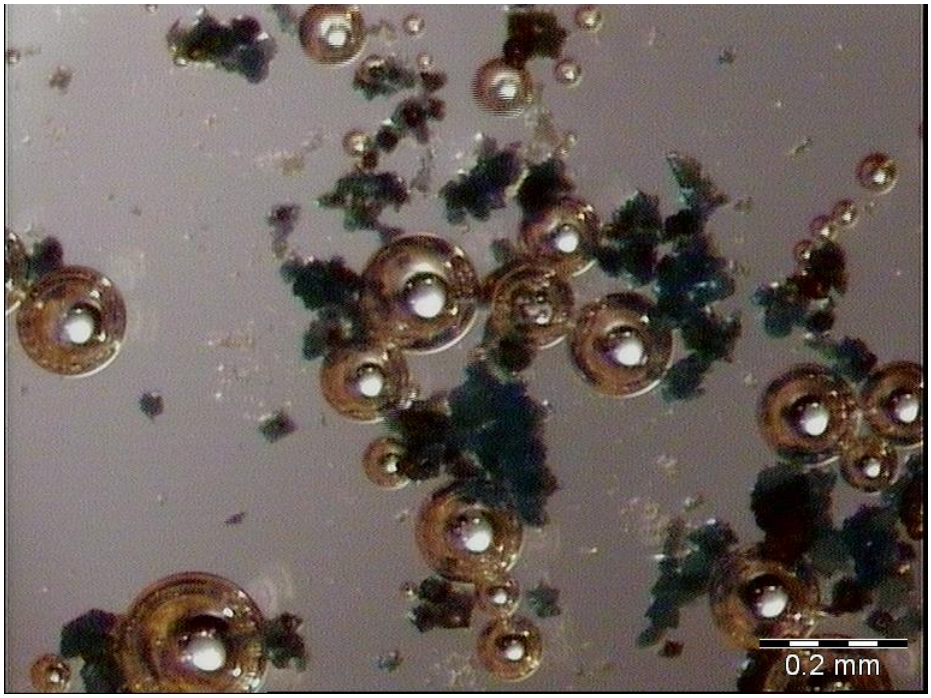

Figure 4.6.3.15 Picture of hot stage microscopy experiment on 1-MBUCT after exposure to DMSO, at 278.2ºC

Given these observations, it was expected that both the TGA and DSC curves would be quite complex, featuring at least three separate thermal events before the decomposition of the material.

Samples exposed to DMSO displayed a puzzling inconsistency in the appearance of their DSC curves. The DSC measurements were obtained from two different batches of samples, which were prepared with the same copper salt and the same methodology, and were both exposed to DMSO for only 24 hours. The only difference between the two batches was that, due to a variety of circumstances, the first batch was left in ethanol for fifteen days prior to being immersed in DMSO, while the second batch was only left in ethanol for two days. The first batch produced various measurements that were inconsistent with each other (Figure 4.6.3.16), while the measurements in the second batches were internally consistent and were in accord with what was shown under the hot stage microscope (Figure 4.6.3.17).

It is therefore likely that the longer exposure to ethanol initiated a partial modification of the structure of 1-MBUCT towards a more thermodynamically stable phase.

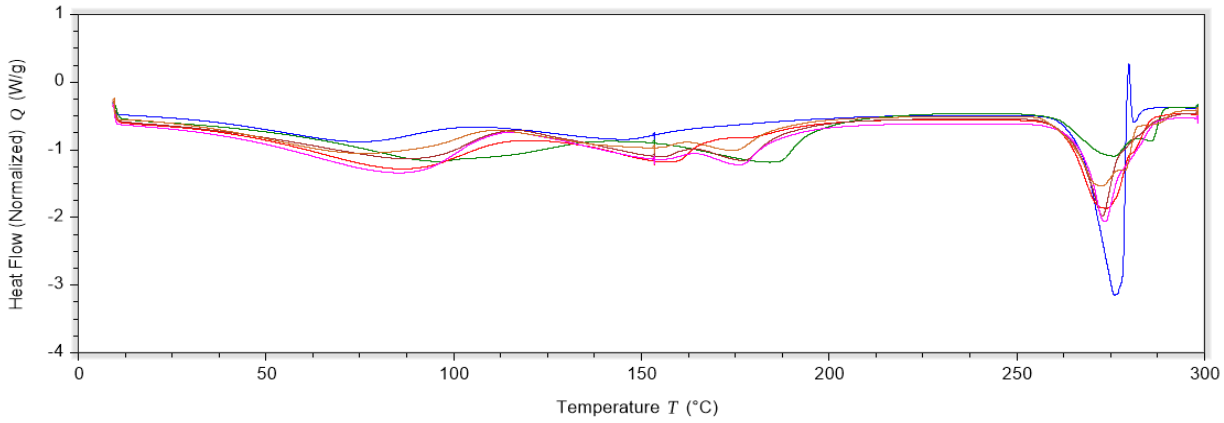

Figure 4.6.3.16 Thermogram of a DSC experiment on 1-MBUCT after exposure to DMSO, overlay of all the experiments in the first batch.

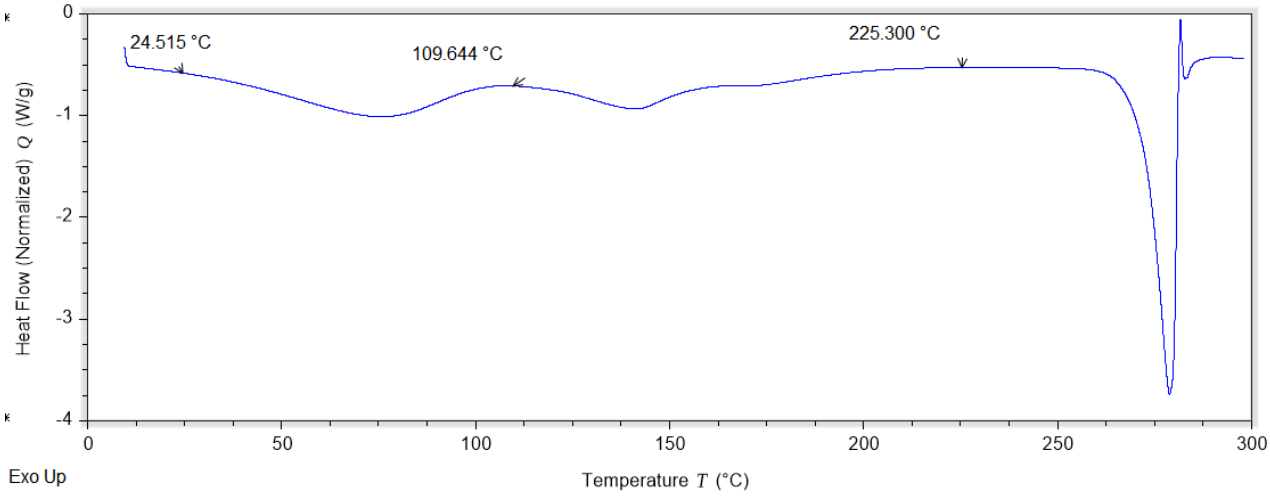

Figure 4.6.3.17 Thermogram of a DSC experiment on 1-MBUCT after exposure to DMSO, example of second batch

The TGA, however, displays even greater variability in its results (Figure 4.6.3.18 and Figure 4.6.3.19), so much so that the proposed explanation for the variability in DSC is not enough to justify it. The issue is that TGA curves varied wildly both within and between sample batches, with especially large variations in mass loss occurring in the temperature range of the first DSC endothermic peak (25 to 110 ºC).

The most likely explanation for this phenomenon is the fact that 1-MBUCT crystals tendend to aggregate into clumps when exposed to DMSO and subsequently removed from the solvent, which made drying each sample before performing an experiment a very challenging task. Thus, the inconsistency of the result can be explained by the permanence of surface solvent inside the small aggregates of crystals that constituted the material.

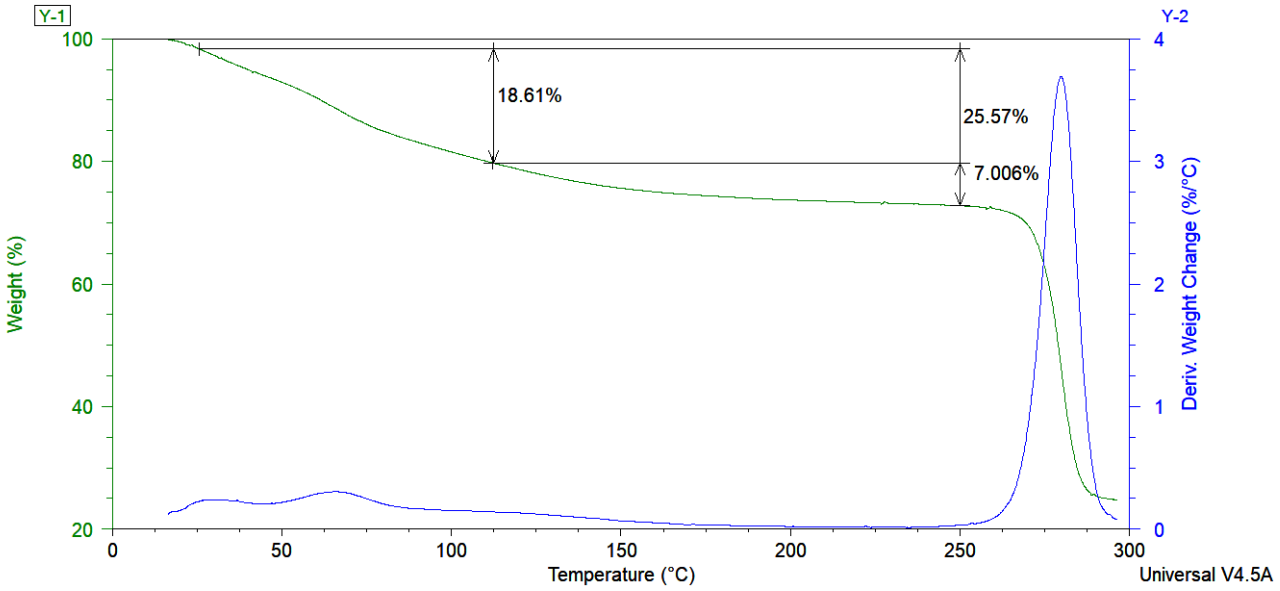

Figure 4.6.3.18 Graphical representation of a TGA experiment on 1-MBUCT after exposure to DMSO, minimum value of the first mass loss

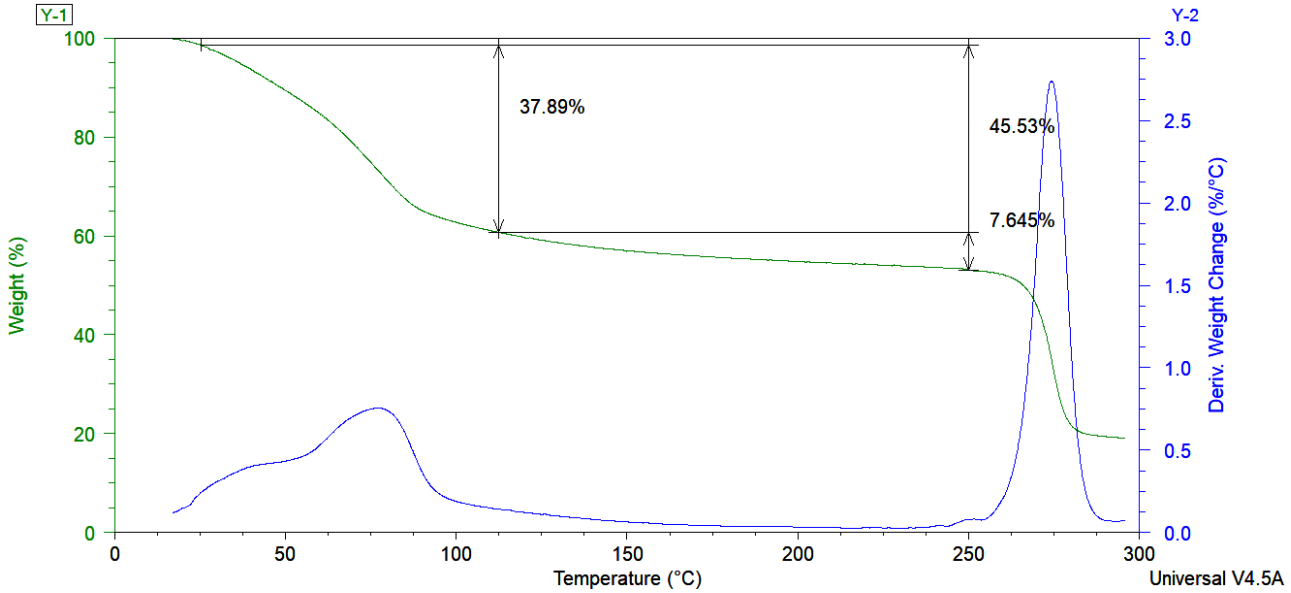

Figure 4.6.3.19 Graphical representation of a TGA experiment on 1-MBUCT after exposure to DMSO, maximum value of the first mass loss

The sample of 1-MBUCT that was exposed to a 1:1 mixture of DMF and DMSO had a similar behavior to the one displayed by the sample immersed in DMSO (Figure 4.6.3.20).

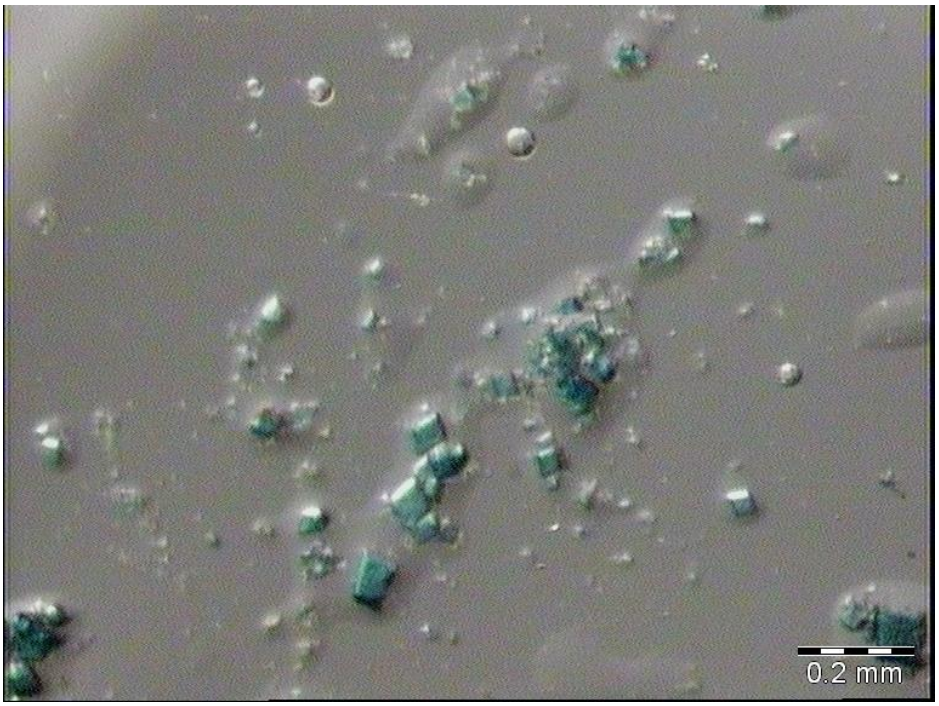

Figure 4.6.3.20 Picture of hot stage microscopy experiment on 1-MBUCT after exposure to 1/1 DMF/DMSO, at 21.3°C

Working within this solvent mixture made it easier to separate single crystals, and thus easier to see the slight shift in color with respect to the standard 1-MBUCT crystals. The pockets of liquid around the crystals are constituted of solvent that could not be removed prior to putting the sample under oil.

In this instance, upon heating, the system simply darkened, maintaining its greenish tinge and changing color around 105ºC (Figure 4.6.3.21).

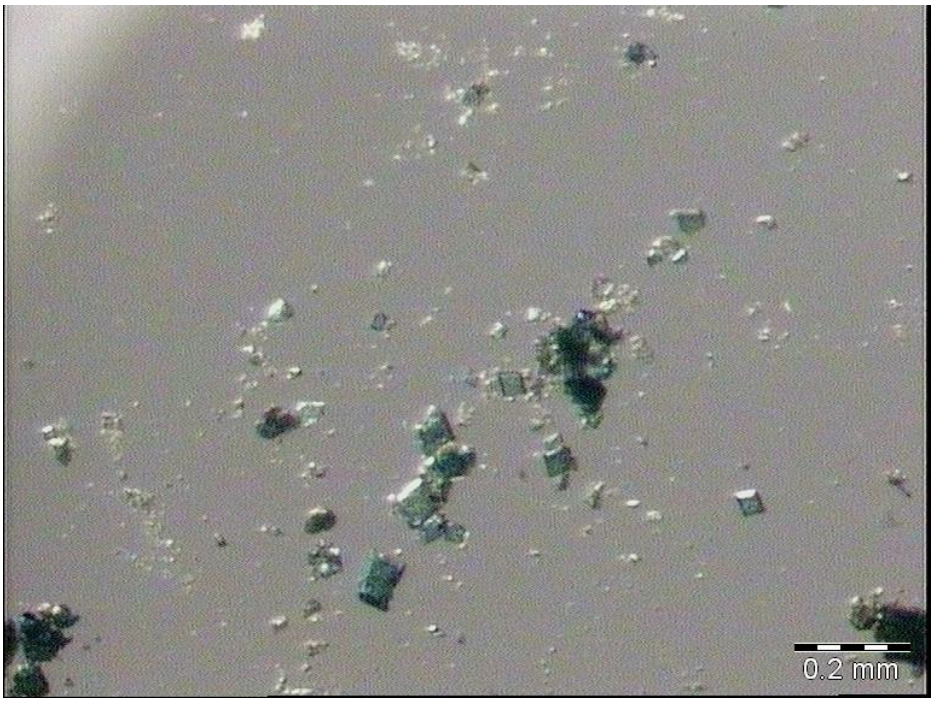

Figure 4.6.3.21 Picture of hot stage microscopy experiment on 1-MBUCT after exposure to 1/1 DMF/DMSO, at 105.3ºC

After this stage, the crystals kept becoming darker and more opaque, maintaining a similar colour until around 250ºC (Figure 4.6.3.22), decomposing shortly thereafter (Figure 4.6.3.23).

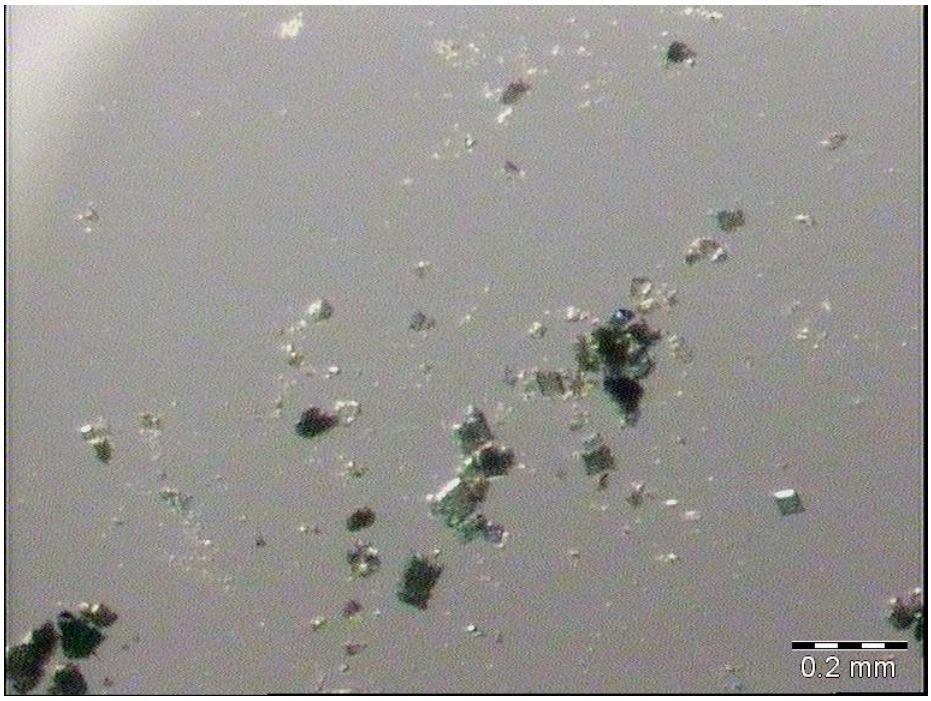

Figure 4.6.3.22 Picture of hot stage microscopy experiment on 1-MBUCT after exposure to 1/1 DMF/DMSO, at 250.2ºC

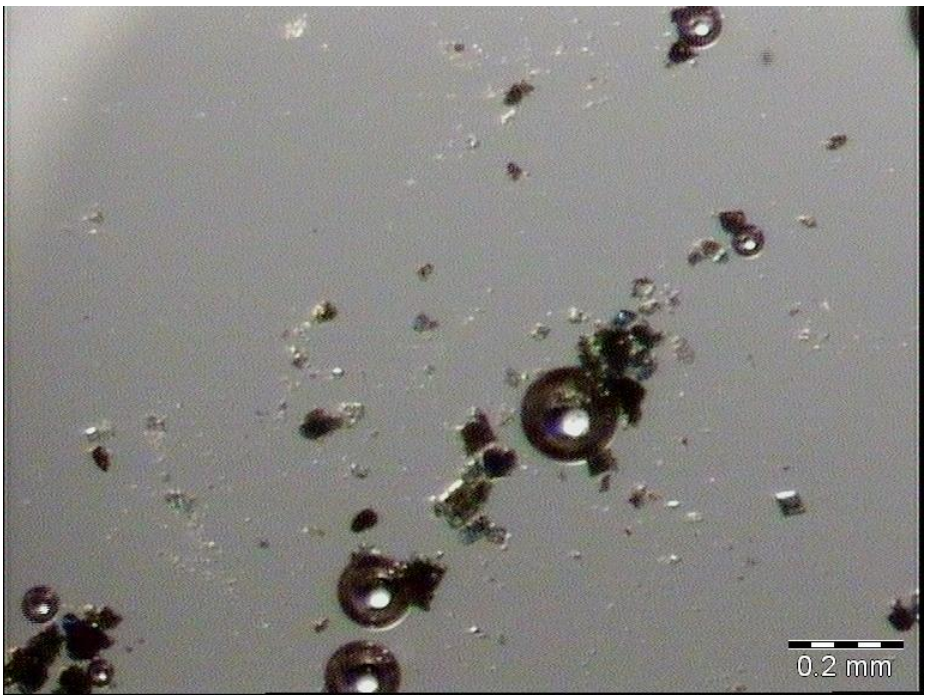

Figure 4.6.3.23 Picture of hot stage microscopy experiment on 1-MBUCT after exposure to 1/1 DMF/DMSO, at 278.5°C

Once again, both DSC and TGA data were registered in two batches, which were handled in the way already detailed when discussing the DMSO solvent exchange samples. The first batch displayed markedly inconsistent results once again (Figure 4.6.3.24).

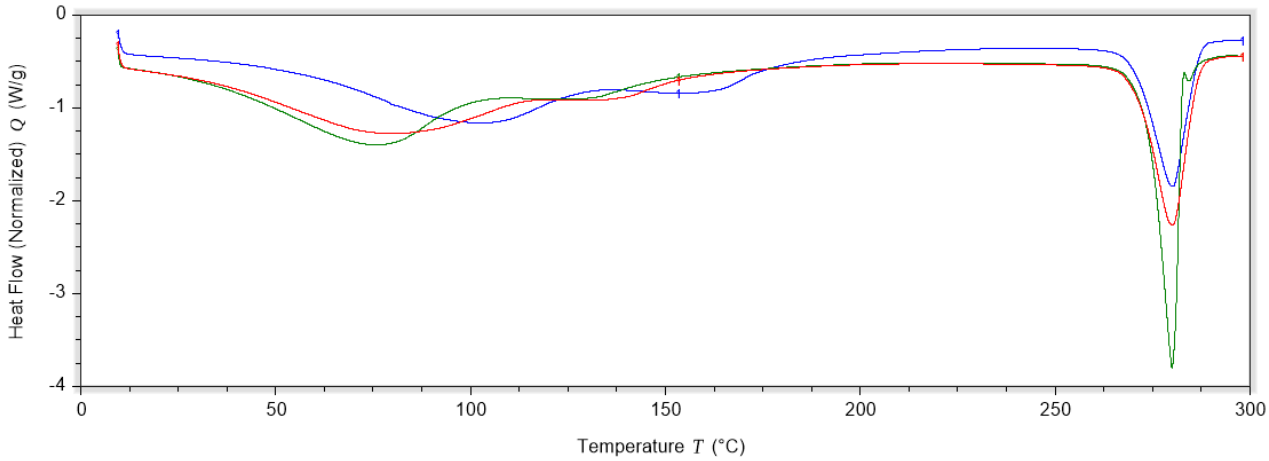

Figure 4.6.3.24 Thermogram of a DSC experiment on 1-MBUCT after exposure to a 1/1 mixture of DMF/DMSO, overlay of all the experiments in the first batch

It should be noted that the FTIR measurements on these samples were quite similar in all samples containing DMSO, regardless of its volume percentage. Thus, the similarity observed in DSC measurements is consistent with that information.

The second batch of DSC measurements on this system is once again much more internally consistent and it resembles the DSC curve for the DMSO system, albeit with a much shallower second endothermic peak (Figure 4.6.3.25).

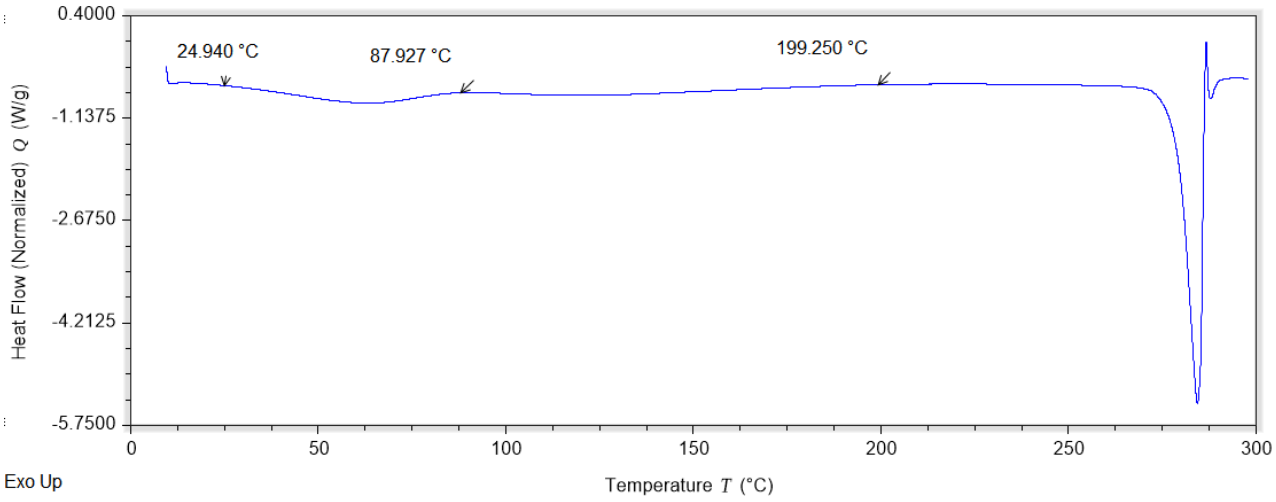

Figure 4.6.3.25 Thermogram of a DSC experiment on 1-MBUCT after exposure to a 1/1 mixture of DMF/DMSO, example of the second batch

Despite the results obtained with DSC, the TGA experiments were plagued by the same issue that characterized the system immersed in pure DMSO, leading once again to extreme variability in the first mass loss (Figure 4.6.3.26 and Figure 4.6.3.27).

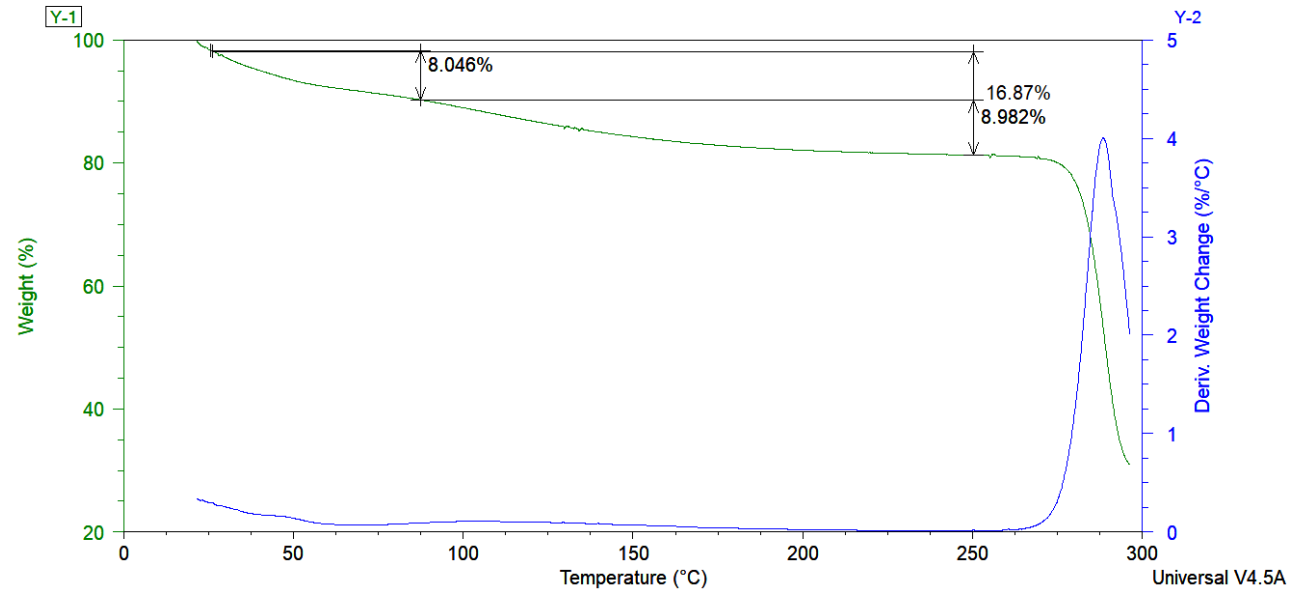

Figure 4.6.3.26 Graphical representation of a TGA experiment on 1-MBUCT after exposure to DMSO, minimum value of the first mass loss

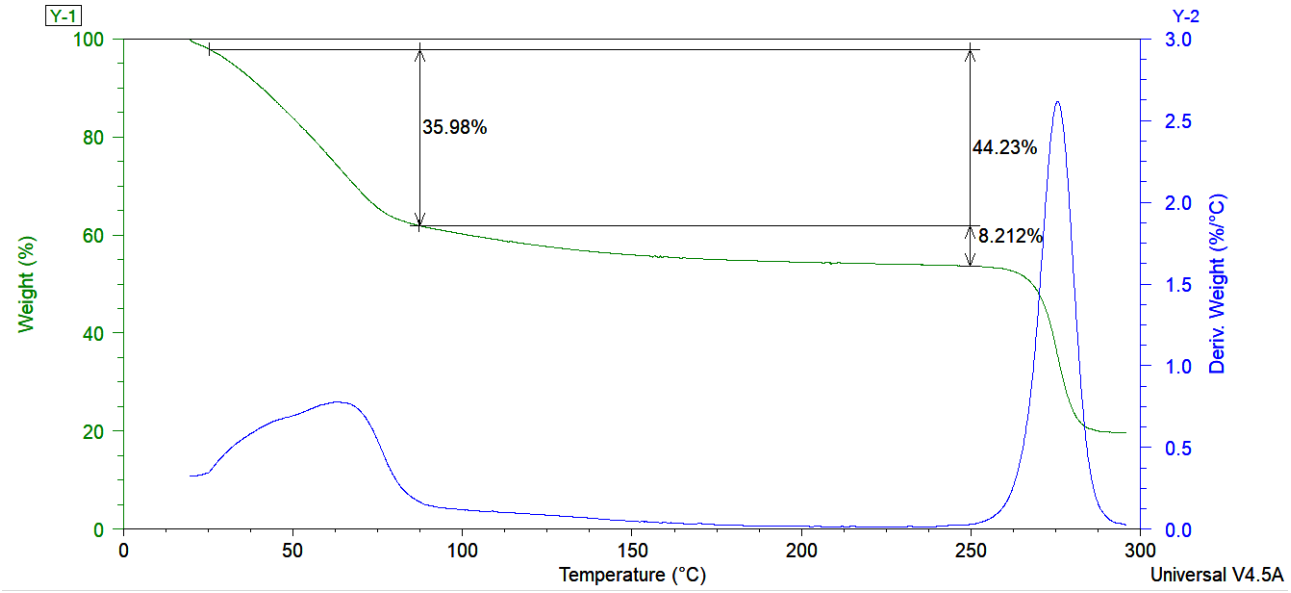

Figure 4.6.3.27 Graphical representation of a TGA experiment on 1-MBUCT after exposure to DMSO, maximum value of the first mass loss

The last sample to analyze in this Section is 1-MBUCT submerged into a 3:1 mixture of DMF and DMSO. Handling this system in an experimental setting proved to be quite problematic, which is why it was not possible to cleanly separate single crystals from the solvent or other smaller crystals around them (Figure 4.6.3.28).

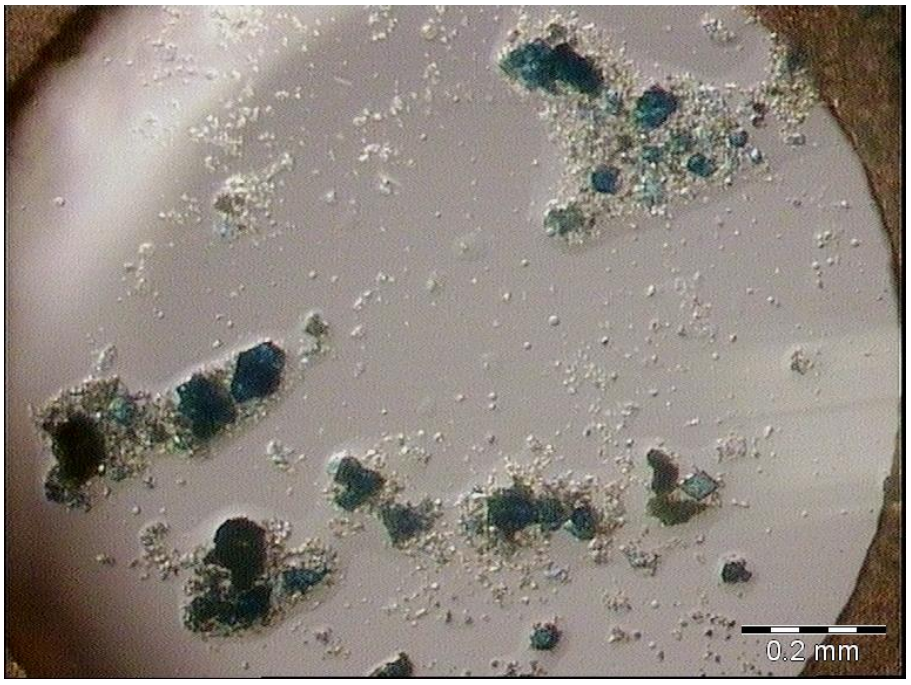

Figure 4.6.3.28 Picture of hot stage microscopy experiment on 1-MBUCT after exposure to 3/1 DMF/DMSO, at 21.6°C

Similarly to the previous sample, the crystals darkened and became more opaque until around 105ºC (Figure 4.6.3.29), then started changing color towards a dark green hue (Figure 4.6.3.30), before finally decomposing around 275ºC (Figure 4.6.3.31).

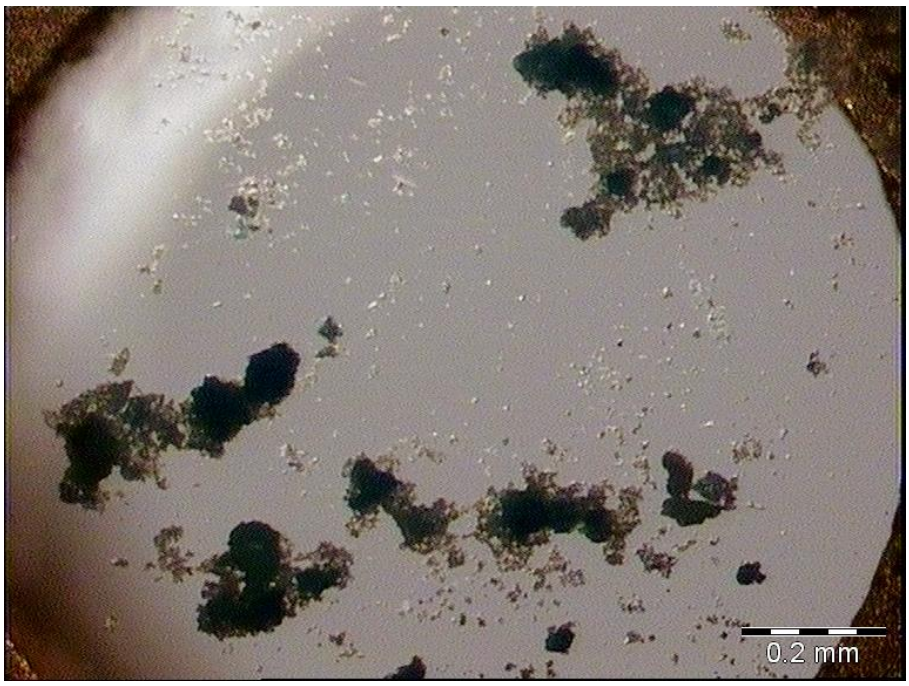

Figure 4.6.3.29 Picture of hot stage microscopy experiment on 1-MBUCT after exposure to 3/1 DMF/DMSO, at 101.3°C

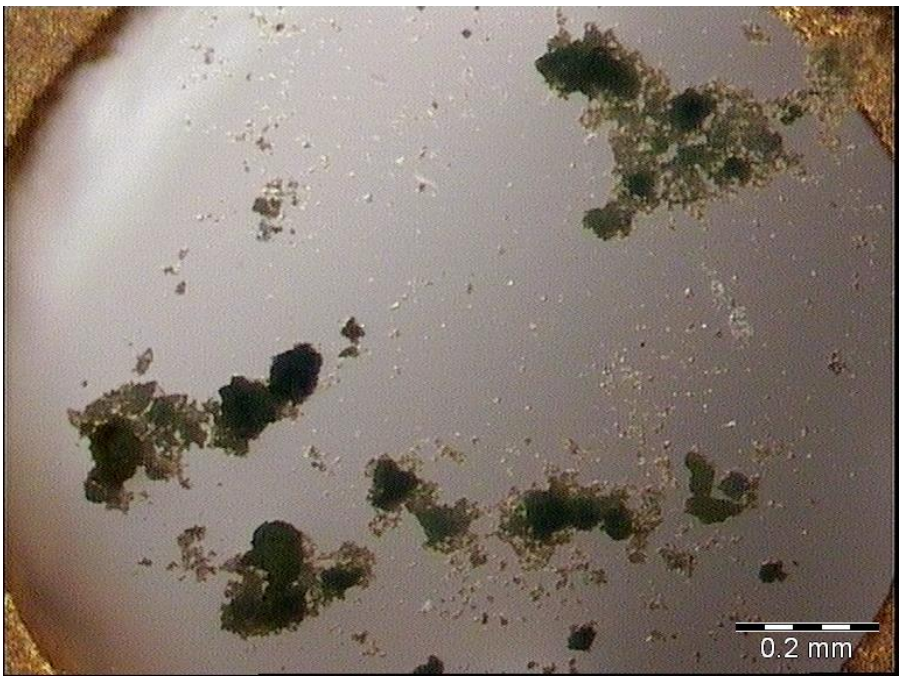

Figure 4.6.3.30 Picture of hot stage microscopy experiment on 1-MBUCT after exposure to 3/1 DMF/DMSO, at 250.1°C

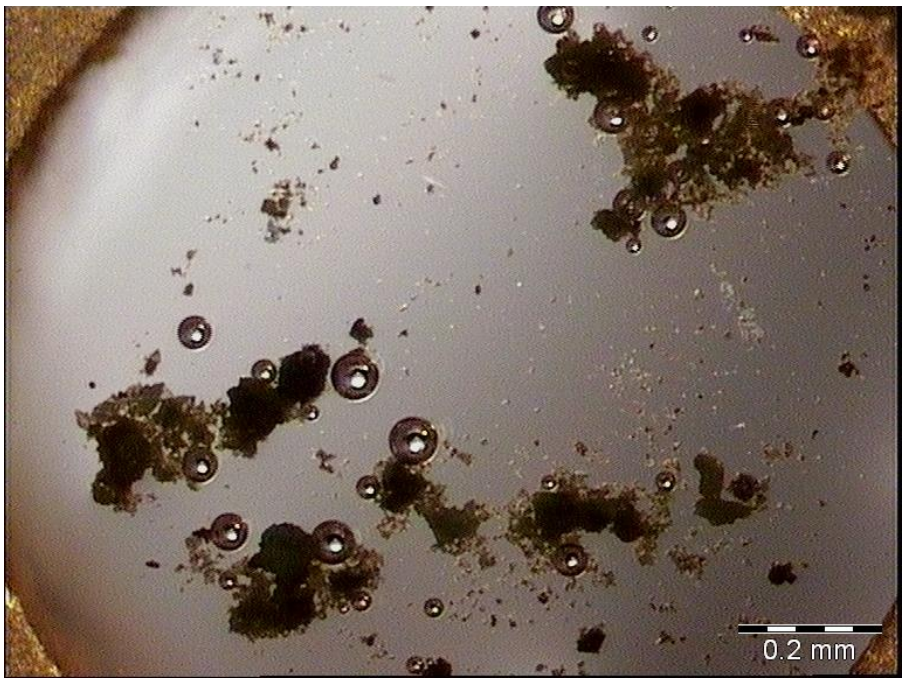

Figure 4.6.3.31 Picture of hot stage microscopy experiment on 1-MBUCT after exposure to 3/1 DMF/DMSO, at 278.1°C

While the DSC and TGA curves obtained from this system are broadly similar to the ones of other samples exposed to DMSO, there are differences that highlight how previously observed tendencies are replicated within this system. Firstly, it is important to note that the decomposition peak of the first batch of DSC experiments shows traces of two thermal events (Figure 4.6.3.32), which lends slightly more weight to the idea that the prolonged wait between synthesis and characterization of this material allowed it to slightly alter its structure in a way that made it react differently to solvent exchange experiments. In fact, the decomposition peak in the second batch does not show any traces of multiple events, and is remarkably similar to DSC measured on previously discussed systems (Figure 4.6.3.33).

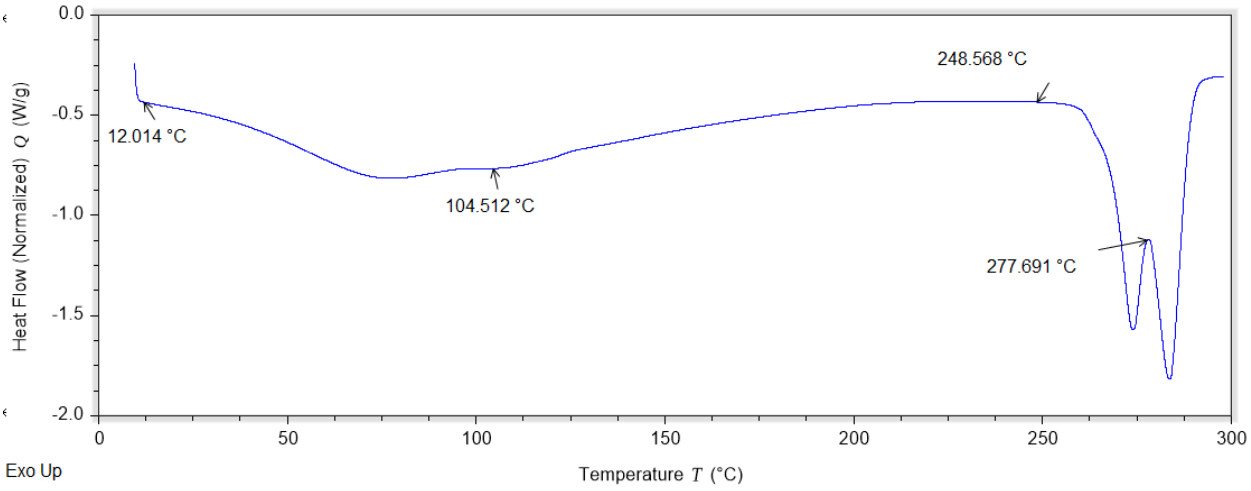

Figure 4.6.3.32 Thermogram of a DSC experiment on 1-MBUCT after exposure to a 3/1 mixture of DMF/DMSO, example of the first batch

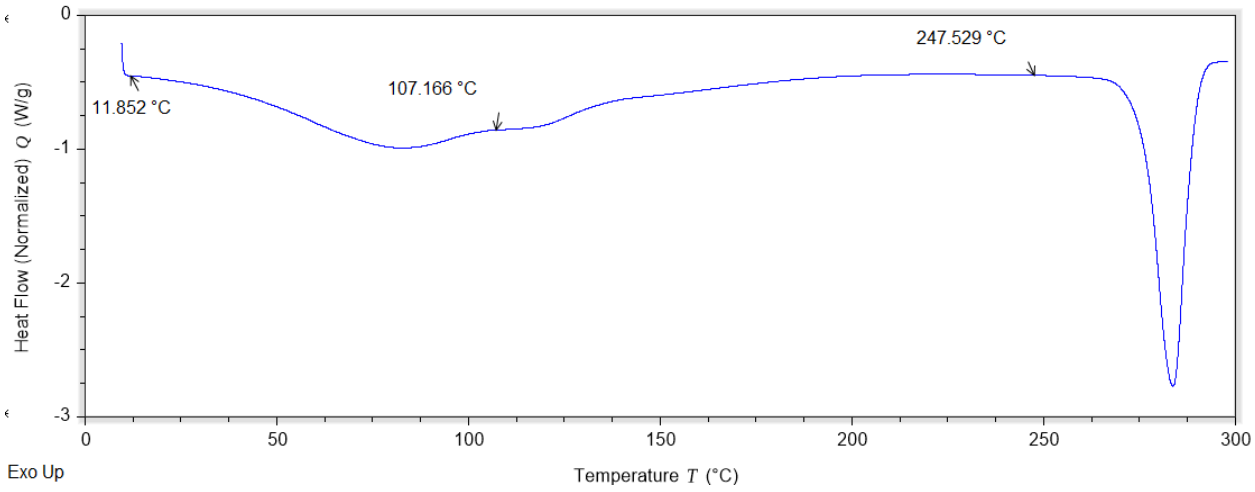

Figure 4.6.3.33 Thermogram of a DSC experiment on 1-MBUCT after exposure to a 3/1 mixture of DMF/DMSO, example of the second batch

When discussing the TGA experiments, instead, the pattern established with the previous systems containing DMSO holds true in this instance as well (Figure 4.6.3.34 and Figure 4.6.3.35). The reason for the wide range of observed mass losses is again most likely the fact that completely drying out the sample was impractical.

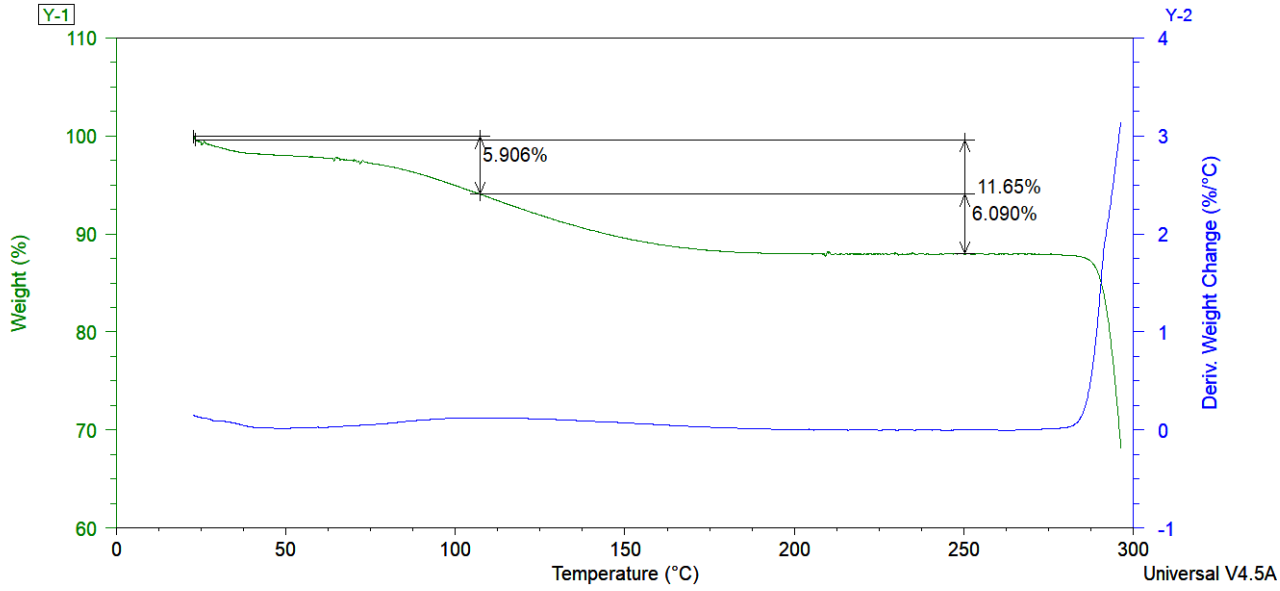

Figure 4.6.3.34 Graphical representation of a TGA experiment on 1-MBUCT after exposure to to a 3/1 mixture of DMF/DMSO, minimum value of the first mass loss.

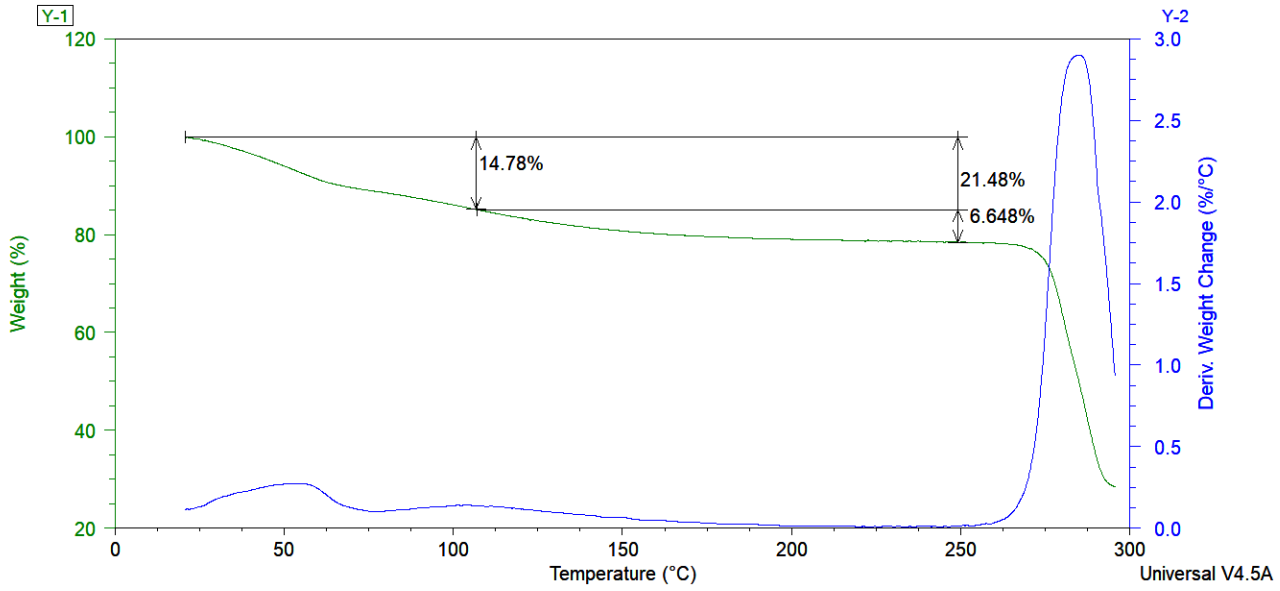

Figure 4.6.3.35 Graphical representation of a TGA experiment on 1-MBUCT after exposure to a 3/1 mixture of DMF/DMSO, maximum value of the first mass loss

4.7. 1-MBUCT DMF Structure

The sample exposed to DMF for 24h was the only solvent exchange experiment which resulted in crystals that produced a diffraction pattern good enough to be harvested for structural information. The data, however, were of poorer quality than the ones on the standard 1-MBUCT system, and this made it quite challenging to model the disorder within the channels of the material. Apart from the unmodeled disorder, the structure (Figure 4.7.1) is almost identical to the one registered before the solvent exchange experiments.

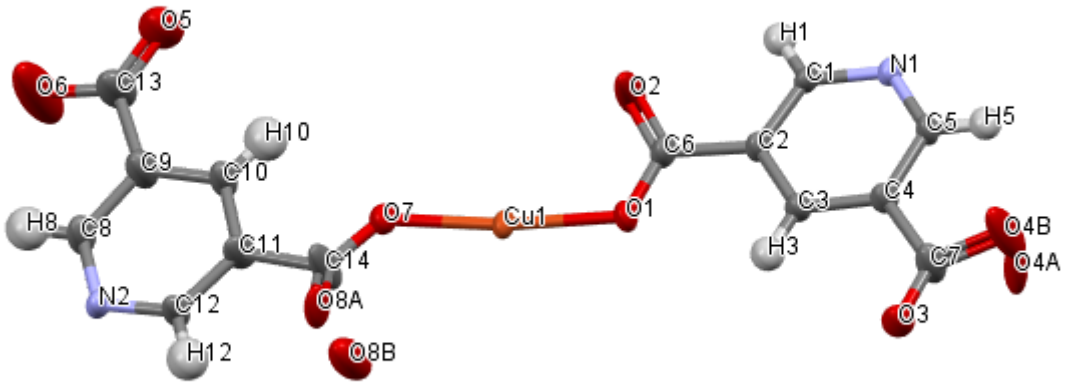

Figure 4.7.1 Structure of 1-MBUCT after exposure to DMF, unresolved channel content was modeled using the “Mask” function in Olex2

The ASU of the system, despite being presented from a slightly different perspective, contains the same atoms that are visible in Figure 4.2.3, after allowing for fractional occupancy of disordered moieties and our inability to effectively model fraction of esterified carboxylate groups present in that structure. It should be noted that the atom O4A in this structure is bonded to C7, but it is placed in another location due to symmetry. If one were to grow the structure of the material it would be possible to see that the isolated O4A atom is indeed bonded to the C7 atom of another ASU. This would mean that C7 appears bonded to three oxygen atoms, but that is not the case because O4A and O4B are the two positions occupied by the disordered O4 atom, with each position displaying a 0.5 occupancy factor.

Expanding the structure also highlights the fact that square channels are also present after the solvent exchange experiment has been completed, though the fact that their content could not be modeled still leaves questions about whether the experiment succeeded (Figure 4.7.2).

For that evaluation to be made, it is useful to consider the electron content of the channels as reported by the Olex2 “Mask” tool, whose accuracy is highly dependent on the degree of accuracy with which the structure was modeled. In this instance, the channels contain 28 electrons for each ASU, which is comparable to the estimate made for the standard 1-MBUCT system. The comparison is outlined in Section 4.6, in which other thermal analyses are discussed. The relevant data relative to the solution of the crystal structure are outlined in Table 4.7.1.

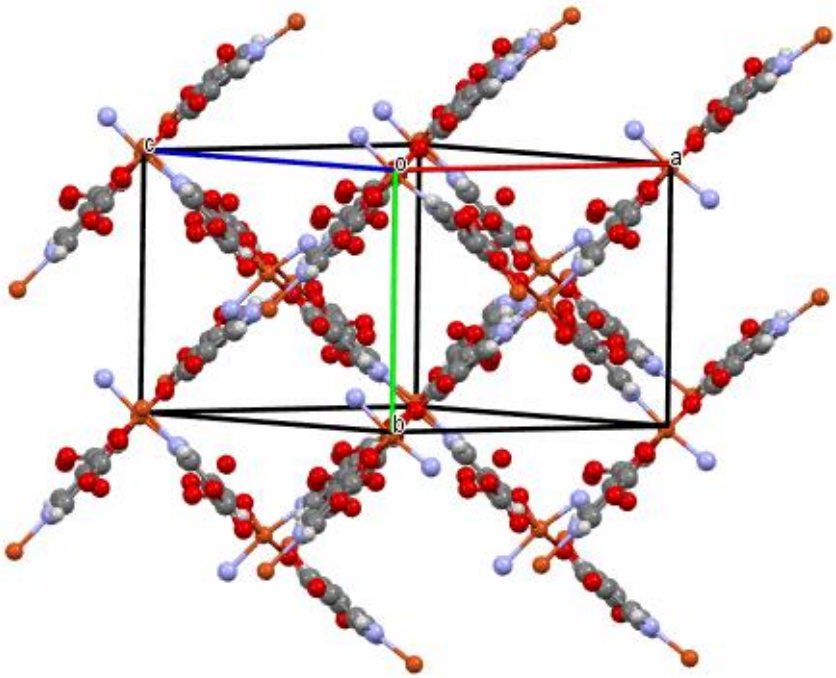

Figure 4.7.2 Structure of 1-MBUCT after exposure to DMF, unresolved channel content was modeled using the “Mask” function in Olex2

Table 4.7.1 Relevant structure solution data for 1-MBUCT-DMF

Identification code	1-MBUCT-DMF
Empirical formula	$C_{12}H_6N_2O_8Cu$
Formula weight	369.57
Temperature (K)	293(2)
Crystal system	monoclinic
Space group	$P2_1/c$
a (Å)	12.647(1)
b (Å)	10.203(1)
c (Å)	15.252(2)
α (°)	90
β (°)	97.661(2)
γ (°)	90
Volume ($Å^3$)	1950.6(4)
Z	24
ρ_{calc} (g/cm^3)	2.177
μ (mm^{-1})	6.453
F(000)	1224.0
Crystal size (mm^3)	0.02 × 0.05 × 0.08
Radiation	MoKα (λ = 0.71073 Å)
2Θ range for data collection (°)	3.25 to 56.634
Index ranges	$-15 \leq h \leq 16$, $-11 \leq k \leq 13$, $-17 \leq l \leq 20$
Reflections collected	11796
Independent reflections	4713 [R_{int} = 0.0711, R_{sigma} = 0.1001]
Data/restraints/parameters	4713/0/244
Goodness-of-fit on F^2	1.016
Final R indexes [I>=2σ (I)]	R_1 = 0.0590, wR_2 = 0.1464
Final R indexes [all data]	R_1 = 0.0978, wR_2 = 0.1623
Largest diff. peak/hole (e $Å^{-3}$)	1.04/-0.73

4.8. Copper Perchlorate synthesis and 1A-MBUCT

As outlined in Section 4.1, the system in which copper perchlorate hexahydrate was utilized as a metal ion source produced markedly different results from all other attempts at synthesizing 1-MBUCT, as is visually apparent in Figure 4.8.1. This section will explain in more detail the

synthetic methods that were utilized for this system, as well as outline all the structural elements that could be determined by analyzing the three materials produced by this reaction.

Figure 4.8.1 The first and third vial from the left are of mother liquor prior to evaporation. Upon slow evaporation of the mother liquor a dark blue solid crystallized within the vials, which is the product displayed in Figure 4.8.1.1. The second and fourth vials contain a powdery crystalline product which did not produce crystals of sufficient dimension for SCXRD.

The first attempt at performing this reaction featured a 48h reaction time and the autoclaves containing the reaction mixtures were left to cool directly at room temperature. With these parameters it was expected that the product would be 1-MBUCT, as was the case with other Cu(II) salts. These conditions, while not ideal, were utilized due to time constraints and should have been enough to obtain a product that could be used to confirm whether the result of the experiment was consistent with previous attempts. The first product found, instead, was an azure powder that, under a microscope, appeared to be constituted mainly of very small crystals. A PXRD pattern of the solid was recorded and the synthesis experiment was repeated with a reaction time of 72h and the same rigid cooling protocol that had been adopted for all the other samples. These efforts resulted in a seemingly identical result, as the product appeared to be a powder of the same quality and crystallinity as the one synthesized previously, save for a slight increase in the dimension of the crystals. After recording a PXRD pattern for the new sample the following comparison was set up (Figure 4.8.2).

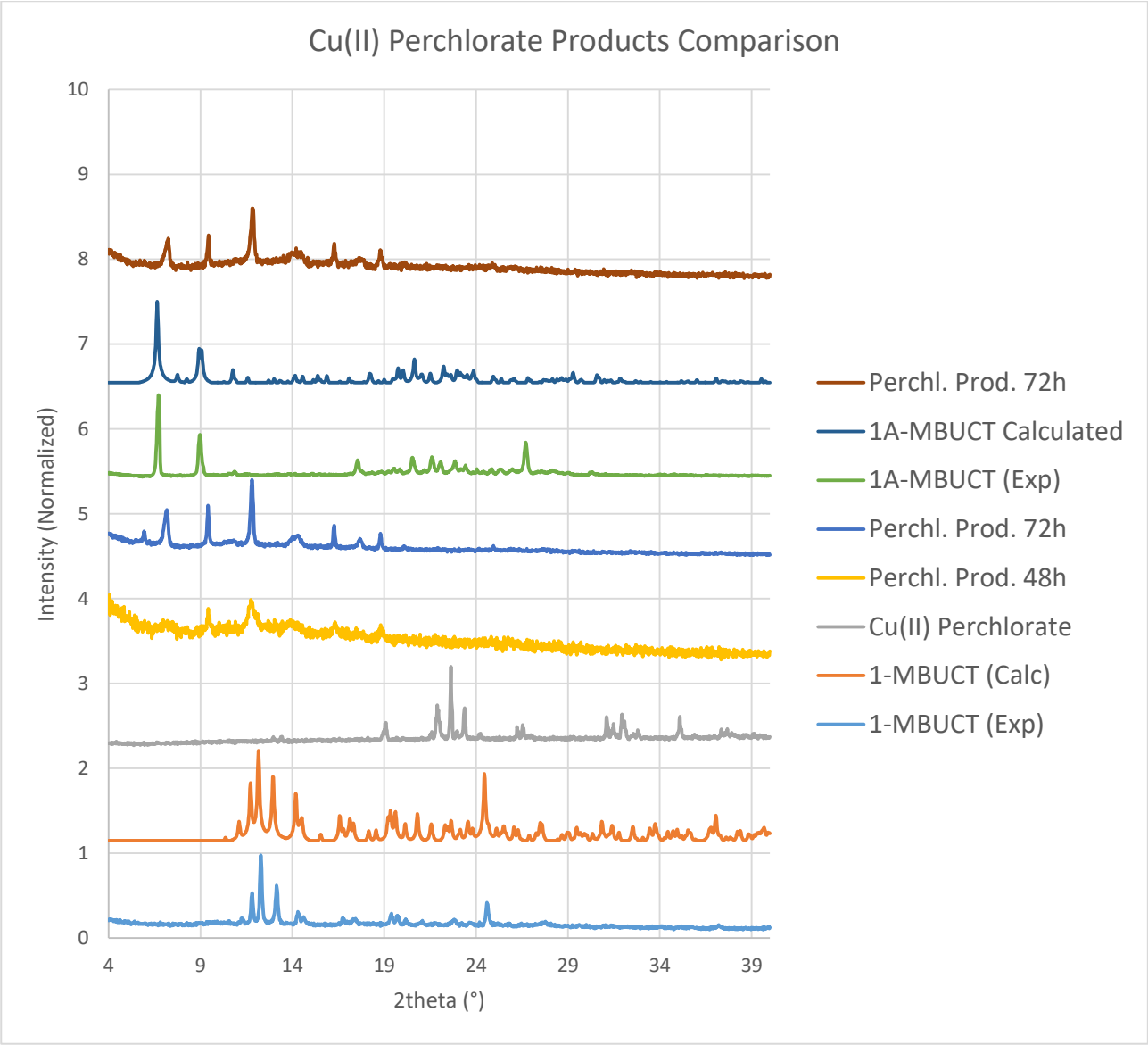

Figure 4.8.2 Comparison between PXRD patterns of products and reagents of the synthesis using copper perchlorate hexahydrate

The comparison shows quite clearly that an increase of 24h in reaction time and the adoption of a different cooling protocol have significantly improved the crystallinity of the powdery product. Furthermore, the peaks that can be seen at 5° and 9° demonstrate that the result of this reaction is a different phase than 1-MBUCT. The reason for this might reside in the coordination properties of the perchlorate anion, since it is present in the coordination sphere of copper within the structure of the second byproduct, a discrete molecular complex.

4.8.1 1A-MBUCT

This section will be dedicated to examining the second product obtained in the reaction with copper perchlorate hexahydrate (Figure 4.8.1.1). Its ASU is pictured in Figure 4.8.1.2, while its packing is depicted in Figure 4.8.1.3 and the relevant information on the solution of the crystal structure are outlined in table 4.8.1.1.

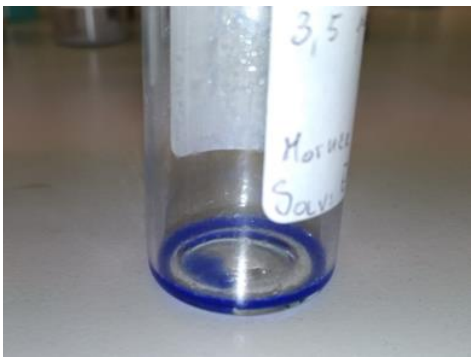

Figure 4.8.1.1 Picture of crystalline solid obtained from evaporation of mother liquor of reaction involving copper perchlorate hexahydrate

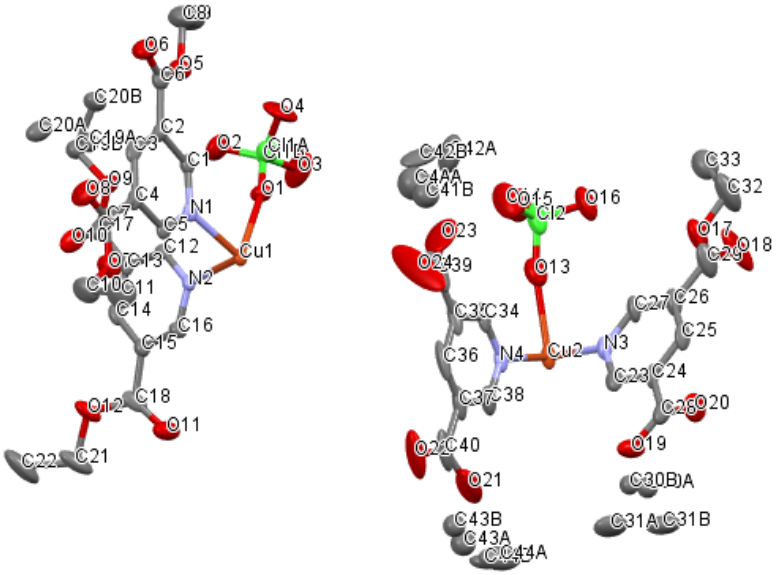

Figure 4.8.1.2 Picture of crystalline structure of 1A-MBUCT complex, crystals obtained from evaporation of mother liquor of reaction involving copper perchlorate hexahydrate. Hydrogens were hidden in the interest of clarity.

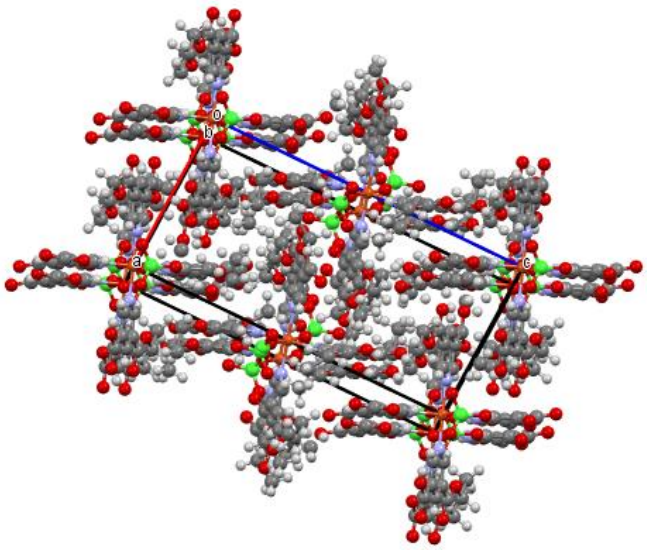

Figure 4.8.1.3 Picture of crystalline structure of 1A-MBUCT complex, crystals obtained from evaporation of mother liquor of reaction involving copper perchlorate hexahydrate.

Table 4.8.1.1 Relevant information on structure solution of 1A-MBUCT

Identification code	1A-MBUCT
Empirical formula	$C_{44}H_{52}Cl_2CuN_4O_{24}$
Formula weight	1155.33
Temperature (K)	293(2)
Crystal system	triclinic
Space group	*P-1*
a (Å)	9.769(2)
b (Å)	13.340(4)
c (Å)	19.856(5)
α (°)	93.775(5)
β (°)	92.224(5)
γ (°)	93.337(5)
Volume ($Å^3$)	2575.5(11)
Z	2
ρ_{calc} (g/cm^3)	1.490
μ (mm^{-1})	0.616
F(000)	1198.0
Crystal size (mm^3)	0.02 × 0.09 × 0.11
Radiation	MoKα (λ = 0.71073 Å)
2Θ range for data collection (°)	2.058 to 50.528
Index ranges	$-11 \leq h \leq 11$, $-15 \leq k \leq 15$, $-23 \leq l \leq 23$
Reflections collected	30223
Independent reflections	9192 [R_{int} = 0.0814, R_{sigma} = 0.1032]
Data/restraints/parameters	9192/24/786
Goodness-of-fit on F^2	1.021
Final R indexes [I>=2σ (I)]	R_1 = 0.0590, wR_2 = 0.1209
Final R indexes [all data]	R_1 = 0.1241, wR_2 = 0.1459
Largest diff. peak/hole (e $Å^{-3}$)	0.65/-0.77

This structure was determined by performing a single crystal X-ray diffraction experiment on the deep blue crystals pictured above, obtained by slowly drying out the mother liquor of the reaction involving copper perchlorate. Both the PXRD pattern calculated from this structure and the one registered experimentally are significantly different from the other solid product of the reaction and

are consistent with each other. As can be seen from the resolved structure, in this complex the perchlorate ion has entered the copper coordination sphere, and the crystal packing appears to consist of cross-like molecules tightly packed within the crystal structure.

Looking at the structure more closely reveals another detail regarding the organic ligands coordinated to the central copper ion. It appears that the best way to model the crystallographic peaks near the oxygen in the carboxylic moieties of 3,5-PDA is to describe them as alkyl carbon atoms bonded to the oxygen itself. In effect, this means that somehow putting the system under solvothermal conditions has promoted an esterification reaction in which the solvent (ethanol) has esterified every carboxylic acid on 3,5-PDA. The esterified compound is named diethyl 3,5-pyridinedicarboxylate (3,5-PDC).

A unit cell research with 3% tolerance in the latest version of the CSD did not yield any prior mention of this structure, and different queries showed that complexes based on Cu(II) or other metals and the perchlorate ion have been extensively researched. There is, however, no analogue to the compound described within this section, i.e. there is no compound with these specific ligands or other esters of 3,5-PDA based on any metal.

4.8.2 Perchlorate 4:4:1

To complete the series of experiments started with other copper salts, the reaction involved copper perchlorate was performed again under the same conditions, but adding 4,4-PBA in the molar ratio specified in Section 3.1. It was expected that this system would follow the pattern set by the other reactions and give out the same product as the reaction involving copper perchlorate without the presence of 4,4-PBA, with some unreacted starting material still present within the reaction vessel. Instead, the introduction of 4,4-PBA inhibited the formation of the powdery product, as well as the formation of the molecular complex dissolved within the mother liquor. The only product resulting from this system was 1-MBUCT, alongside some unreacted starting material suspended in a clear mother liquor. This result suggests that 4,4-PBA either prevents the perchlorate ion from coordinating the Cu(II) ions within the systems or acts as a templating agent for the aggregation of 1-MBUCT.

5. 2-MBUCT

5.1. General Synthetic Conditions

In the same way as 1-MBUCT, discussed in Section 3, this system was synthesized by varying the conditions previously used in the UCT laboratories to prepare a molecular complex. In this instance the solvent of choice was a 3 to 1 (V/V) mixture of N,N-dimethylformamide (DMF) and dimethylsulphoxyde (DMSO) and the starting copper salt was copper sulfate pentahydrate, while the

organic linkers were the same utilized for Section 4, 3,5-PDA and 4,4-PBA. It is worth noting that the solvent mixture was initially prepared right before putting the other reagents into the system, but the continued presence of impurities in the product as well as other practical considerations made it necessary to prepare the solvent mixture in advance and to then let it rest in a container with molecular sieves. The sieves were previously treated multiple times with acetone and dried in an oven at 250ºC for 8 hours to eliminate any trace of impurities within their pores.

The initial reaction procedure consisted in inserting the reagents (same 1/4/4 molar ratio utilized in Section 4, same concentration, around 0.02 M) into a Teflon-lined autoclave and leaving the system at 105ºC in an oven for 24h, cooling the autoclaves directly at room temperature after the reaction was completed. The initial results were encouraging, but rather poor, which meant it was best to immediately switch to a reaction time of 72h and adopt the more controlled cooling protocol outlined in Section 3. The final iteration of the synthetic conditions was refined enough to eliminate almost every impurity from the system, and the remaining traces of unreacted material were easily removed through washing with fresh solvent. There was, however, a byproduct so marginal that it could not be removed by any means other than manual separation under a microscope with upwards of 6x magnification. This byproduct was present in extremely small quantities, and its morphology and structure will be discussed in more depth in Section 6.1.

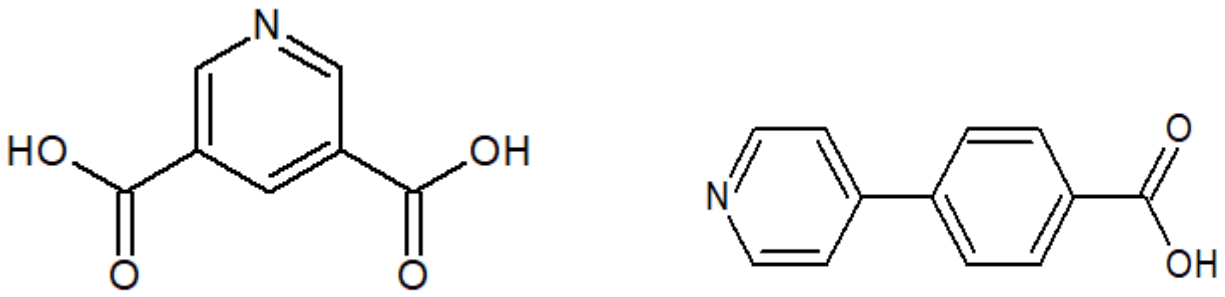

Figure 5.1.1 The two ligands utilized in the synthesis, 3,5-pyridinedicarboxylic acid (3,5-PDA) on the left and 4-pyridin-4-yl-benzoic acid (4,4-PBA) on the right.

In this instance, copper sulfate was the only salt that was used for the reaction, and this was the case for a number of reasons, chief among them the fact that the complexity of this system relative to 1-MBUCT made it a lot more challenging to gain useful information by introducing even minor variations into the system. It is also worth noting that the optimization of the synthetic process outlined in this Section required a considerable amount of time and effort, which meant that the amount of time left to closely examine the results of slightly different synthesis methods would have been very small.

The main features of this material are its extremely large unit cell, the diverse coordination environments of the five copper ions within the unit cell itself, the large amount of solvent in the channels and the fact that at least two of those copper ions are coordinated by a molecule of solvent.

5.2. Structure

The crystal pictured in Figure 5.2.1 is a good sample of what the crystal habit of the system appears as: thin, rectangular plates that can reach 2mm in length and 0.5 mm in width. This system tends to produce clusters of crystals that need to be broken up before a single crystal can be isolated, and even single crystals are quite frail, making them tricky to manipulate and study.

Figure 5.2.2 and Figure 5.2.3 show that this system has a very complex internal structure that incorporates five copper ions with five different coordination spheres within its ASU. This MOF also includes solvent molecules within its coordination structure, unlike the previous systems, and two of the copper ions that constitute it (Cu4 and Cu5 in Figure 5..2.2 and Figure 5.2.3) have arranged themselves in a so-called “paddlewheel” structure. 2-MBUCT also presents a wealth of partially disordered or completely uncharacterizable solvent within its channels, which contributes to the complexity of its TGA and DSC curves, which will be discussed in other sections. The relevant structure solution data are outlined in Table 5.2.1.

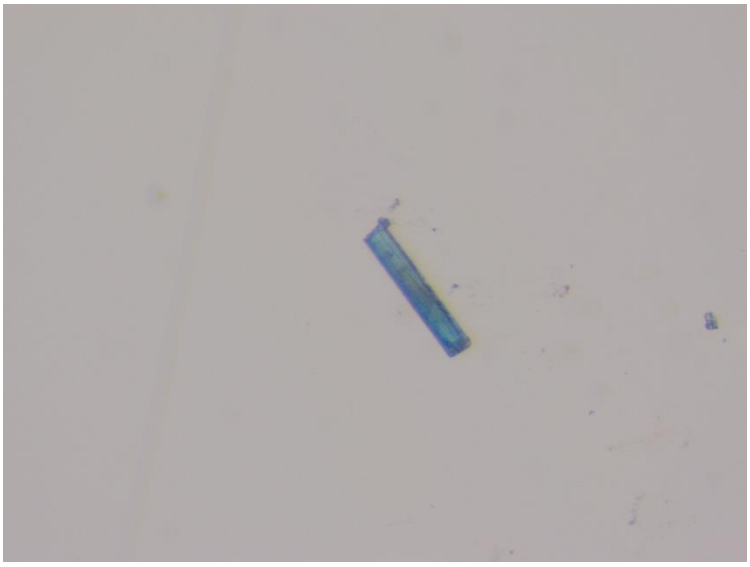

Figure 5.2.1 Picture of 2-MBUCT crystal

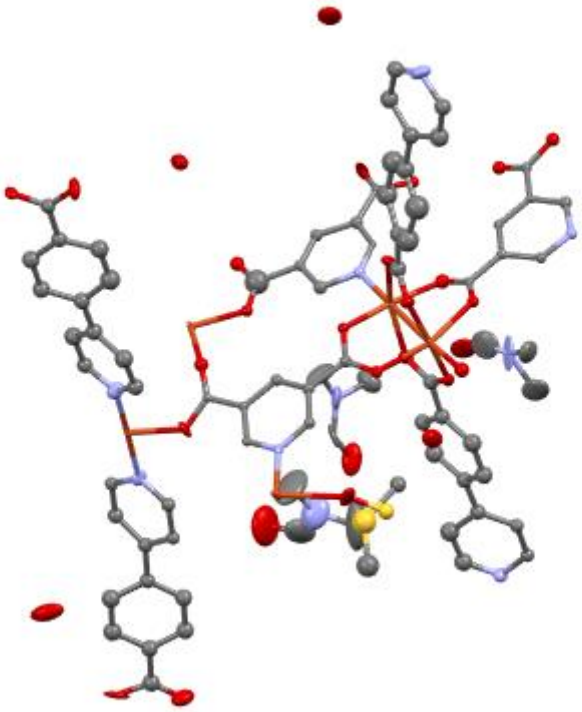

Figure 5.2.2 2-MBUCT crystal structure, hydrogens and labels were omitted for clarity

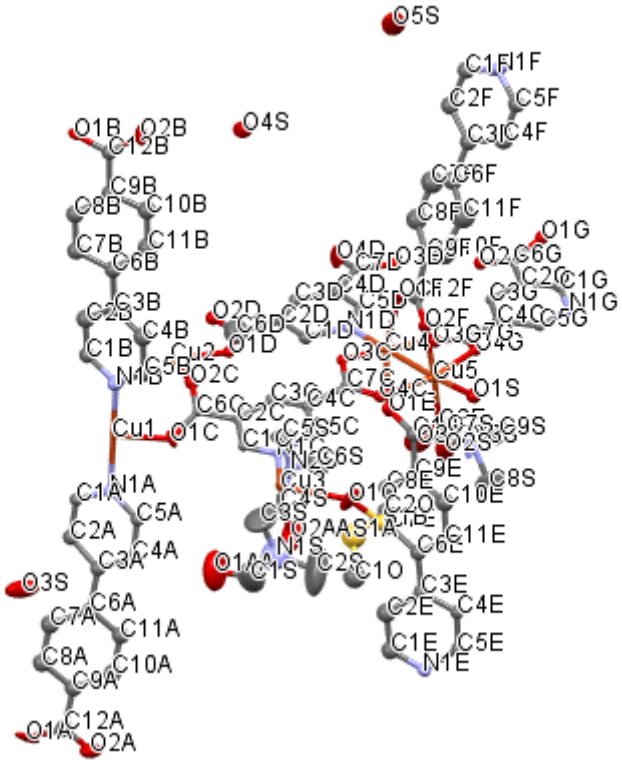

Figure 5.2.3 2-MBUCT crystal structure, hydrogens were omitted for clarity

Table 5.2.1 Relevant information for structure solution of 2-MBUCT

Identification code	2-MBUCT
Empirical formula	$C_{76}H_{62}Cu_5N_9O_{28}S$
Formula weight	1899.10
Temperature (K)	113.15
Crystal system	monoclinic
Space group	$P2_1/c$
a (Å)	25.868(5)
b (Å)	14.833(3)
c (Å)	29.222(6)
α (°)	90
β (°)	103.556(4)
γ (°)	90
Volume ($Å^3$)	10900(4)
Z	4
ρ_{calc} (g/cm^3)	1.157
μ (mm^{-1})	1.043
F(000)	3864.0
Crystal size (mm^3)	0.04 × 0.3 × 0.13
Radiation	MoKα (λ = 0.71073 Å)
2Θ range for data collection (°)	2.868 to 54.294
Index ranges	$-33 \leq h \leq 31$, $-19 \leq k \leq 18$, $-37 \leq l \leq 37$
Reflections collected	117610
Independent reflections	23976 [R_{int} = 0.1350, R_{sigma} = 0.1138]
Data/restraints/parameters	23976/91/716
Goodness-of-fit on F^2	1.080
Final R indexes [I>=2σ (I)]	R_1 = 0.1645, wR_2 = 0.3924
Final R indexes [all data]	R_1 = 0.1999, wR_2 = 0.4103
Largest diff. peak/hole (e $Å^{-3}$)	2.87/-3.27

Before discussing the specific structural characteristics of 2-MBUCT it is necessary to point out that the refinement of this structure was by necessity not optimal, for a variety of reasons. Firstly, the quality of the diffraction data is quite poor, as evidenced by the parameter R_{int} = 0.1350, in Table 5.2.1, which gives an estimate of the degree to which the registered diffraction peak are consistent

with the symmetry of the system. Furthermore, it should also be noted that the structure solution program modeled the presence of a significant electron density "hole" (Table 5.2.1), thereby overestimating the intensity of residual unresolved maximum peaks.

These features of the system made it quite challenging to fully model the solvent within the channels of the material. As shown in Figure 5.2.2 and Figure 5.2.3, it was possible to model three DMF molecules within the channels of the material, as well as three water molecules, alongside a water molecule (O1S) coordinated to Cu5 and a DMSO molecule coordinated to Cu1. While it is apparent why the solvent molecules coordinated to metal atoms were in fixed positions in every unit cell, and thus easier to model, not knowing much of the chemical environment around the solvent molecules within the channels makes it hard to determine why exactly those molecules would be in a specific position consistently enough to be solved correctly (Figure 5.2.4).

The use of the Mask function was necessary to estimate the remaining volume occupied by solvent within the material, as well as the number of electrons occupying said volume. Apart from some small pockets of void space measuring around 42 $Å^3$ one main channel per unit cell can be recognized. The channel measures 2427 $Å^3$ and contains roughly 873 electrons, for an average electron density value of 2.7 $e^-/ Å^3$. The shape of the channels and the specific area of the unit cell it occupies is shown in Figure 5.2.5.

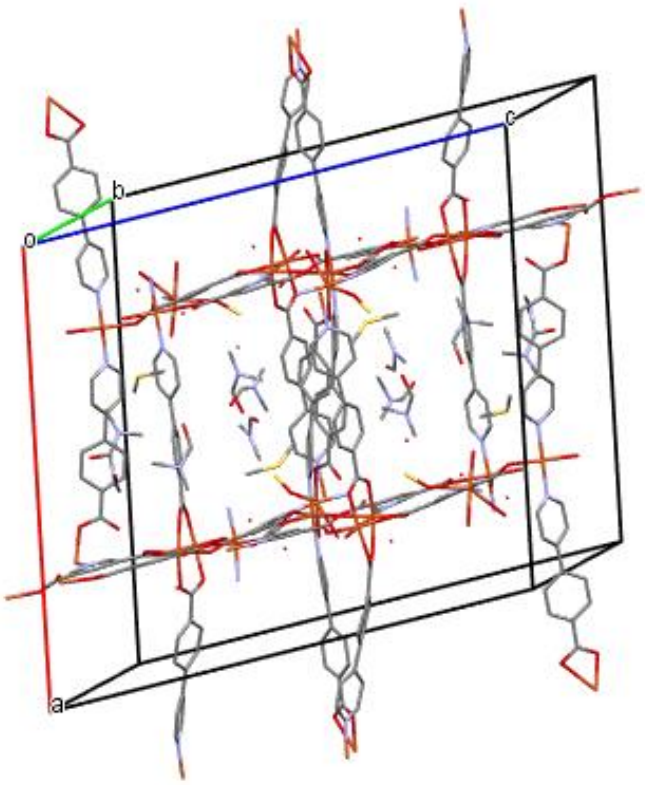

Figure 5.2.4 2-MBUCT crystal structure, hydrogens were omitted for clarity. The aim of this picture is to highlight the position of solvent molecules within the channels of the material.

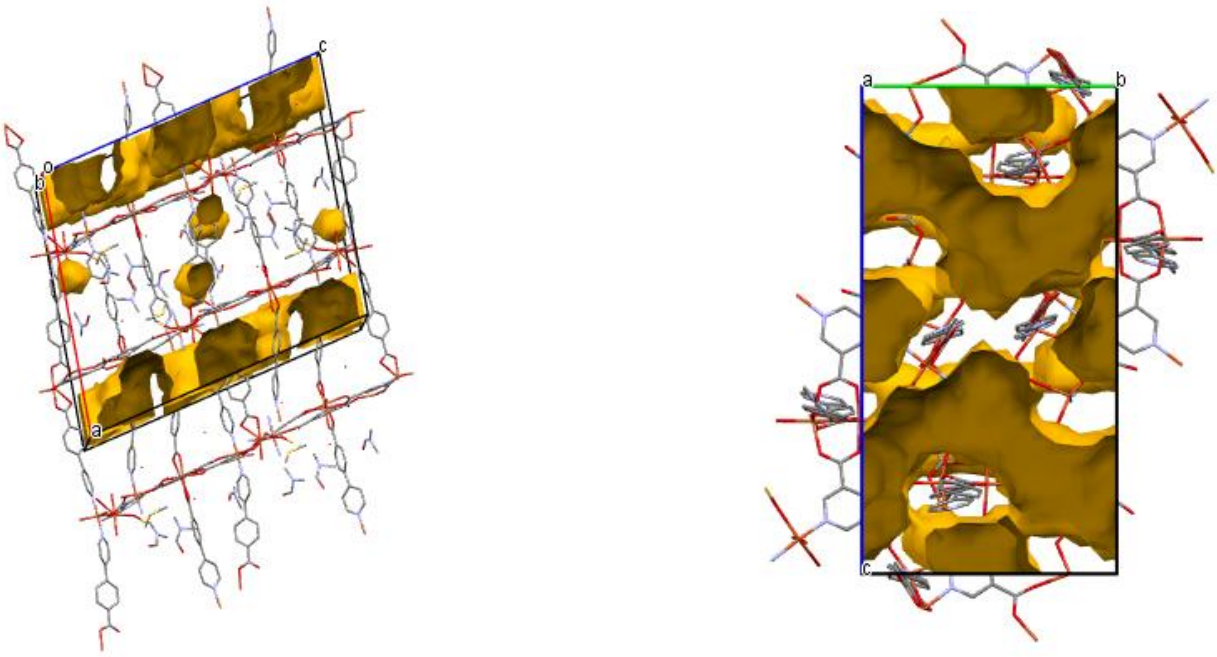

Figure 5.2.5 2-MBUCT crystal structure, hydrogens were omitted for clarity. The picture on the left is a view of the space occupied by unmodeled solvent within the channels of the material, the picture on the right is an overhead view meant to capture the shape of that space.

Lastly, searching for the unit cell parameters of this structure in the CSD with a 3% tolerance did not find any reports of a similar compound. Looking at the most salient aspect of the structure of 2-MBUCT, the paddlewheel, it is quite well-known that MOFs containing copper clusters with geometries have been extensively investigated and have shown to possess interesting properties in a variety of applications.[5,47,48]

5.3.PXRD Analysis

Despite having attempted to synthesize 2-MBUCT numerous times with different synthetic parameters, it was impossible to completely eliminate all byproducts from the system even after washing the solid with fresh solvent. A very small quantity of another crystalline species (a [12]crown-6 compound) remained within the product vial, and will be examined in more depth in Section 6 of this work. For the purposes of analyzing the behavior of 2-MBUCT, it was important to evaluate whether this tiny amount of impurities would in any way compromise the result of bulk analysis of this MOF. This was done by comparing the calculated PXRD pattern of the byproduct with the PXRD patterns generated by 2-MBUCT, as illustrated in Figure 5.3.1.

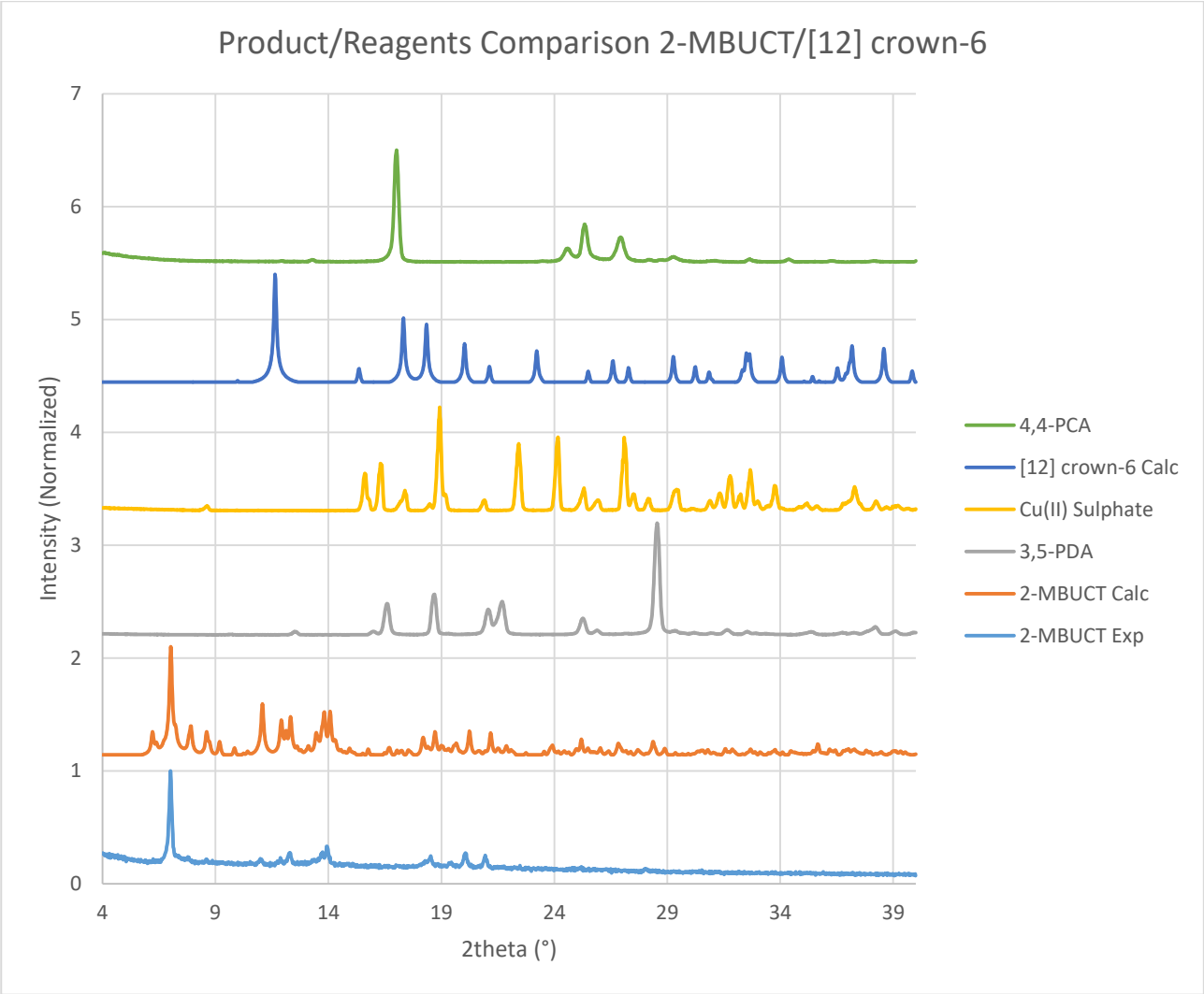

Figure 5.3.1 Comparison of reagents and products PXRD of 2-MBUCT reaction.

This comparison shows that the development of better reaction conditions was worthwhile, as it is readily apparent that the experimental PXRD of 2-MBUCT is consistent with the calculated pattern and there are no traces of impurities in a quantity larger than 5% of the total mass, given by either the reagents or the only byproduct of the reaction. There is, however, one feature of the patterns that could dispute this interpretation, and that is the difference in relative intensities of the peaks between the calculated and experimental patterns. This feature might be due to preferential orientation of the crystallites, but further research would be needed to draw precise conclusions.

5.4. Thermal Analysis

Another way in which I could gain information on this MOF both before and after the solvent exchange experiment was through TGA/DSC bulk analysis which necessitated a prior HSM experiment in order to be performed successfully.

The crystal on the left of the picture (Figure 5.4.1) is actually a cluster of various plate-like single crystals, while the smaller crystal on the right is a single crystal displaying the standard crystal habit of the material, a thin, rectangular plate. The color is slightly different from Figure 5.2.1 because of different lighting.

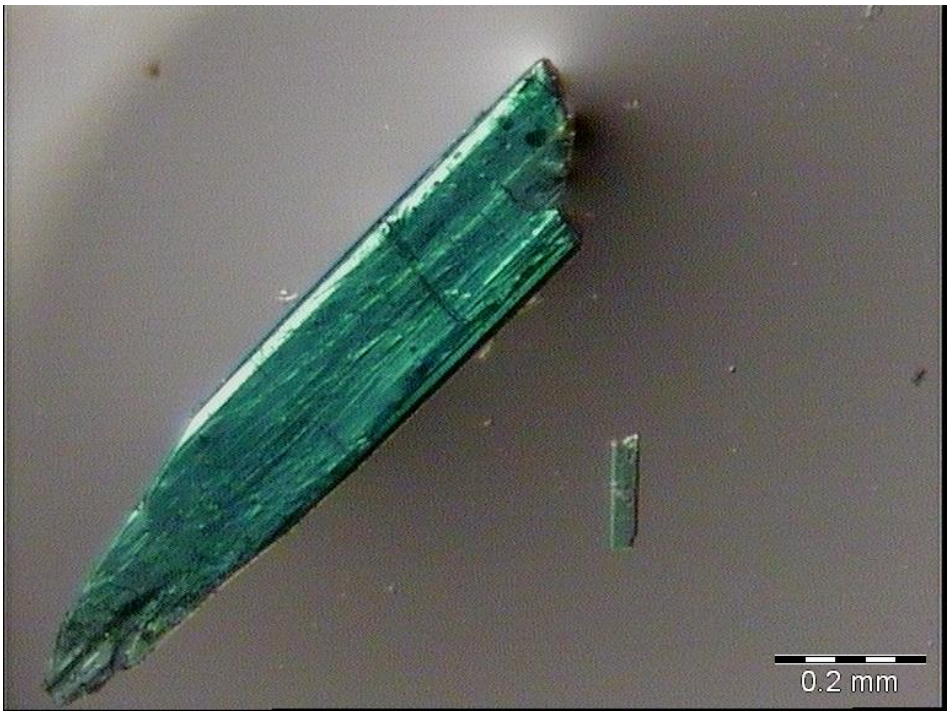

Figure 5.4.1 Picture of hot stage microscopy experiment on 2-MBUCT without solvent exchange, 26.0°C

Upon heating, the crystals slowly and subtly veer towards a greener colour, a process that stops around 150ºC (Figure 5.4.2), the material then starts darkening, and this second change accelerates significantly around 200ºC, ending with a dark green crystal at around 230ºC (Figure 5.4.3), which then decomposes shortly thereafter (Figure 5.4.4).

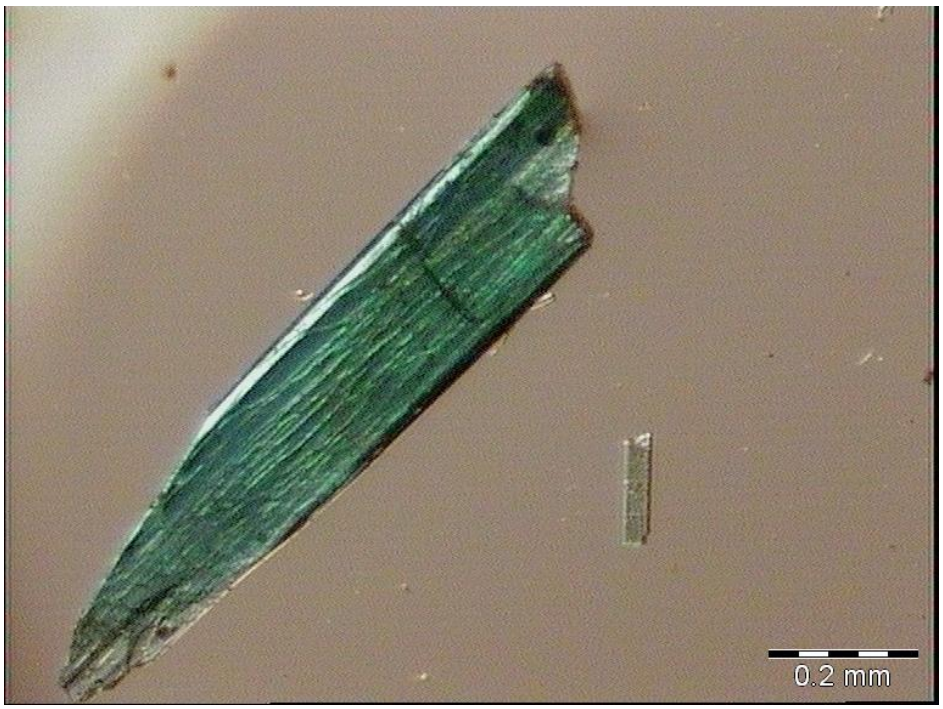

Figure 5.4.2 Picture of hot stage microscopy experiment on 2-MBUCT without solvent exchange, 130.5°C

Figure 5.4.3 Picture of hot stage microscopy experiment on 2-MBUCT without solvent exchange, 228.0°C

Figure 5.4.4 Picture of hot stage microscopy experiment on 2-MBUCT without solvent exchange, 278.2°C

The DSC data for this system are consistent with these observations, as one can see three endothermic peaks in the DSC curve before the decomposition of the material. The first signal is quite clearly visible, while the other two are somewhat enmeshed, with the third signal being a sharper peak that emerges from a broad, shallow one, reminiscent of the peaks displayed in previous DSC curves (Figure 5.4.5).

It is also evident in the shape of the decomposition peak that the material undergoes another change after its structure collapses. It is very likely that part of the MOF structure detaches itself from the rest of the material once the heat is intense enough to cause some chemical bonds to break (the most likely candidates for this are carboxylate groups, expelled as CO_2) and that this event causes the decomposition of the material. The sharp exothermic peak that follows the decomposition, then, most likely represents a rearrangement in the rest of the material that transforms it into a more stable phase, which would be consistent with a substantial release of internal energy as heat. Regardless of the nature of the process, it is certainly irreversible, because an experiment in which the sample was heated to 300ºC, then cooled back down to 10ºC, then heated again showed no further thermal activity, meaning that the new phase is stable within this temperature range.

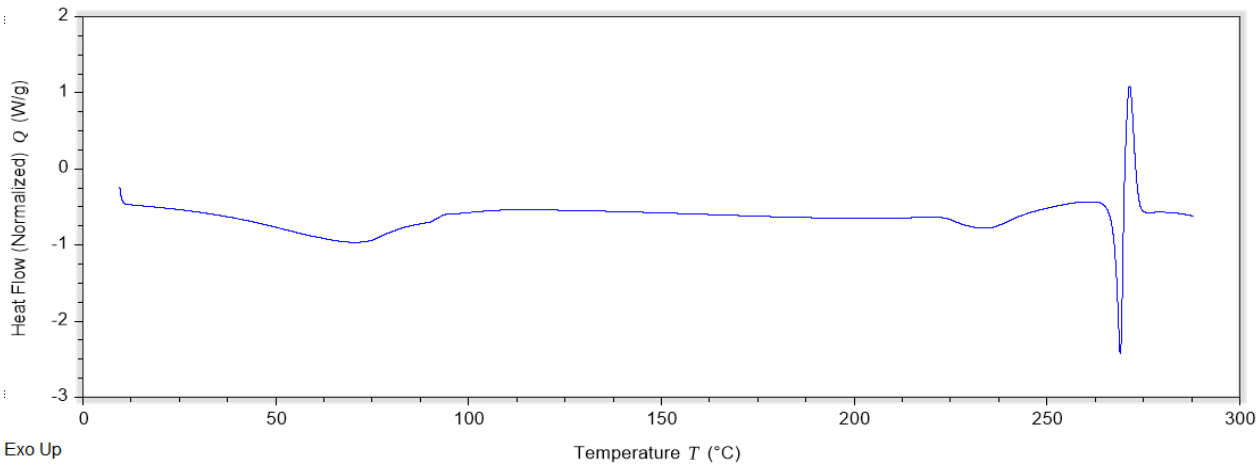

Figure 5.4.5 Thermogram of a DSC experiment on 2-MBUCT

Applying these information to the TGA measurement registered on the sample it can be determined that a 40% total mass loss occurs before decomposition, divided into three separate mass losses, one around 20%, the second one around 17% and the last one a little under 4%. Given the quantity and variety of solvent within the unit cell of the system it is no wonder that the thermal data are so complex, and show such a large mass loss. Unfortunately, the same characteristic of the material makes it impossible to perform accurate calculations on which mass loss corresponded to which solvent within the channels of 2-MBUCT (Figure 5.4.6).

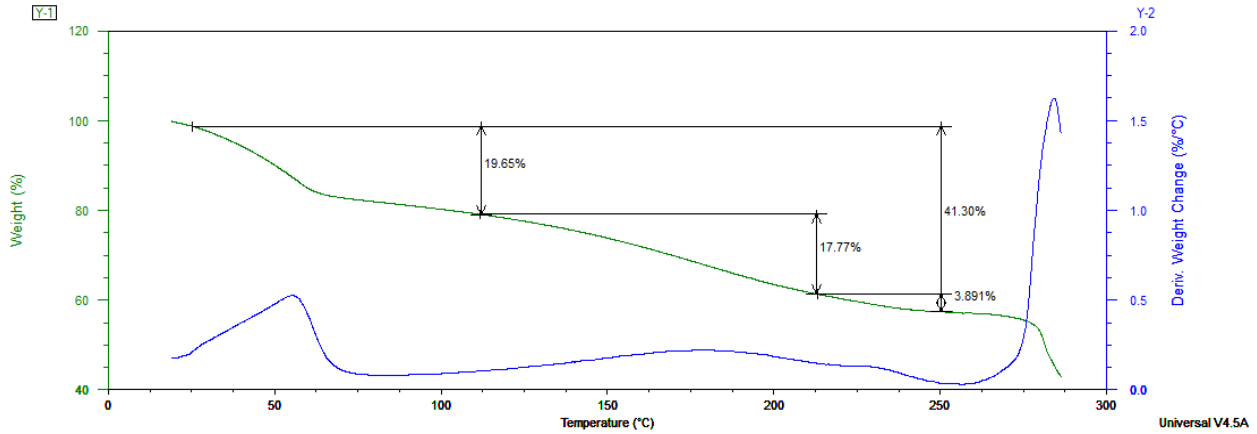

Figure 5.4.5 Graphical representation of a TGA experiment on 2-MBUCT

5.5.Solvent Exchange Experiment

The fact that one of the copper ions within the structure of the material coordinates a molecule of DMSO made it possible to see this molecule of solvent very clearly within the structure. It was therefore possible to infer that if the material could be exposed to a solvent that could substitute DMSO within the coordination sphere of the ligand then the substitution would happen. Thus, a small vial containing crystals of 2-MBUCT was put into a bigger vial containing a small quantity of acetone,

tightly sealing the bigger vial to isolate the system, but leaving the smaller vial open. Overnight the acetone evaporated and slowly condensed within the smaller vial, submerging the crystals. After 24h of immersion in acetone there were no visible changes in the material.

5.5.1. PXRD Analysis

It was not possible to find a single crystal which could generate a diffraction pattern of high enough quality to obtain a crystal structure of the compound. For this reason, the first measurement that could provide significant information about whether or not the crystal structure of the compound had been modified was a comparison of its PXRD patterns before and after the solvent exchange experiment (Figure 5.5.1.1):

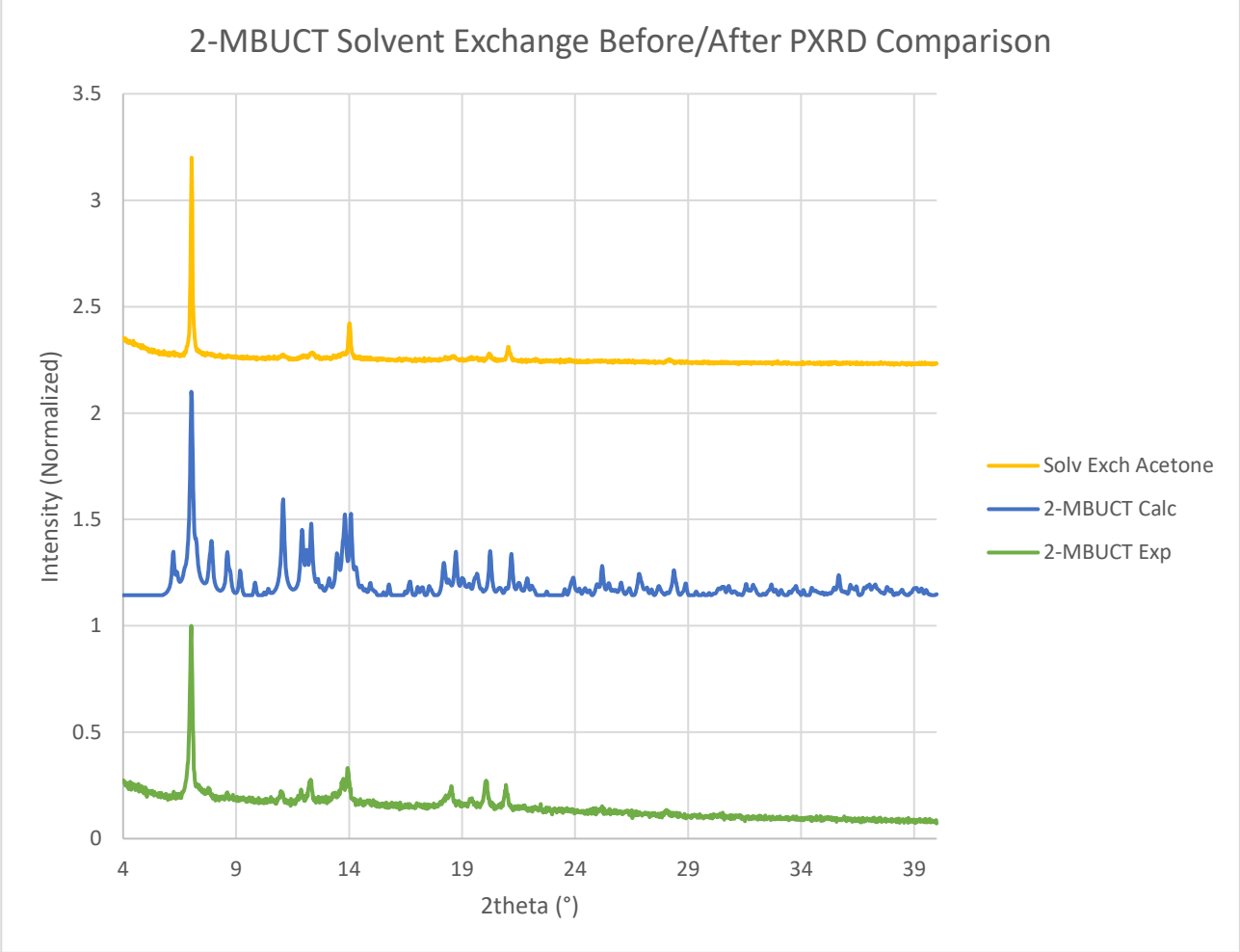

Figure 5.5.1.1 Comparison of products PXRD of 2-MBUCT, before and after a solvent exchange experiment in acetone

This comparison is enough to say that the crystals have most likely preserved their overall structure, given the presence of a few diagnostic peaks both before and after the solvent exchange experiment. The disappearance of other peaks, however, shows that there has been some degradation within the solvent exchange sample, which might be why it was not possible to obtain a new structure from single crystal X-ray diffraction experiments.

Another way in which I could gain information on this MOF after the solvent exchange experiment was through TGA/DSC bulk analysis, which necessitated a prior HSM experiment in order to be performed successfully.

5.5.2. Thermal Analysis

Similarly to the way in which 1-MBUCT was tested to ascertain whether it could substitute the solvent within its channels with another. To test this, the material was subjected to the previously discussed solvent exchange experiment, and thermal data were registered on the result.

The crystals look very similar to the ones in the previous sample (Figure 5.5.2.1), and the change color at roughly the same rate, going from an aquamarine color to an indigo hue at around 110ºC (Figure 5.5.2.2).

Figure 5.5.2.1 Picture of hot stage microscopy experiment on 2-MBUCT after solvent exchange with acetone, 21.3ºC

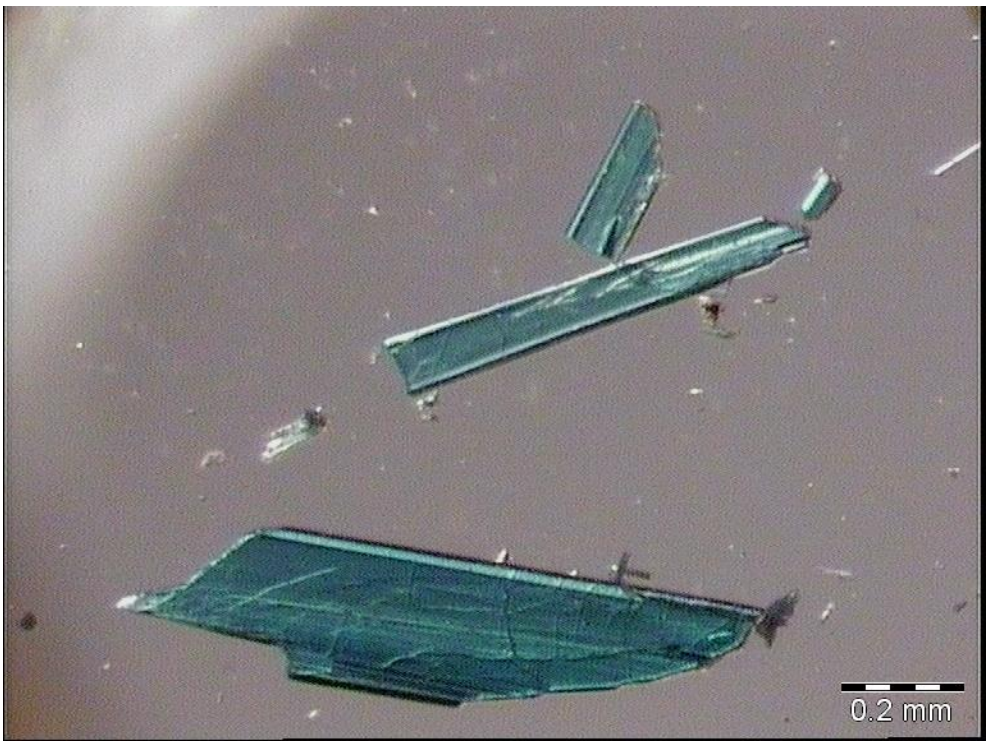

Figure 5.5.2.2 Picture of hot stage microscopy experiment on 2-MBUCT after solvent exchange with acetone, 119.8°C

After the initial color change, the material starts to darken in a similar way to what was shown in the previous set of thermal data, and the process accelerates significantly around 200ºC (Figure 5.5.2.3), ending around 250ºC (Figure 5.5.2.4), with decomposition following in short order (Figure 5.5.2.5).

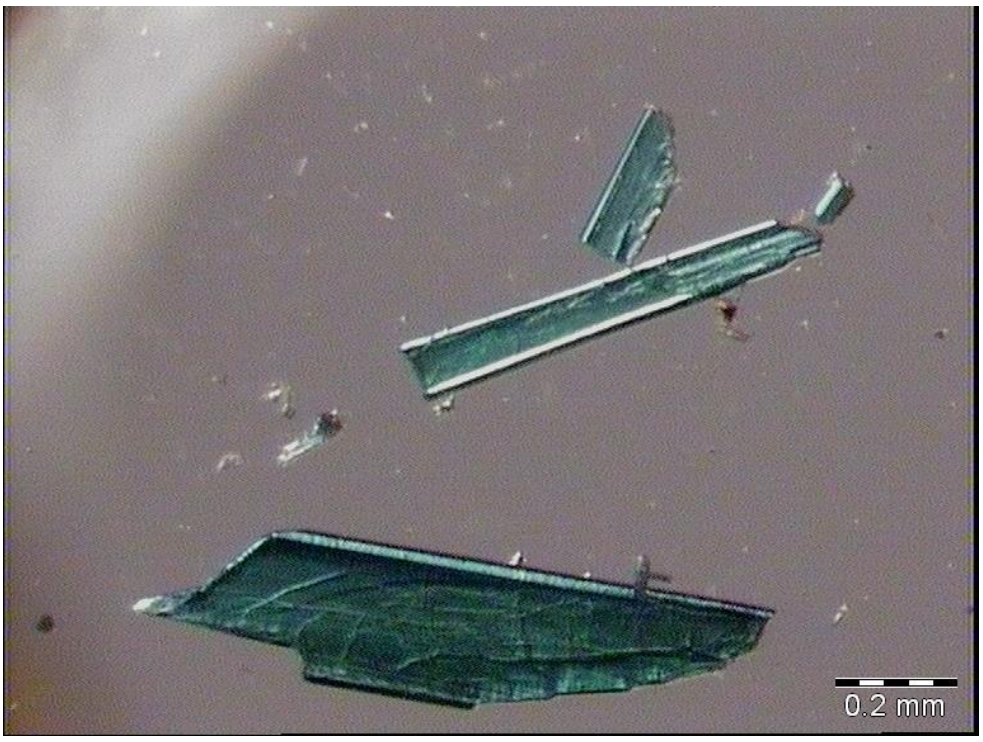

Figure 5.5.2.3 Picture of hot stage microscopy experiment on 2-MBUCT after solvent exchange with acetone, 200.0°C

Figure 5.5.2.4 Picture of hot stage microscopy experiment on 2-MBUCT after solvent exchange with acetone, 250.1°C

Figure 5.5.2.5 Picture of hot stage microscopy experiment on 2-MBUCT after solvent exchange with acetone, 289.1°C

The DSC data were once again consistent with both this set of HSM data and the previous DSC curves, displaying three relevant thermal events before the eventual decomposition of the material (Figure 5.5.2.6).

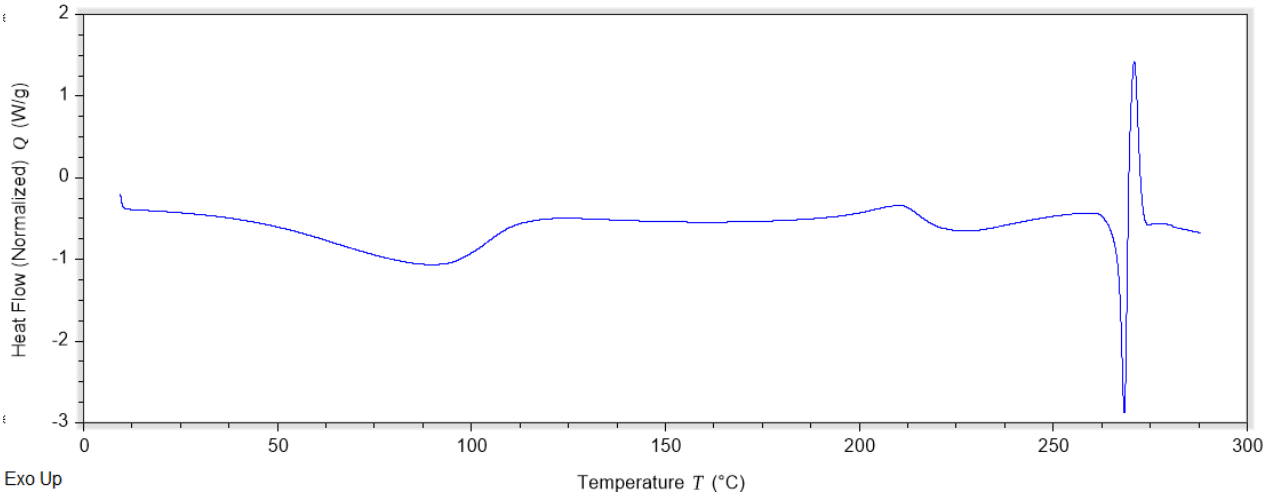

Figure 5.5.2.6 Thermogram of a DSC experiment on 2-MBUCT after acetone solvent exchange

As in the previous instance, there is an initial significant endothermic peak, followed by a much broader, shallower peak interrupted by the third thermal event. The sharp peak around 270ºC, as always, represent the decomposition of the material. The TGA of the solvent exchange experiment is represented in Figure 3.6.17.

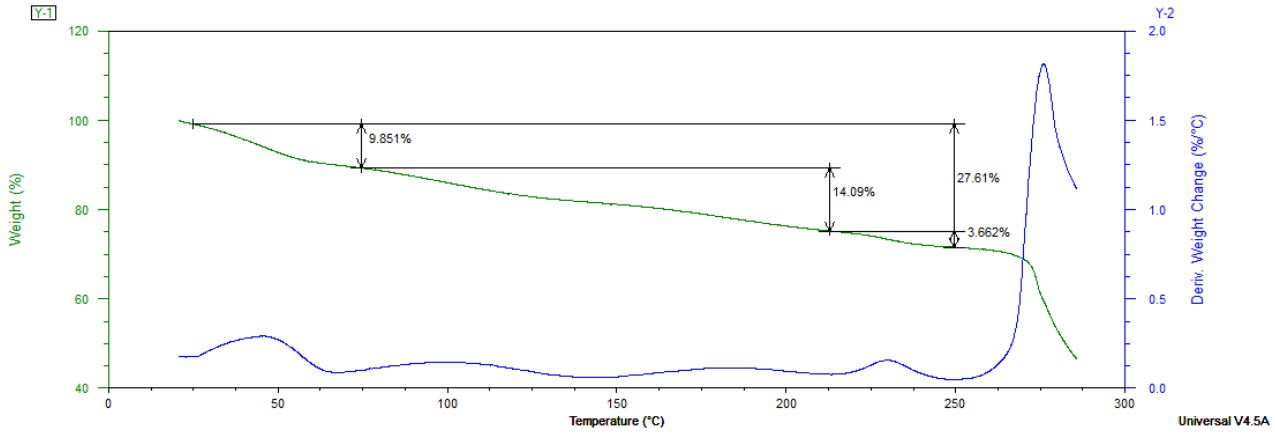

Figure 3.6.17 Graphical representation of a TGA experiment on 2-MBUCT after acetone solvent exchange

Given the DSC, the mass losses for this material were calculated with the same onset and end temperatures utilized when measuring the sample that had not undergone any solvent exchange experiments. The result is on average a 27% mass loss, much lower than the one registered for the previous system. It was not possible to obtain a single crystal suitable for SCXRD after performing the solvent exchange experiment on this material, therefore it was also impossible to compare structural information, and it can only be inferred that the solvent within the channels was at least partially substituted. Another possible explanation is the presence of residual solvent on the surface of the sample that did not undergo solvent exchange, but that is unlikely, as this system did not show the tendency to aggregate displayed by 1-MBUCT when exposed to DMF and DMSO.

6. Miscellaneous Compounds

6.1. [12] Metallacrown-6 Copper (II) Compound, MC-1

This Section will focus on the byproduct to the reaction that produced 2-MBUCT, pictured in Figure 6.1.1. The ASU and unit cell of the system are shown in Figure 6.1.2 and the relevant information on the crystal structure solution is outlined in Table 6.1.1.

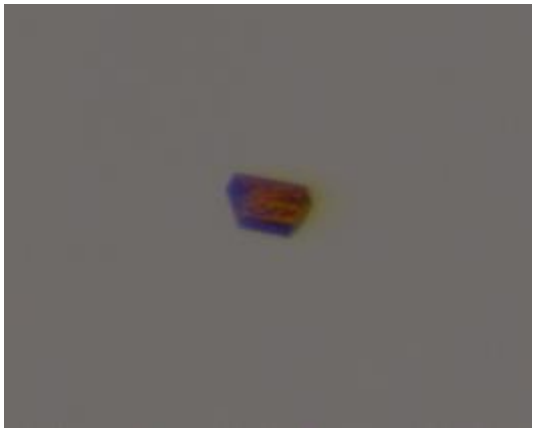

Figure 6.1.1 Picture of [12] crown-6 byproduct of mixed ligand system, present in extemely small quantities

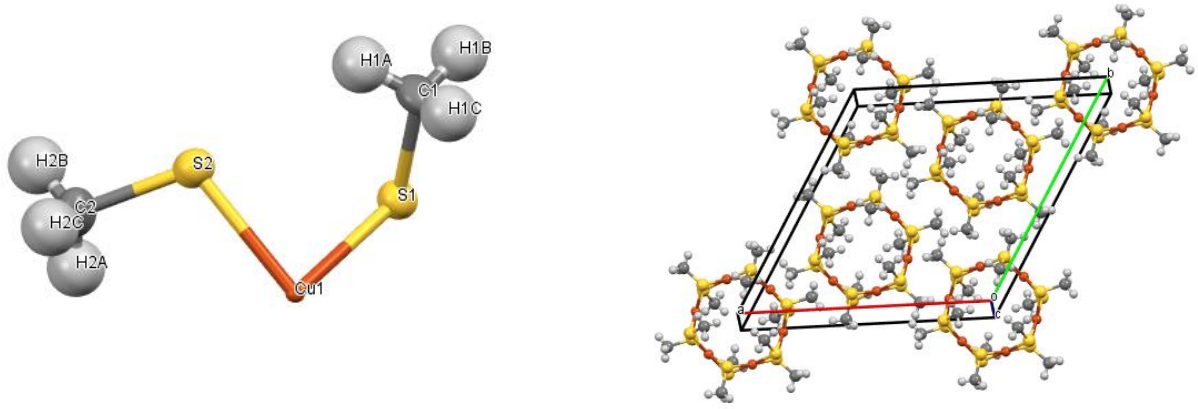

Figure 6.1.2 Picture of [12] crown-6 structure, collected from byproduct of mixed ligand system, only two analogues in CSD, none with copper. The left side of the image is a representation of the ASU with labeled atoms, while the right side shows the ring-like structure of the complex with its unit cell

Table 6.1.1 Relevant crystal structure solution data for MC-1

Identification code	[12]crown-6
Empirical formula	$C_2H_6CuS_2$
Formula weight	158.30
Temperature (K)	293(2)
Crystal system	trigonal
Space group	*R-3*

a (Å)	17.722(2)
b (Å)	17.722(2)
c (Å)	8.739(2)
α (°)	90
β (°)	90
γ (°)	120
Volume ($Å^3$)	2376.7(7)
Z	18
ρ_{calc} (g/cm^3)	2.323
μ (mm^{-1})	5.151
F(000)	1611.0
Crystal size (mm^3)	0.06 × 0.05 × 0.06
Radiation	MoKα (λ = 0.71073 Å)
2Θ range for data collection (°)	4.596 to 56.688
Index ranges	$-21 \leq h \leq 23$, $-23 \leq k \leq 23$, $-11 \leq l \leq 11$
Reflections collected	16136
Independent reflections	1321 [R_{int} = 0.1019, R_{sigma} = 0.0456]
Data/restraints/parameters	1321/0/48
Goodness-of-fit on F^2	1.127
Final R indexes [I>=2σ (I)]	R_1 = 0.0642, wR_2 = 0.2056
Final R indexes [all data]	R_1 = 0.0785, wR_2 = 0.2183
Largest diff. peak/hole (e $Å^{-3}$)	1.46/-2.13

As mentioned before, this product was present in extremely low quantities in the reaction output. A rough estimate would infer the presence of around fifty crystals of the size reported in Table 6.1.1 for every cubic centimeter of material. For this reason it was impossible to conduct any bulk analysis on this material. Thus, comparing PXRD patterns with the other elements of this system was done using the calculated pattern from the single crystal structure (Figure 6.1.3).

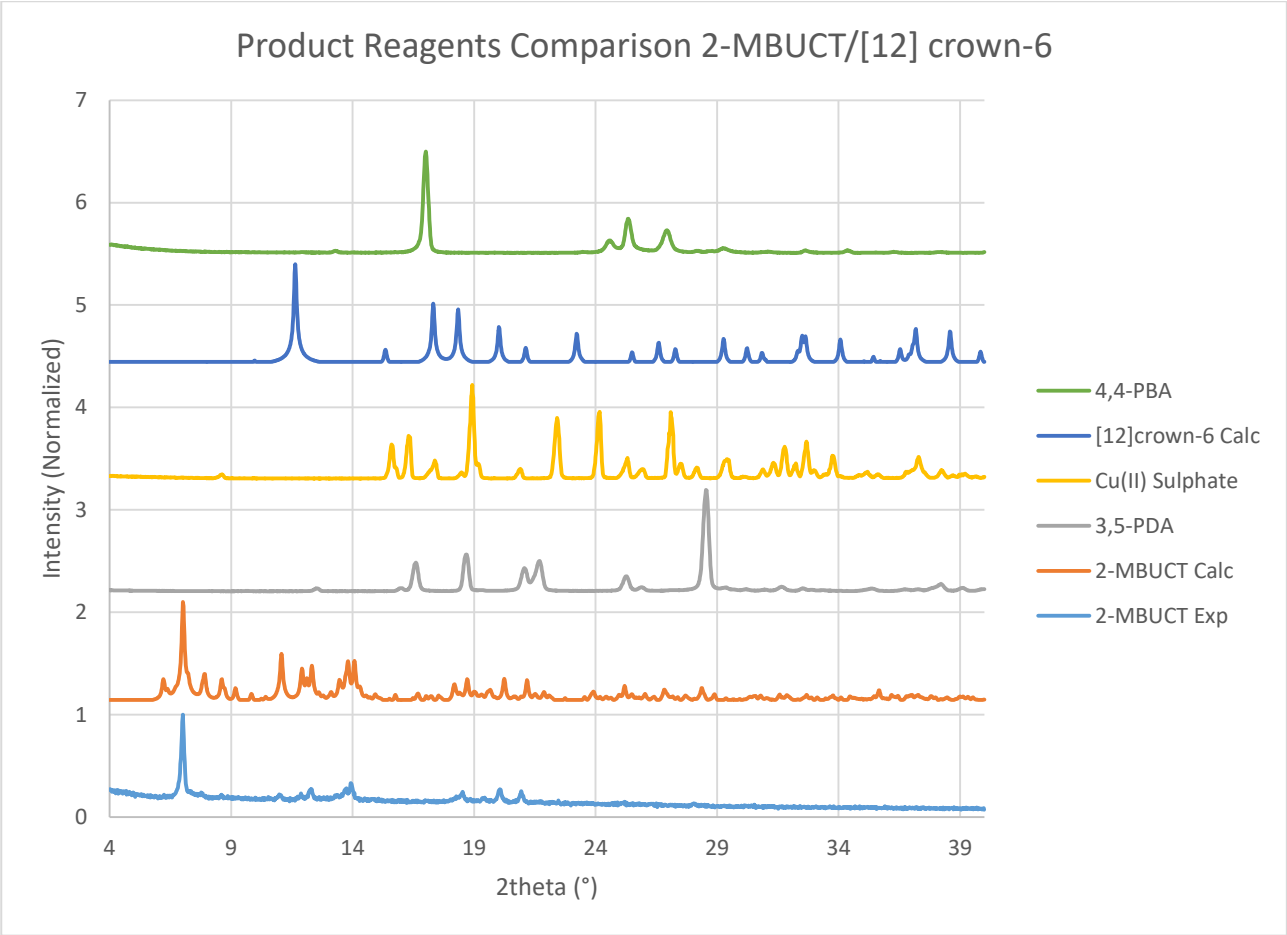

Figure 6.1.3 Comparison of PXRD patterns of reagents and products of the reactionfrom which 2-MBUCT was produced

It is readily apparent that [12]crown-6 is dissimilar from any of the other components of the system, and, given its structure, that it has formed due to the decomposition of a small quantity of DMSO, which gave rise to the methylsulphides that coordinate copper in the ring-like structure. This type of complex, in fact, has only two known analogues in the CSD, both of which include different metals (their CSD reference codes are AFACUG and DUZWIF).

Both of these compounds are also categorized as [12]crown-6 structures, and both were synthesized by decomposing DMSO at a high temperature in the presence of salts of the metal that needed to be incorporated within the structure. The metallacrown containing palladium was part of a series of oxo-linked and thio-linked cyclical palladium compounds used for fluorescence studies,[49] while the metallacrown containing ruthenium was utilized for catalysis of organic substrates.[50] In the same article in which the ruthenium-containing compound was reported, it was also stated that it was possible to synthesize a similar cycle using Zn(II), but no single crystal structure of such a compound was reported. The intriguing properties of similar compounds suggest that it might be interesting to improve the synthetic method to selectively obtain this product and test its properties.

It should be noted that, while the examples of compounds structured exactly as the one described in this work are few and far between, the use of sulfur-based ligands in cyclical metallacrown structures is far more widespread and well understood.[49] Thus, it is likely that previous research on this family of compounds would be a precious source of information when trying to examine potential application for the [12]crown-6 compound examined in this section.

6.2. $Cu(2,6PDA)_2$, MC-2

By filtering and slowly evaporating the mother liquor from the synthesis in Section 2.2 it was possible to isolate and solve the structure of a byproduct of the reaction. The crystal is shown in Figure 6.2.1, while its ASU is shown in Figure 6.2.2 and Figure 6.2.3. The relevant information for its crystal structure solution are outlined in Table 6.2.1.

Figure 6.2.1 Crystal of $Cu(2,6PDA)_2$, long edge of the plate measures 0.67mm while the short edge measures 0.27mm

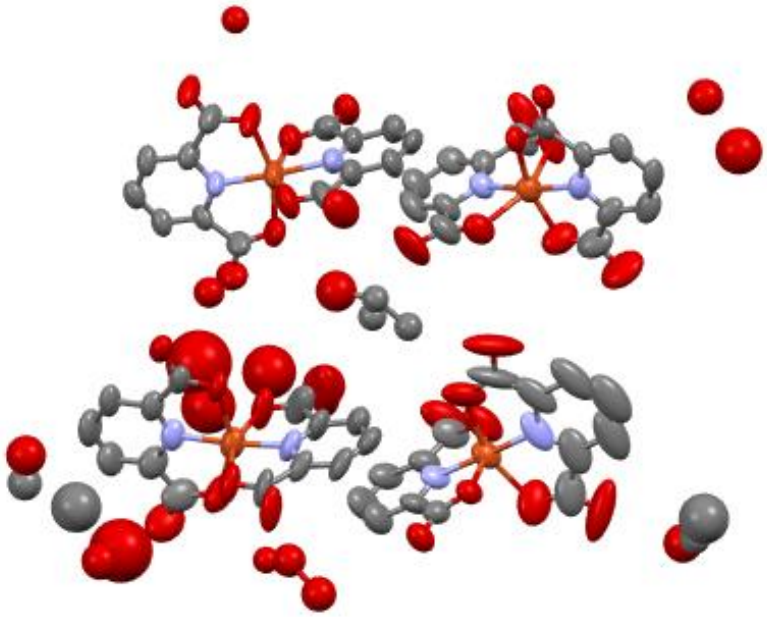

Figure 6.2.2 Single crystal structure of MC-2, image of the ASU. Hydrogens and labels were omitted for clarity

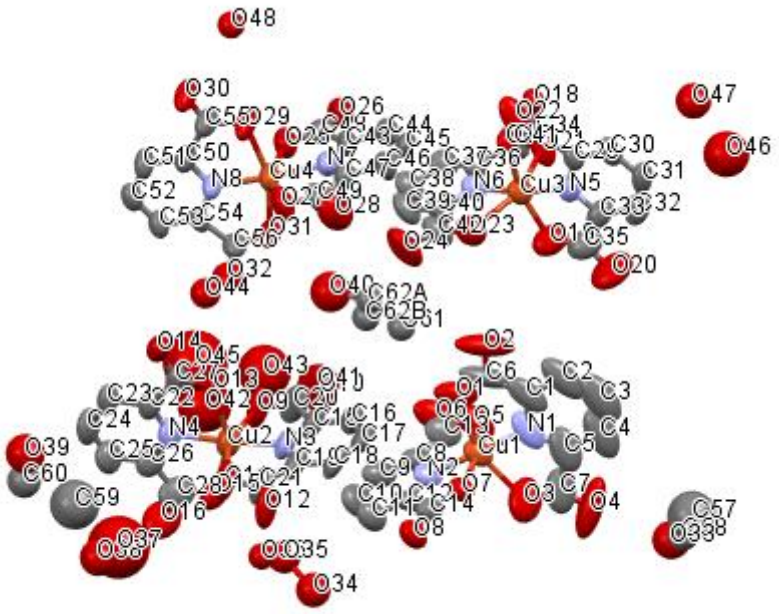

Figure 6.2.3 Single crystal structure of MC-2, image of the ASU. Hydrogens were omitted for clarity

Table 6.2.1 Relevant structure solution information for MC-2

Identification code	MC-2
Empirical formula	$C_{14.75}H_{6.5}CuN_2O_{10.38}$
Formula weight	441.26
Temperature (K)	104.15
Crystal system	triclinic
Space group	*P-1*
a (Å)	15.570(2)
b (Å)	16.205(2)
c (Å)	16.887(2)
α (°)	87.594(2)
β (°)	67.314(2)
γ (°)	70.343(2)
Volume ($Å^3$)	3683.0(9)
Z	8
ρ_{calc} (g/cm^3)	1.592
μ (mm^{-1})	1.245
F(000)	1768.0

Crystal size (mm^3)	0.67 × 0.27 × ?
Radiation	MoKα (λ = 0.71073 Å)
2Θ range for data collection (°)	2.628 to 50.198
Index ranges	$-18 \leq h \leq 18$, $-19 \leq k \leq 19$, $-20 \leq l \leq 20$
Reflections collected	36593
Independent reflections	12900 [R_{int} = 0.0452, R_{sigma} = 0.0585]
Data/restraints/parameters	12900/123/983
Goodness-of-fit on F^2	1.323
Final R indexes [I>=2σ (I)]	R_1 = 0.1161, wR_2 = 0.3390
Final R indexes [all data]	R_1 = 0.1763, wR_2 = 0.3857
Largest diff. peak/hole (e $Å^{-3}$)	1.81/-1.26

It is apparent from Figure 6.2.2 and 6.2.3 that the structure is very disordered, so much so that it was not possible to model some solvent present in the space between the discrete complex molecules. The disorder itself, however, alongside the magnitude of the anisotropy of electronic density on the ligands, offers important information on the behavior of this compound.

Measuring the distances between pairs of copper atoms in adjacent complexes, in fact, one can see that the vectors identifying said distances are parallel to each other and to one cell axis, allowing for small differences given the disorder inherent in the structure. Furthermore, the magnitude of the distance vector corresponds more or less to the module of a cell axis divided by an integer (e.g. the Cu1 to Cu2 distance measures 8.2 Å). Moreover, changing the orientation of the unit cell it is possible to capture multiple orientations in which the complex molecules are superimposable in pairs. Two examples of this are shown in Figures 6.2.4 and 6.2.5.

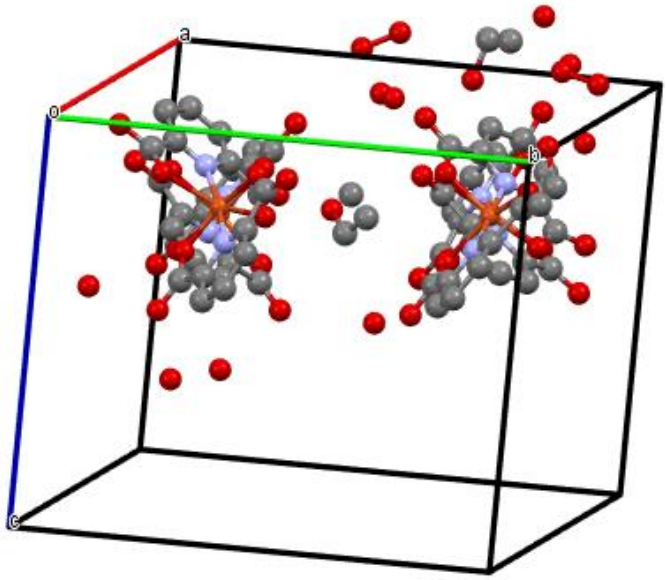

Figure 6.2.4 Single crystal structure of MC-2, image of the ASU. Hydrogens and labels were omitted for clarity. Superimposition of Cu3 with Cu4 (left) and Cu1 with Cu2 (right)

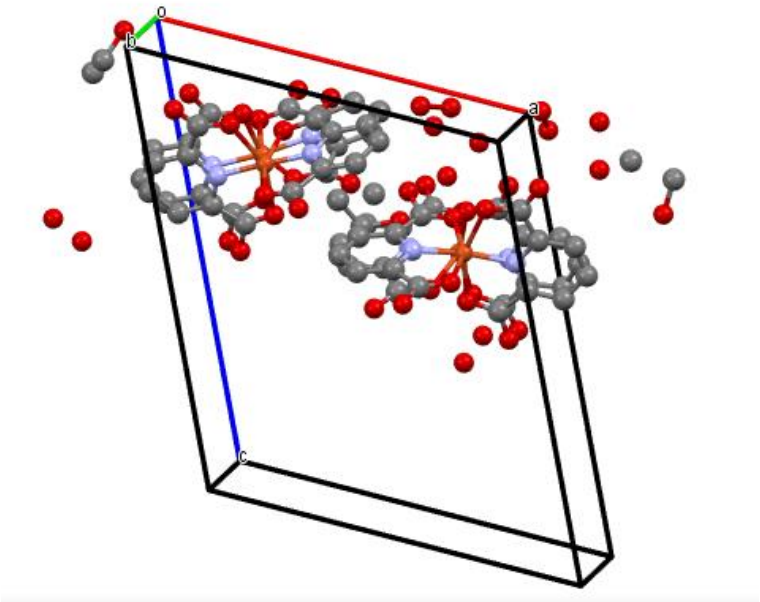

Figure 6.2.5 Single crystal structure of MC-2, image of the ASU. Hydrogens and labels were omitted for clarity. Superimposition of Cu3 with Cu1 (left) and Cu4 with Cu2 (right)

It should also be noted that the SCXRD measurement was performed at around 104K, therefore it is possible that this system at room temperature would display a much smaller unit cell because the temperature drop has probably locked the complex molecules in specific positions that would just be temporary states of molecular dislocation at room temperature. This is corroborated by the large

thermal ellipsoids of the complexes, which might indicate that the atoms of the pyridyl rings are in slightly different positions for each unit cell.

The reduction in molecular mobility correlated with the temperature decrease might also contribute to the extremely disordered nature of the solvent molecules between complexes, since they are probably locked into different positions in each unit cell, making it difficult for them to generate crystallographic peaks during single crystal experiments.

6.3. MC-3

Given its structural similarity to DMSO there was an attampt to use acetone in its place to synthesize a MOF in the same conditions used for 2-MBUCT, but the result of the attempt was a powder so fine that its components could not be observed even under a microscope. After drying out some of the product measuring its PXRD pattern was necessary to verify whether or not the product was crystalline. The solid is shown in Figure 6.3.1.

Figure 6.3.1 Product of copper sulfate, 3,5-PDA and 4,4-PBA reaction in 3/1 DMF/Acetone. Product in the process of drying (left) and wet product in its mother liquor (right)

Upon drying, there is a stark change in the color of the material from dark red to a uniform grey, which might be caused by the presence of a byproduct within the mother liquor which makes the liquid itself assume an orange tinge and causes the light grey solid to look reddish-brown. There was no attempt to isolate such a molecule due to time constraints, but a simple repetition of the experiment

could give more information on this system. A comparison between the PXRD of this system and the one obtained from 2-MBUCT is pictured in Figure 6.3.2.

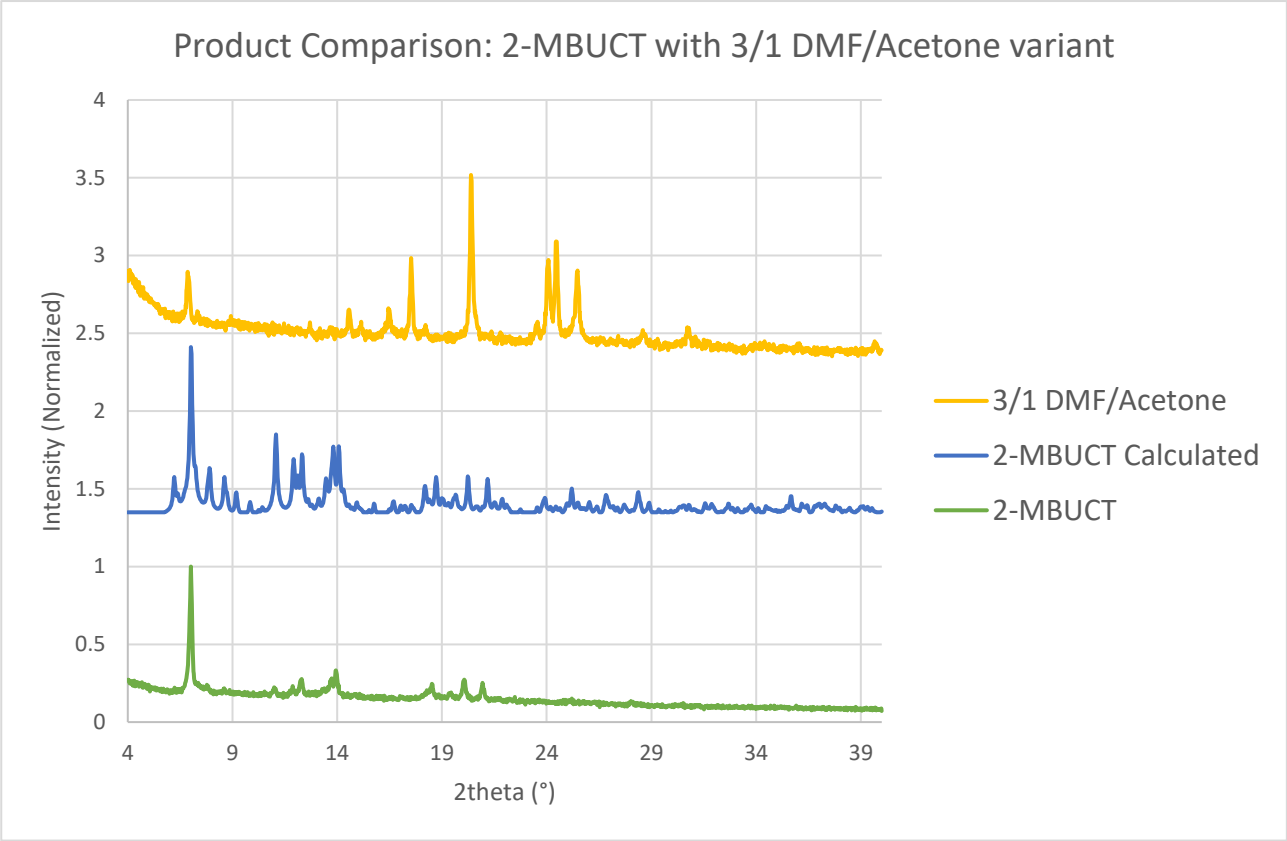

Figure 5.3.2 Comparison of PXRD patterns of 2-MBUCT (both experimental and calculated) and pattern of product synthesized in a 3/1 mixture of DMF and Acetone

The comparison shows quite clearly that there is a crystalline product within the grey solid obtained from the reaction and that it is not the same material as 2-MBUCT. It would be possible to draw better conclusions by refining the synthetic method, as it is quite likely that the different interactions between acetone and DMF with respect to those between DMSO and DMF have a profound effect on not only the nature of the product of this reaction, but also the size of its crystals. In particular it is important to point out that the boiling point of acetone, and therefore of the solvent mixture, is considerably lower than the one of DMSO. Thus, it is possible that if the reaction were to be repeated at lower temperatures and in milder synthetic conditions the size and quality of the crystals would be good enough to perform more accurate analysis.

This reaction was an attempt to investigate whether the similar geometries that these two interactions would have had if the one between Cu and acetone had taken place would have been enough to preserve the structure despite the obvious differences in Cu-O bonds in the two instances taken into consideration.

6.4. MC-4

Given the results obtained by removing 4,4-PBA from the ethanol reaction there was a reason to try to make a similar change in a reaction in a 3/1 mixture of DMF/DMSO, which resulted in octagonal thin plates of a deep blue colour. It is the only product found within the system and the crystals were of a high enough quality that it was possible to perform a single crystal X-ray diffraction experiment. Unfortunately, anomalies within the SCXRD data made it very challenging to solve the structure of the compound, and it was not possible to do so within the time allotted for the experiments on which this work is based. The crystal of this product is shown in Figure 6.4.1.

Preliminary checks of the unit cell parameters during the single-crystal data refinement process showed what appeared to be a cubic space group. The parameters of the unit cell are the following: a=22.946(3); b=22.946(3); c=22.946(3); α=90°; β=90°; γ=90°; space group $F_{m\text{-}3}$.

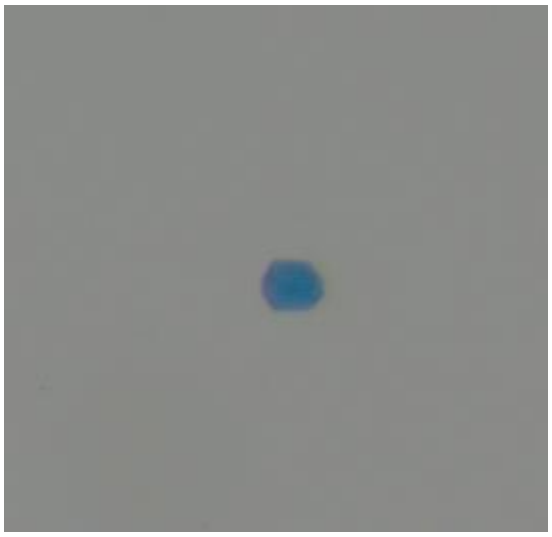

Figure 6.4.1 Crystal of MC-4, product of a solvothermal synthesis at 105°C in a 3/1 mixture of DMF/DMSO. Copper sulfate and 3,5-PDA. Approximating the crystal to a rectangular plate, its long edge would measure 0.34mm and its short edge would measure 0.26mm

Given the purity of the product it was possible to obtain FTIR, PXRD and thermal data. The usefulness of these data is, however, limited until the structure is solved. For this reason, most of those data will be confined to the Appendix.

The PXRD data shown in Figure 6.4.2 highlight the crystallinity of the material and the consistency with which it can be synthesized. Given this measurement, it is thought that the reason for the extreme difficulty in modeling SCXRD data relative to this system lies in widespread presence of twinning inside the crystals belonging to these samples.

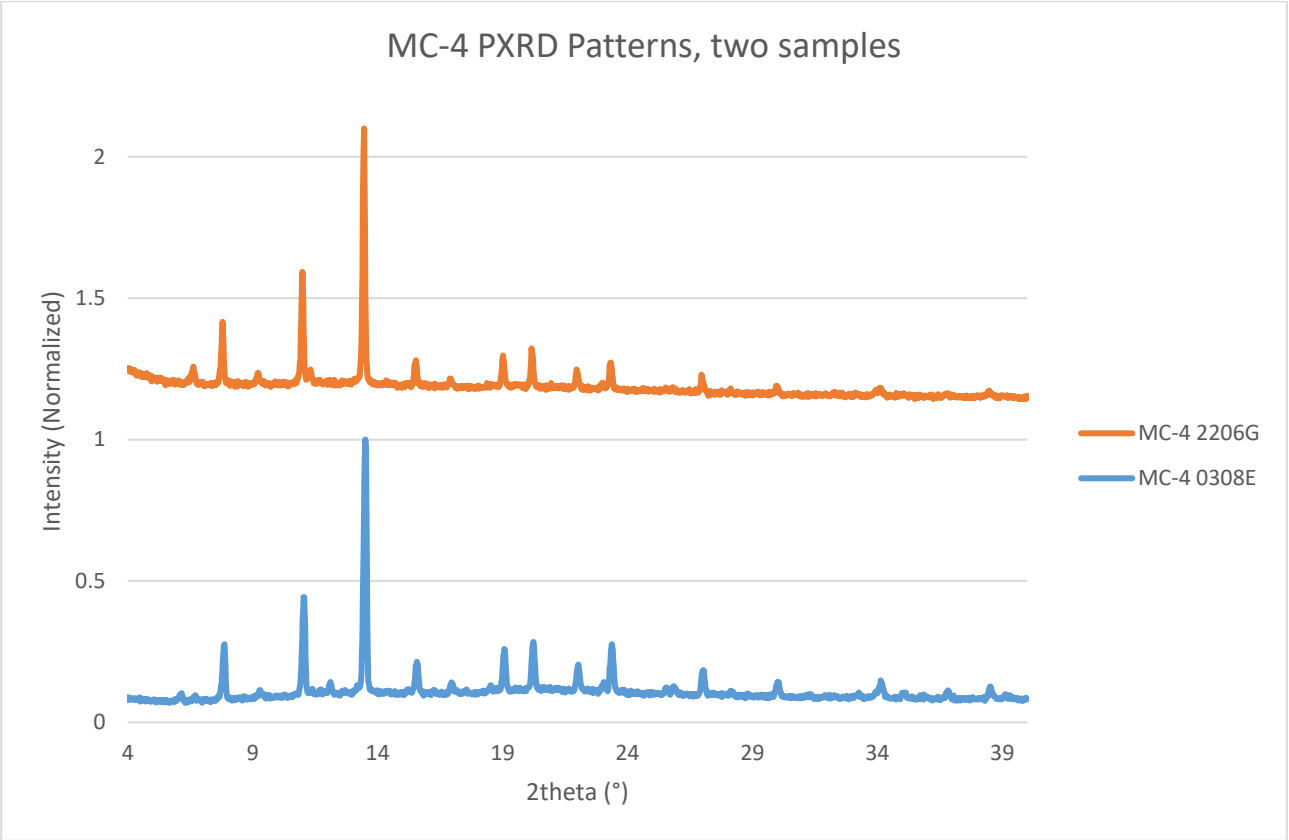

Figure 6.4.2 PXRD patterns of MC-4

7. Conclusions

This project started by asking the following questions: can MOFs be made by changing one ligand within three complexes of the same components produced using three different solvents? Can the MOFs produced in this manner substitute the solvent in their channels with a new one when immersed into the new solvent?

The structure of MOFs is by definition porous, and the presence of pores containing disordered solvent means that there are fewer ordered atoms to diffract the incoming X-ray radiation, thus the resulting diffraction data will be of poorer quality and it will be more difficult to determine the structure of the material. Another issue found in the materials synthesized for this work is that the pores of the material were filled by solvent that was largely disordered, thus creating a background of diffused X-ray radiation that worsens the overall quality of the data and the correlation between the raw data and the proposed crystal structure.

This issue, among others, also impacts materials after they have undergone solvent exchange experiments, which is why it is challenging to draw meaningful conclusions from the experiments outlined in this work. Given the nature of this research, it would have been necessary to conduct experiments for a much more extended period in order to answer the question of whether the MOFs obtained in this work do indeed possess stable porosity.

Even so, it is clear that coordination polymers can indeed be consistently synthesized by only varying one ligand in the initial systems. Such polymers would by some definitions be called MOFs and, in some instances, it is likely that they can exchange the solvent that is present within their channels. Further research would be needed to both confirm this statement and establish whether the porosity in these materials can withstand gas sorption experiments and therefore qualify 1-MBUCT and 2-MBUCT as full-fledged MOFs.

Analyzing specifically 1-MBUCT, it was discovered that the synthesis of this material depends quite heavily on both the copper salt used as a source of Cu(II) ions and the presence of 4,4-PBA in the reaction mixture, despite the fact that this ligand is never incorporated into the MOF structure. Specifically, it was concluded that it was possible to synthesize 1-MBUCT by using copper sulfate pentahydrate, copper bromide, copper acetate, copper chloride dihydrate and copper perchlorate hexahydrate.

When using copper perchlorate it was demonstrated that the perchlorate anion in some way inhibited the formation of 1-MBUCT, leading instead to the synthesis of two different products, one of which was not structurally characterized, and the second of which contained perchlorate ions coordinated to

Cu(II) ions. In the same product the ligand 3,5-PDA was also coordinated to Cu, but all the carboxylic acid moieties on these ligands had been esterified during the reaction. It is possible that this is the feature of the reaction that prevents 1-MBUCT from forming, as the esterification of the carboxylate groups prevents them from coordinating other Cu(II) ions. Another interesting feature of the system was that the reaction could be forced to produce 1-MBUCT just by adding 4,4-PBA in stoichiometric quantity to the system, which might imply that the carboxylate moiety of that ligand was selectively esterified, thus preventing 3,5-PDA from being able to propagate the MOF network structure.

By using copper chloride, instead, a light blue gel was produced alongside 1-MBUCT, which implies that the chloride anion must have played a role in the formation of the gel. SEM experiments showed a significant quantity of Cu and Cl atoms within the gel, but a large excess of N atoms in every part of the material. This means that there is a large excess of ligand with respect to metal ions within the gel structure, and therefore that the gel is mostly held together by weak interactions, such as hydrogen bonding between carboxylic acid dimers of different ligands. The gel surface was covered in two distinct crystalline phases of unknown composition, which displayed vastly different crystal habits.

As for 2-MBUCT it was not feasible to employ so many different permutations of the synthetic process due to the time-consuming nature and complexity of refining the existing reaction, which utilized copper sulfate. This MOF incorporated both 3,5-PDA and 4,4-PBA within its structure, and was notable for its remarkably large unit cell, as well as five Cu(II) ions with different coordination environments within its ASU. 2-MBUCT also featured a free coordination site on two of its Cu(II) centers, which coordinated a DMSO and a water molecule from the reaction mixture. This material is an example of a very well-known class of materials containing a Cu-based paddlewheel cluster. Such materials are utilized for a variety of applications in numerous fields, which suggests that further studies into this system could lead to the discovery of useful and interesting properties.

Solvent exchange experiments on 1-MBUCT showed that heterocyclic solvents such as pyridine or THF partly decomposed the material, shifting a large part of it into a solution, which made it impossible to analyze the results of such experiments through bulk thermal analysis. Solvent exchange experiments with smaller solvent molecules, such as acetonitrile or DMF, were instead moderately successful, as it was possible to demonstrate that the structure of the MOF remained mostly intact throughout the experiment, and it was possible to do so for all solvent exchange experiments. It is also possible that there was at least partial substitution of the solvent within the channels of the material with various other solvents, but even though multiple pieces of information suggest that this is the case, the data are still inconclusive. A similar experiment run on 2-MBUCT by utilizing acetone as the new solvent led to similarly inconclusive results, because of the impossibility to model part of the solvent within the channels of 2-MBUCT.

Lastly, it should be mentioned that the wide variety of byproducts obtained from this system offers an opportunity to optimize the system to obtain larger quantities of these molecules in order to investigate their properties, which, in some cases, might be worthy of exploration given the potential demonstrated by other materials in their respective classes (e.g. metallacrowns or metallogels).

8. Appendix

8.1.SEM Elements Analysis

This section will be dedicated to examples from the SEM dataset that illustrate the range in molar ratios between N and Cu atoms found in various parts of the gel sample. One example will demonstrate the maximum mass percentage of Cu atoms found in the material, while the second example will focus on the opposite edge of the mass percentage range.

Example of dataset with a 1:5 Cu:N molar ratio:

Table 8.1.1 SEM elements analysis data set for Sample 2, the ratio between mass percentages found in this dataset is the maximum found in the sample. It translates to an approximate 1:5 Cu:N molar ratio. Sample 2 is a fragment of the white region of the dry gel, contained in vial 2.

Sample: Sample 2
Type: Default
ID:

Processing option : All elements analysed (Normalised)

All results in weight%

Spectrum	In stats.	C	N	O	Cl	Cu	Total
Spectrum 1	Yes	47.99	7.74	24.8	12.59	6.9	100
Spectrum 2	Yes	48.09	7.88	26.89	11.22	5.91	100
Spectrum 3	Yes	49.47	8.36	30.61	7.31	4.24	100
Spectrum 4	Yes	50.1	8.01	28.97	8.03	4.89	100
Mean		48.91	8	27.82	9.79	5.49	100
Std. deviation		1.04	0.27	2.53	2.53	1.16	
Max.		50.1	8.36	30.61	12.59	6.9	
Min.		47.99	7.74	24.8	7.31	4.24	

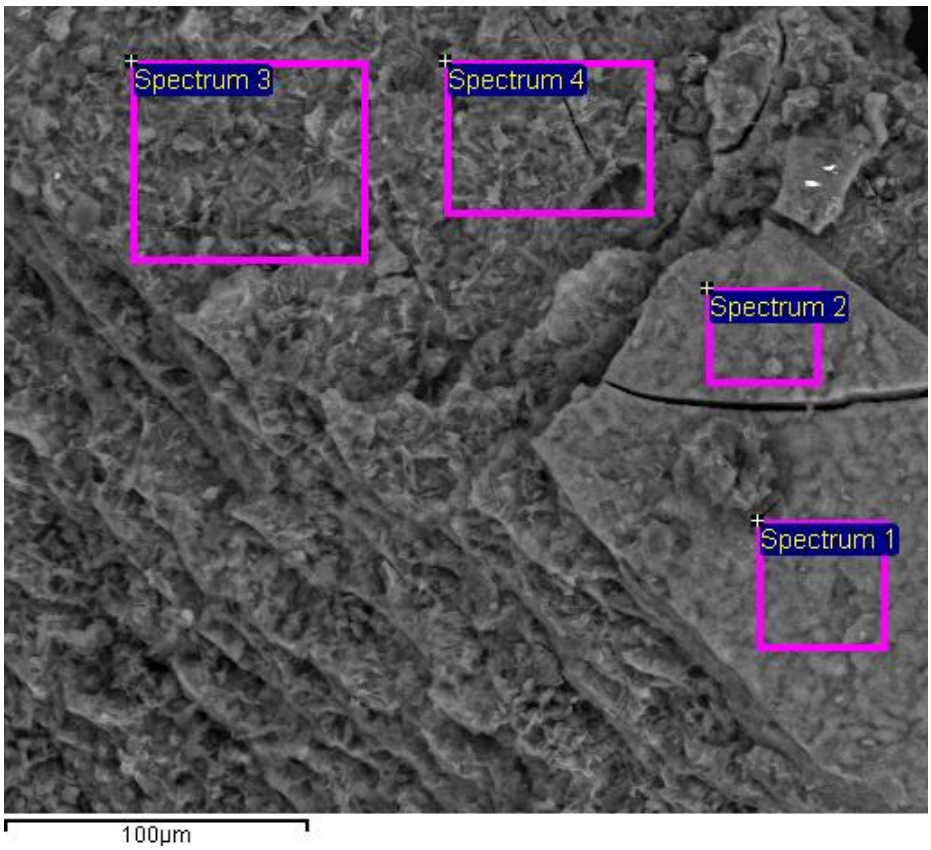

Figure 8.1.1 SEM elements analysis data set for Sample 2, picture associated with Table 8.1.1, white region of the dry gel, vial 2

Example of dataset with a 1:30 Cu:N molar ratio:

Table 8.1.2 SEM elements analysis data set for Sample 4, the ratio between mass percentages found in this dataset is the minimum found in the sample. It translates to an approximate 1:30 Cu:N molar ratio. Sample 4 is a fragment of the light blue region of the dry gel, contained in vial 4.

Sample: Sample 4
Type: Default
ID:

Processing option : All elements analysed (Normalised)

All results in weight%

Spectrum	In stats.	C	N	O	Cl	Cu	Total
Spectrum 1	Yes	50.52	9.01	37.75	1.48	1.25	100
Spectrum 2	Yes	50.37	8.48	38.57	1.55	1.04	100
Spectrum 3	Yes	50.54	8.11	38.6	1.62	1.13	100
Mean		50.47	8.53	38.31	1.55	1.14	100
Std. deviation		0.1	0.45	0.48	0.07	0.11	
Max.		50.54	9.01	38.6	1.62	1.25	
Min.		50.37	8.11	37.75	1.48	1.04	

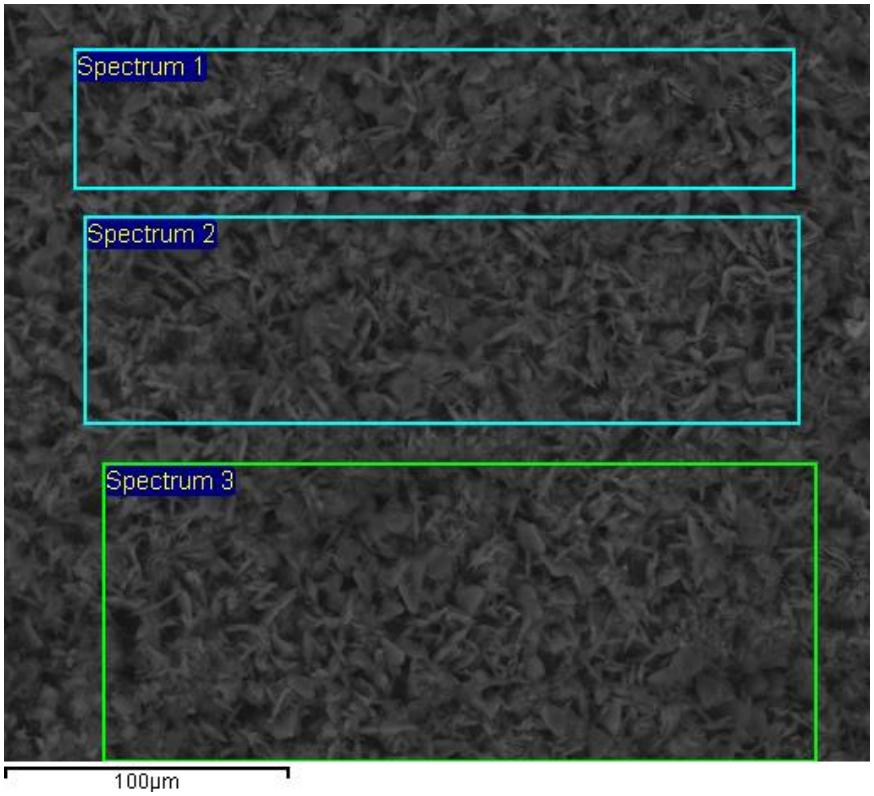

Figure 8.1.2 SEM elements analysis data set for Sample 4, picture associated with Table 8.1.2, light blue region

8.2. SEM Pictures

This section will be dedicated to SEM images that were not used for elements analysis but were useful for interpreting other data on the material, despite not being directly referenced.

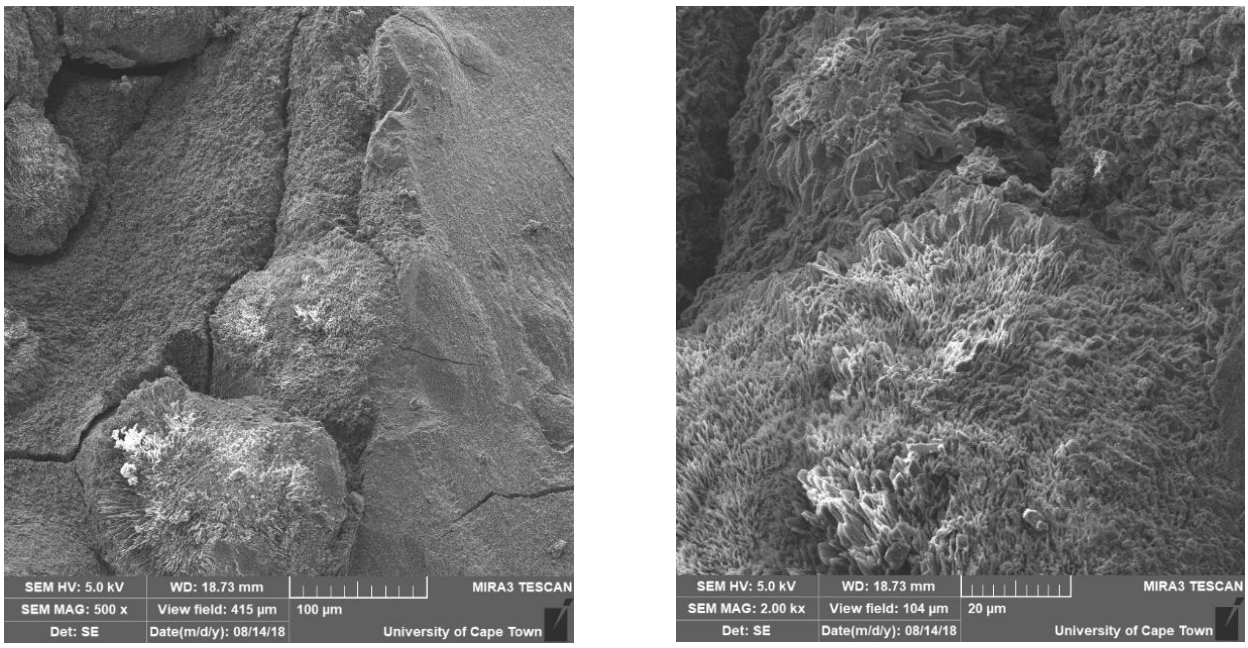

Figure 8.2.1 SEM images 5.2 (left) and 5.4 (right), representing fragments of the dark blue region of the dry gel, vial 5

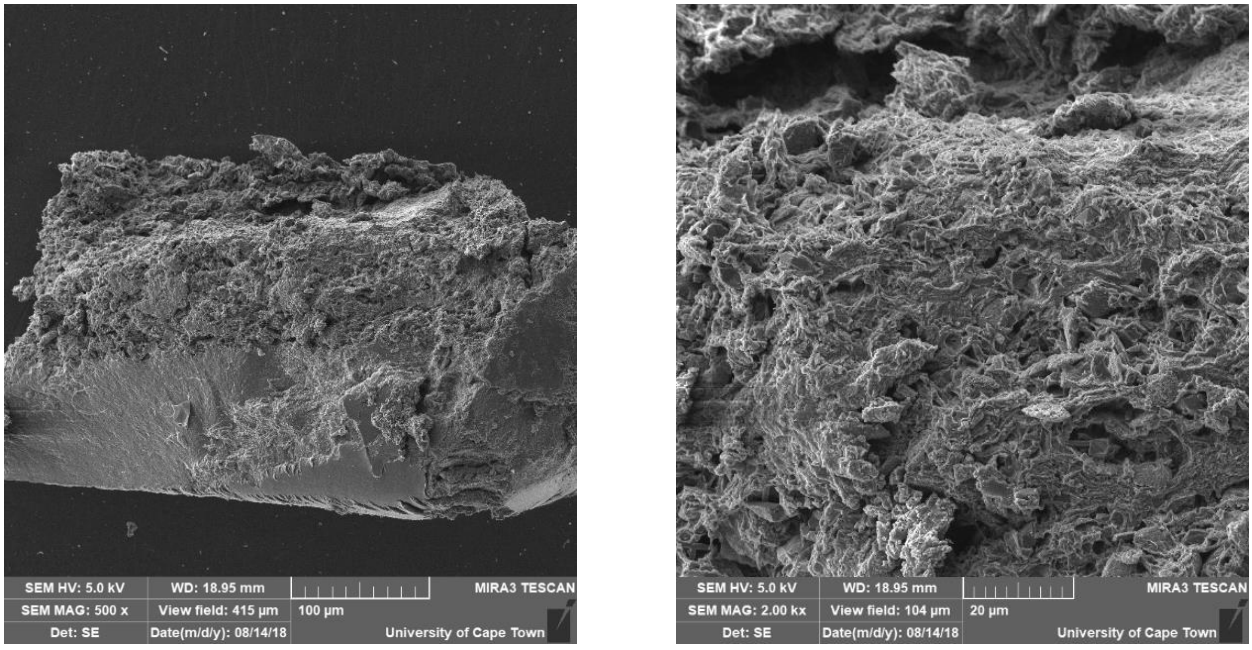

Figure 3.8.21 SEM images 3.3 (left) and 3.4 (right), representing fragments of the light blue region of the dry gel, vial 3

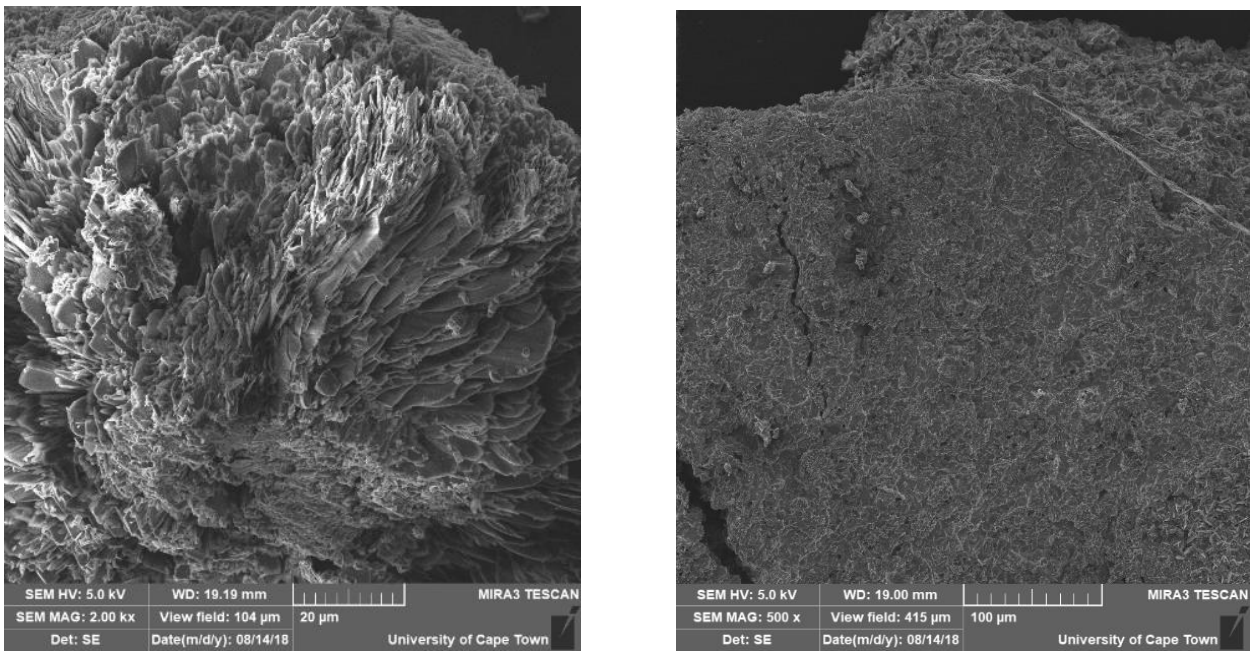

Figure 3.8.30 SEM images 4.5 (left) and 1.4 (right), representing fragments of the light blue region and white region of the dry gel respectively, vial 4 (left) and vial 1 (right)

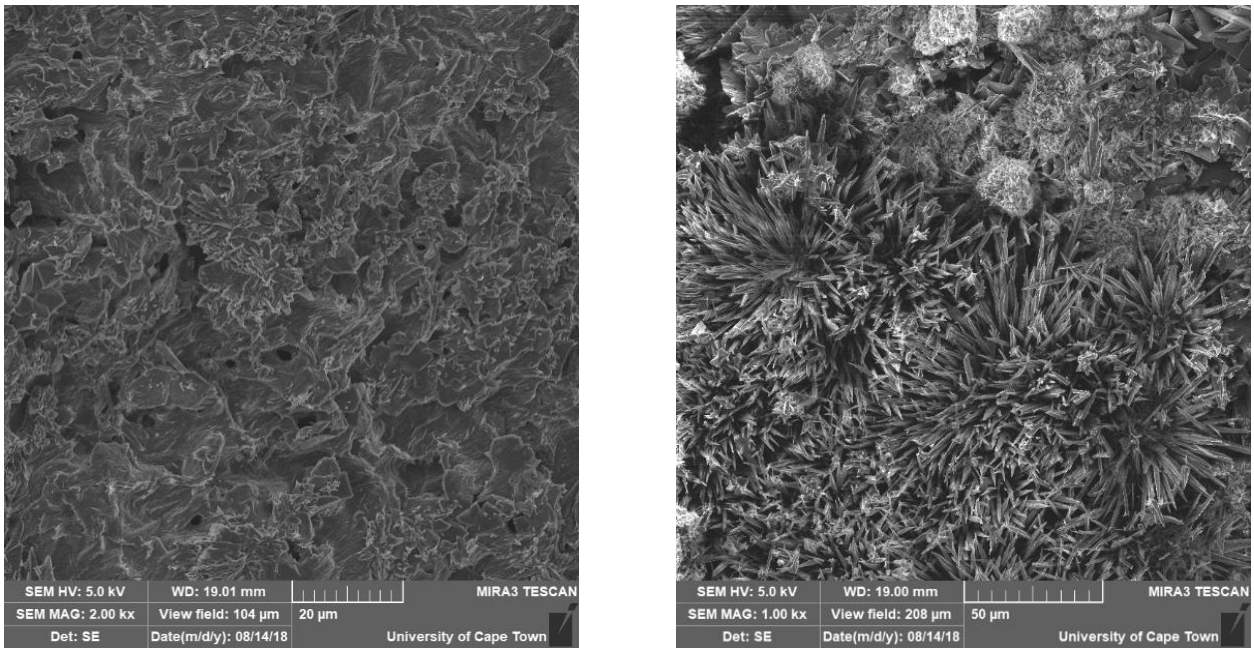

Figure 3.8.31 SEM images 1.5 (left) and 1.3 (right), representing fragments of the white region of the dry gel, vial 1

8.3.FTIR Spectra

This section collects all FTIR spectra of products and starting materials that were not utilized during this work.

The spectrum in Figure 8.3.1 was obtained from the unknown compound MC-4.

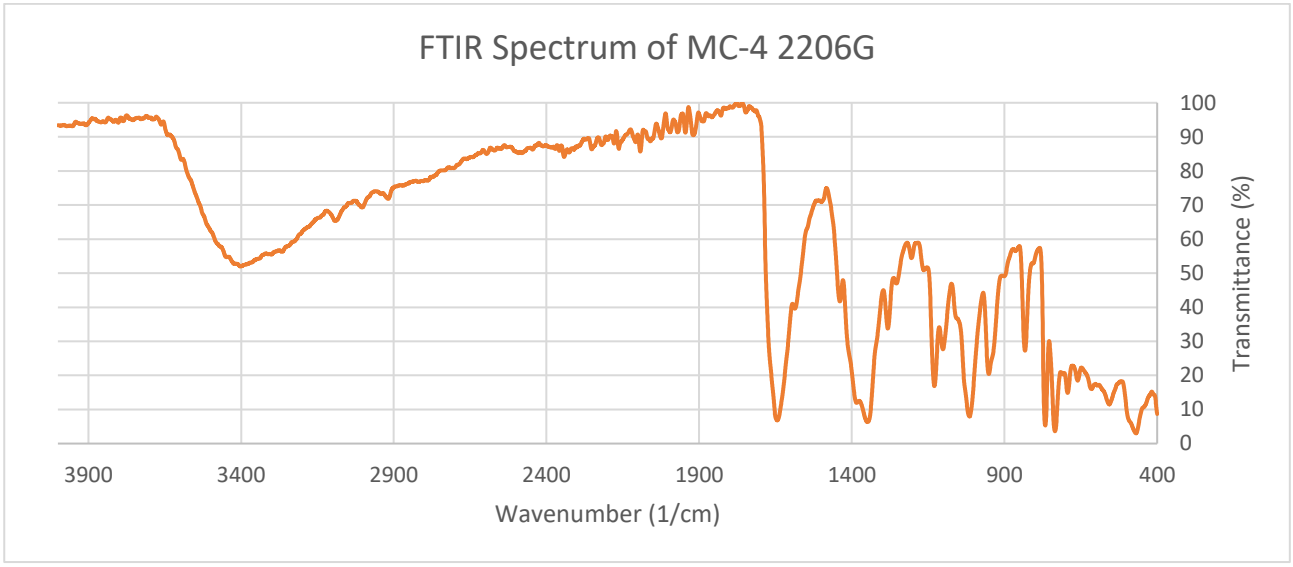

Figure 8.3.1 FTIR Spectrum of MC-4

The spectrum in Figure 8.3.2 was obtained from a standard 2-MBUCT batch.

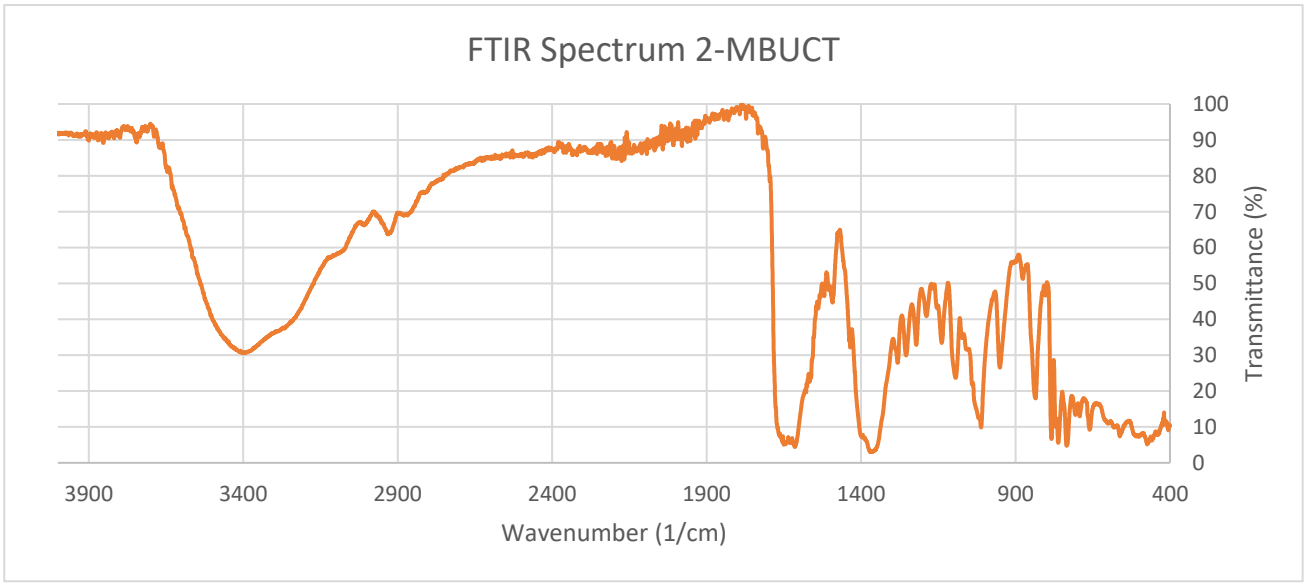

Figure 8.3.2 FTIR Spectrum of 2-MBUCT

The spectrum in Figure 8.3.3 was obtained from a 2-MBUCT batch after it was submerged in acetone:

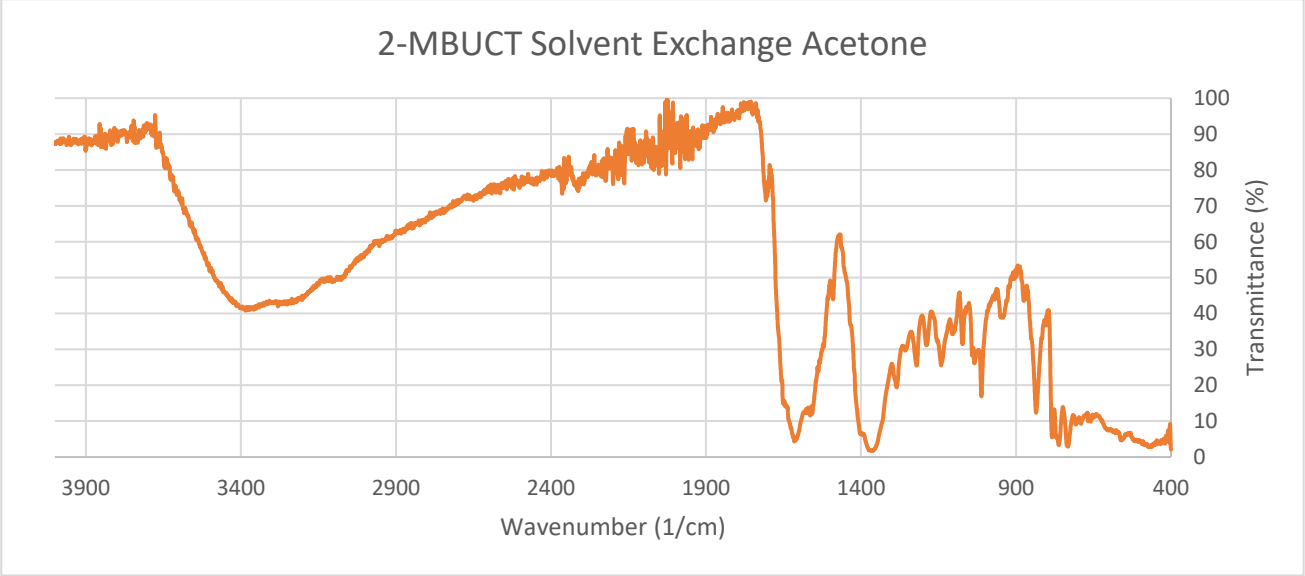

Figure 8.3.3 FTIR Spectrum of 2-MBUCT after being submerged in acetone

8.4. HSM Pictures

The first series of HSM pictures refers to the powdery product of the reaction to synthesize 1-MBUCT involving copper perchlorate, discussed in Section 4.8

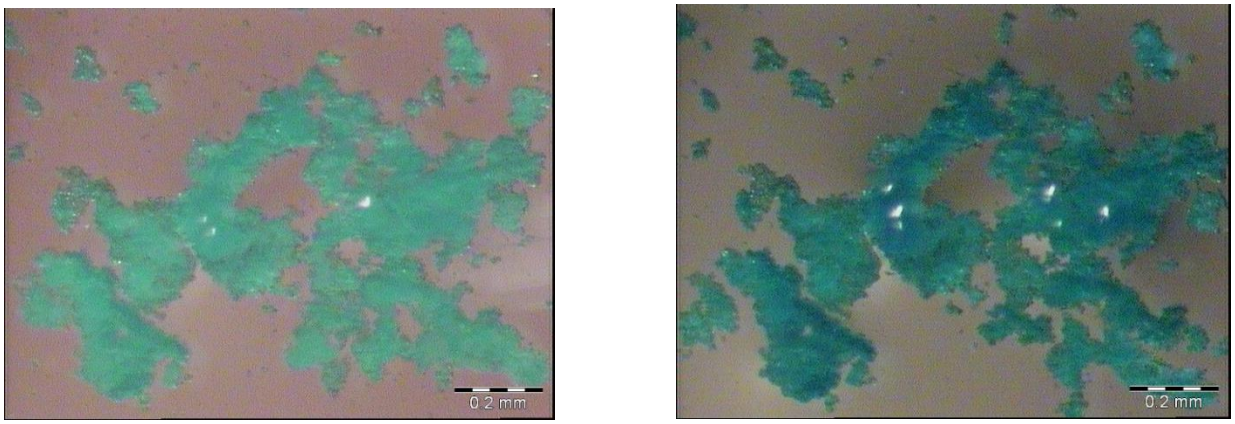

Figure 8.4.1 HSM picture of powder product at 21.1°C (left) and 120.5°C (right)

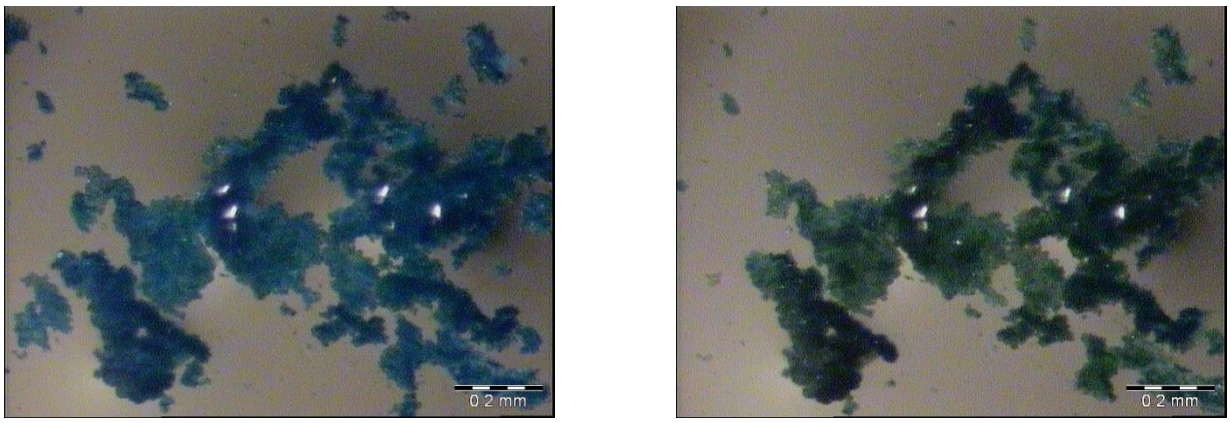

Figure 8.4.2 HSM picture of powder product at 190.5°C (left) and 280.2°C (right)

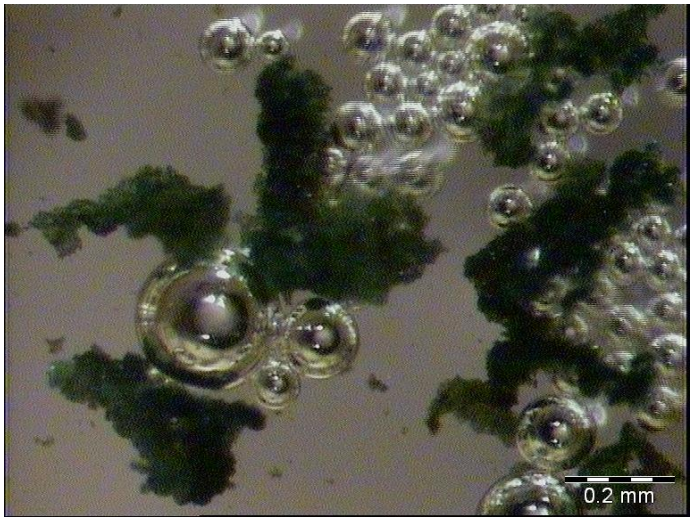

Figure 8.4.3 HSM picture of powder product at 302.0°C

Another compound for which the obtained thermal data were unusable, given that it was impossible to solve its structure, is MC-4.

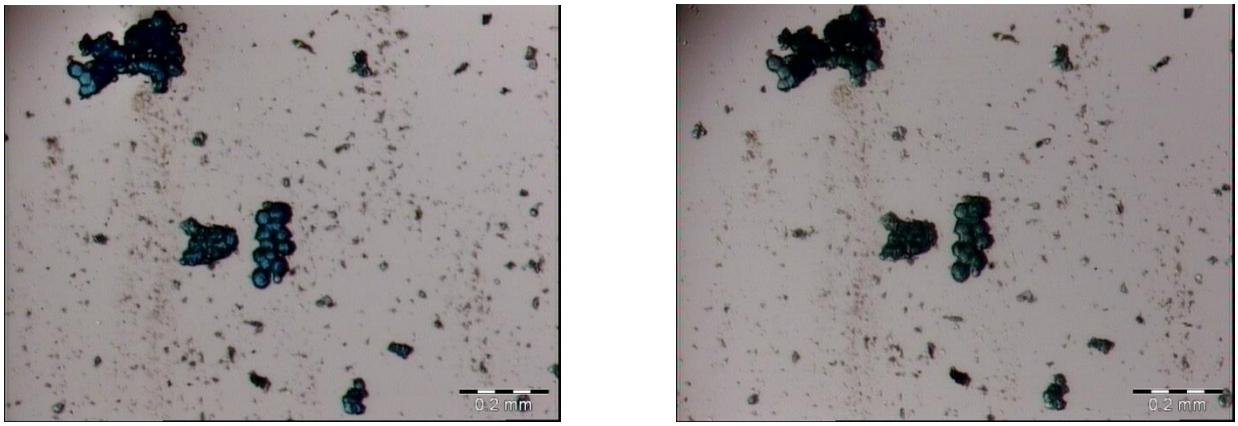

Figure 8.4.4 HSM picture of MC-4 at 22.4°C (left) and 210.1°C (right)

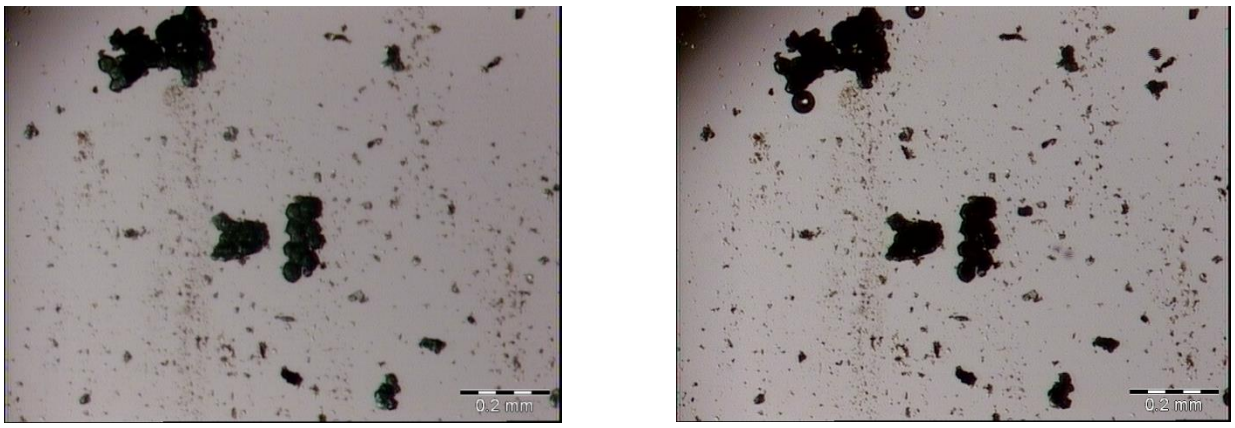

Figure 5.4.7 HSM picture of MC-4 at 234.8°C (left) and 257.0°C (right)

8.5. Thermal Analysis

This section collects TGA/DSC curves that were indirectly referenced in some thermal analysis sections of this work or were not relevant for the overall argument presented in this work due to the lack of other pieces of data.

The curve in Figure 8.5.1 refers to a sample of 1-MBUCT exposed to DMF that displayed unexplained impurities in its DSC measurement. Figure 8.5.2 and Figure 8.5.3 refer respectively to DSC and TGA measurements conducted on MC-4, which were not utilized in the main body of this work since it was not possible to solve the structure of MC-4 within a reasonable timeframe. Figure 8.5.4 refers to a cyclical DSC measurement performed on 2-MBUCT to gather more information on its decomposition peak.

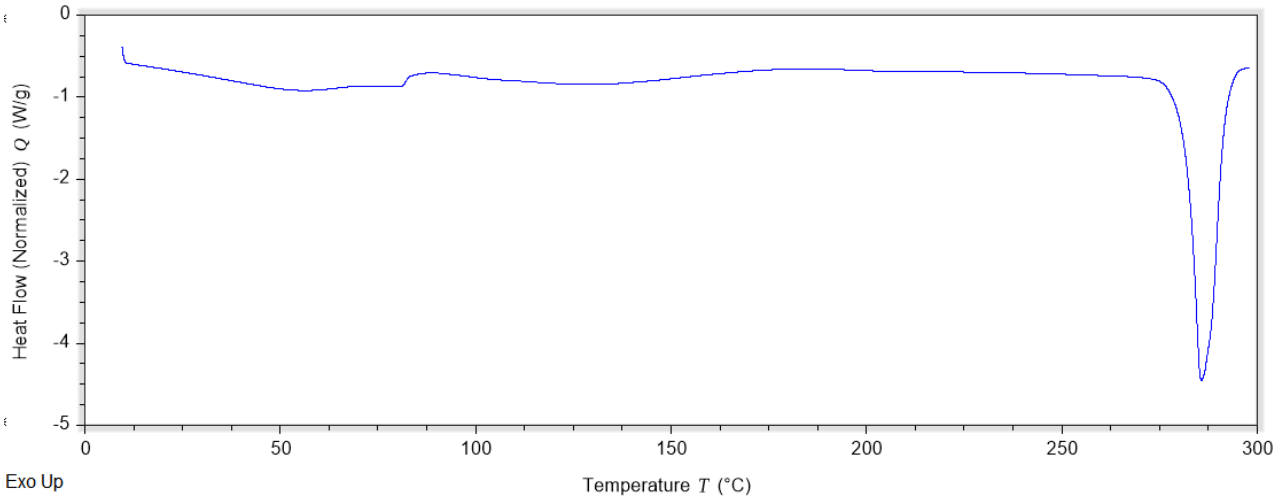

Figure 8.5.1 Thermogram of a DSC experiment on 1-MBUCT after exposure to DMF. Unexplained impurities are present

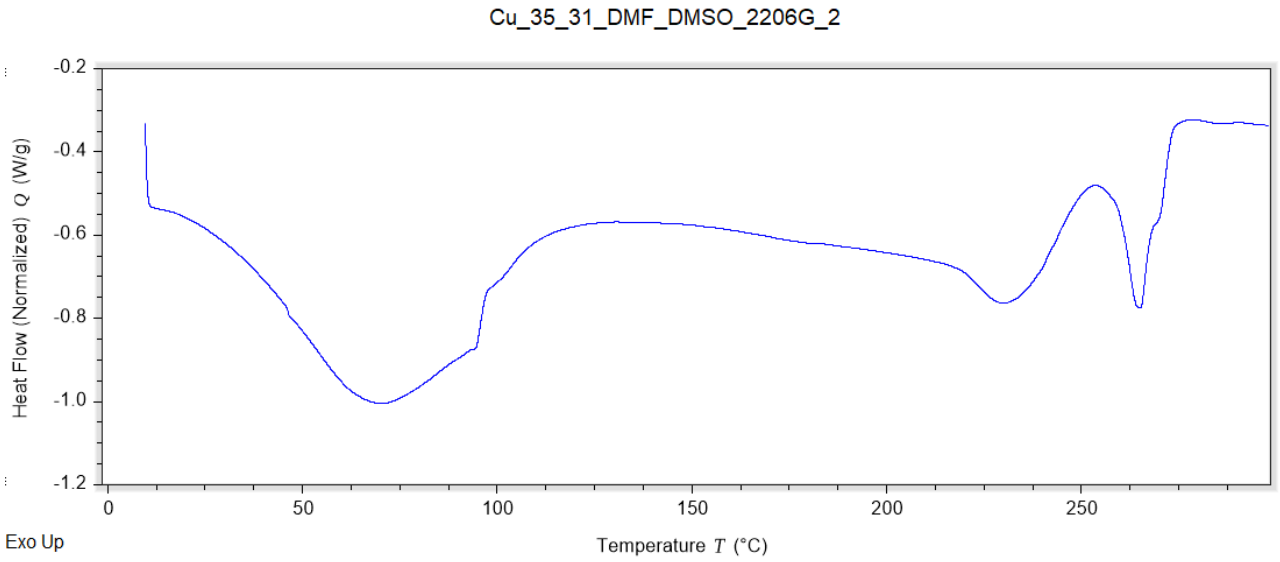

Figure 8.5.2 Most representative DSC pattern of the average of five replications, MC-4

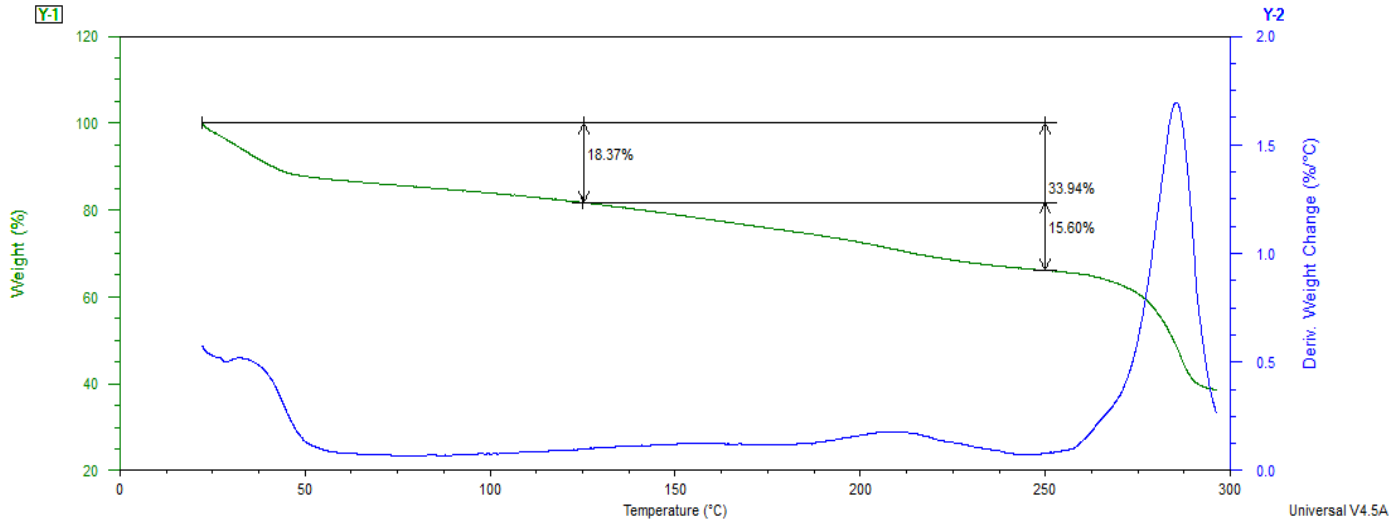

Figure 8.5.3 Most representative TGA pattern of the average of five replications, MC-4

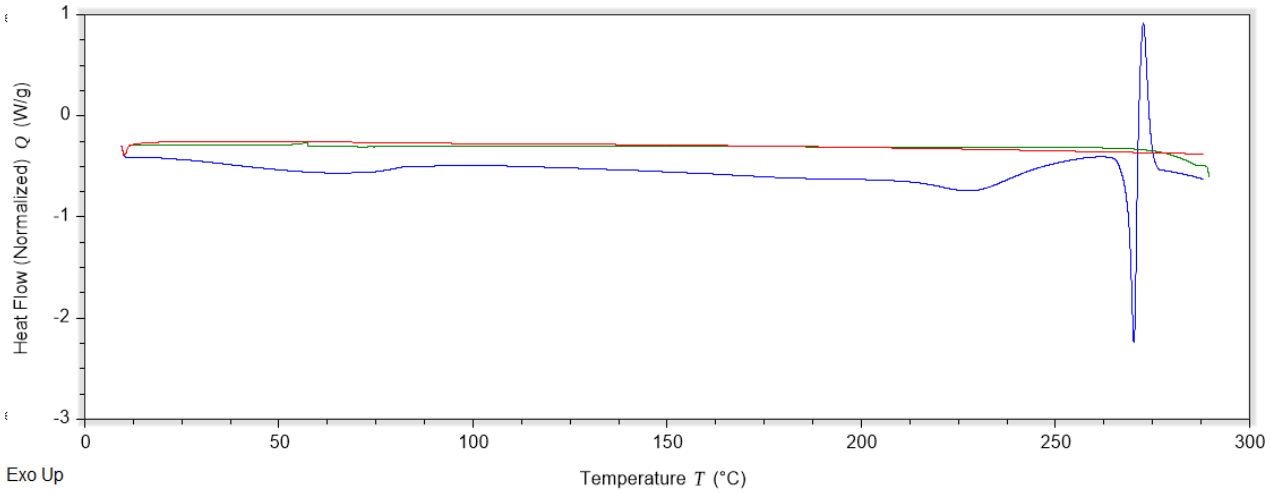

Figure 8.5.4 DSC curves obtained by heating (blue) a sample of 2-MBUCT, then cooling the sample down at the same rate (green) and finally heating the sample up again at the same rate (red).

In Figure 8.5.4 the sample was heated from 10ºC to 290ºC at a rate of 10 ºC/min, generating a DSC curve that is in line with all previous experiments on the same material (blue curve). The curves generated by cooling from 290ºC to 10ºC at a rate of 10 ºC/min (green) and heating back up from 10ºC to 290ºC at a rate of 10 ºC/min (red) are instead completely flat, suggesting that the system is table within this temperature range and that the process catalyzed by the first heating cycle is irreversible.

9. Bibliography

1. Wang, J. *et al.* Multifunctional Luminescent Eu(III)-Based Metal-Organic Framework for Sensing Methanol and Detection and Adsorption of Fe(III) Ions in Aqueous Solution. *Inorg. Chem.* **55**, 12660–12668 (2016).

2. Roth Stefaniak, K. *et al.* Photo-triggered release of 5-fluorouracil from a MOF drug delivery vehicle. *Chem. Commun.* **54**, 7617–7620 (2018).

3. Liu, J. *et al.* Applications of metal-organic frameworks in heterogeneous supramolecular catalysis. *Chem. Soc. Rev.* **43**, 6011–6061 (2014).

4. Pettinari, C., Marchetti, F., Mosca, N., Tosi, G. & Drozdov, A. Application of metal − organic frameworks. *Polym. Int.* **66**, 731–744 (2017).

5. Cortés-Súarez, J. *et al.* Synthesis and Characterization of an SWCNT@HKUST-1 Composite: Enhancing the CO_2 Adsorption Properties of HKUST-1. *ACS Omega* **4**, 5275–5282 (2019).

6. Furukawa, H. & Yaghi, O. M. Storage of hydrogen, methane, and carbon dioxide in highly porous covalent organic frameworks for clean energy applications. *J. Am. Chem. Soc.* **131**, 8875–8883 (2009).

7. Zou, L. & Zhou, H. C. Hydrogen storage in metal-organic frameworks. *Nanostructured Mater. Next-Generation Energy Storage Convers. Hydrog. Prod. Storage, Util.* **11**, 143–170 (2017).

8. Morris, R. V. *et al.* Identification of carbonate-rich outcrops on Mars by the spirit rover. *Science (80-.).* **329**, 421–424 (2010).

9. Zhang, F. *et al.* Two metal-organic frameworks based on a flexible benzimidazole carboxylic acid ligand: Selective gas sorption and luminescence. *Dalt. Trans.* **46**, 15118–15123 (2017).

10. Postnikov, P. S. *et al.* Solid-state transformation in porous metal-organic frameworks based on polymorphic-pillared net structure: Generation of tubular shaped MOFs. *Microporous Mesoporous Mater.* **278**, 99–104 (2018).

11. Kondo, A., Suzuki, T., Kotani, R. & Maeda, K. Liquid/vapor-induced reversible dynamic structural transformation of a three-dimensional Cu-based MOF to a one-dimensional MOF showing gate adsorption. *Dalt. Trans.* **46**, 6762–6768 (2017).

12. Yang, H. Y. *et al.* An Interpenetrated Pillar-Layered Metal-Organic Framework with Novel

Clusters: Reversible Structural Transformation and Selective Gate-Opening Adsorption. *Cryst. Growth Des.* **18**, 3044–3050 (2018).

13. Dittrich, B. Crystal engineering: a textbook, by Gautam R. Desiraju, Jagadese J. Vittal and Arunachalam Ramanan. *Crystallogr. Rev.* **18**, 312–314 (2012).

14. Chen, X.-M. *et al.* Terminology of metal–organic frameworks and coordination polymers (IUPAC Recommendations 2013). *Pure Appl. Chem.* **85**, 1715–1724 (2013).

15. Kitagawa, S. & Uemura, K. Dynamic porous properties of coordination polymers inspired by hydrogen bonds. *Chem. Soc. Rev.* **34**, 109–119 (2005).

16. Furukawa, H., Cordova, K. E., O'Keeffe, M. & Yaghi, O. M. The chemistry and applications of metal-organic frameworks. *Science (80-.).* **341**, (2013).

17. Li, H., Eddaoudi, M., O'Keeffe, M. & Yaghi, O. M. Design and synthesis of an exceptionally stable and highly porous metal- organic framework. *Nature* **402**, 276–279 (1999).

18. S.S.Y. Chui, S.M.F. Lo, J.P.H. Charmant, A.G. Orpen & I.D. Williams. *A Chemically Functionalizable Nanoporous Material [Cu3(TMA)2(H2O)3]n*. *Science* **283**, (1999).

19. Lee, Y. R., Kim, J. & Ahn, W. S. Synthesis of metal-organic frameworks: A mini review. *Korean J. Chem. Eng.* **30**, 1667–1680 (2013).

20. Stock, N. & Biswas, S. Synthesis of metal-organic frameworks (MOFs): Routes to various MOF topologies, morphologies, and composites. *Chem. Rev.* **112**, 933–969 (2012).

21. Mueller, U.; Puetter, H.; Hesse, M. . W. No Title. (2005).

22. Klinowski, J., Almeida Paz, F. A., Silva, P. & Rocha, J. Microwave-Assisted Synthesis of Metal-Organic Frameworks. *Dalt. Trans.* **40**, 321–330 (2011).

23. Bang, J. H. & Suslick, K. S. Applications of ultrasound to the synthesis of nanostructured materials. *Adv. Mater.* **22**, 1039–1059 (2010).

24. Ameloot, R. *et al.* Interfacial synthesis of hollow metal–organic framework capsules demonstrating selective permeability. *Nat. Chem.* **3**, 382 (2011).

25. Shi, Q., Chen, Z., Song, Z., Li, J. & Dong, J. Synthesis of ZIF-8 and ZIF-67 by steam-assisted conversion and an investigation of their tribological behaviors. *Angew. Chemie - Int. Ed.* **50**, 672–675 (2011).

26. Friščić, T. *et al.* Ion- and liquid-assisted grinding: Improved mechanochemical synthesis of metal-organic frameworks reveals salt inclusion and anion templating. *Angew. Chemie - Int.*

Ed. **49**, 712–715 (2010).

27. Barbour, L. J. Crystal porosity and the burden of proof. *Chem. Commun.* 1163–1168 (2006). doi:10.1039/b515612m

28. Ramsay, O. B. *Serendipity: Accidental Discoveries in Science (Roberts, Royston M.)*. *Journal of Chemical Education* **67**, (John Wiley & Sons, 2009).

29. Company, E. C. Paratone N oil.

30. Otwinowski Z, M. W. Processing of X-ray diffraction data collected in oscillation mode. Methods in enzymology. Macromolecular Crystallography, part A,. *Methods Enzymol.* **276**, pp 307–326 (1997).

31. Bruker AXS Inc., APEX2, Version 1.0-27.

32. Bruker AXS Inc., Program SAINT.

33. Sheldrick, G. M. Program SADABS.

34. SADABS, APEX2 & SAINT. Bruker AXS Inc. (2009).

35. Sheldrick, G. M. A short history of SHELX. *Acta Crystallogr. Sect. A* (2008). doi:10.1107/S0108767307043930

36. Barbour, L. J. X-seed - A software tool for supramolecular crystallography. *J. Supramol. Chem.* **1**, 189–191 (2001).

37. Dolomanov, O. V., Bourhis, L. J., Gildea, R. J., Howard, J. A. K. & Puschmann, H. OLEX2: A complete structure solution, refinement and analysis program. *J. Appl. Crystallogr.* **42**, 339–341 (2009).

38. Macrae, C. F. *et al.* Mercury CSD 2.0 - New features for the visualization and investigation of crystal structures. *J. Appl. Crystallogr.* **41**, 466–470 (2008).

39. Olympus. Soft Imaging System GmbH, Digital Solutions for Imaging and Microscopy.

40. Lu, Y.-L. *et al.* Influence of Water Content on the Self-Assembly of Metal−Organic Frameworks Based on Pyridine-3,5-dicarboxylate. *Inorg. Chem.* 24302437 (2006). doi:10.1021/ic0512577

41. Lu, J. Y. & Schauss, V. Crystal Engineering of a three-dimensional coordination polymer based on both covalent and hydrogen bonding interactions of bifunctional ligands. *CrystEngComm* **26**, (2001).

42. Dang, D., Gao, H., Bai, Y. & Zhang, G. Synthesis, Crystal Structure and Luminescent Properties of One Coordination Polymer of Copper(II) Achieved from Pyridine-3,5-dicarboxylate. doi:10.1007/s10870-009-9657-2

43. Zacharias, S. C., Ramon, G. & Bourne, S. A. Supramolecular metallogels constructed from carboxylate gelators. *Soft Matter* **14**, 4505–4519 (2018).

44. Piepenbrock, M. O. M., Clarke, N. & Steed, J. W. Metal ion and anion-based 'tuning' of a supramolecular metallogel. *Langmuir* **25**, 8451–8456 (2009).

45. Nandi, G., Titi, H. M., Thakuria, R. & Goldberg, I. Solvent dependent formation of metallogels and single-crystal MOFs by La(III) and Ce(III) connectors and 3,5-pyridinedicarboxylate. *Cryst. Growth Des.* **14**, 2714–2719 (2014).

46. Dukh, M. *et al.* Metal coordination as a tool for controlling the self-assembling and gelation properties of novel type cholic amide-phenanthroline gelating agent. *Tetrahedron* **59**, 4069–4076 (2003).

47. Perman, J. A., Chen, M., Mikhail, A. A., Niu, Z. & Ma, S. Acid-base directed supramolecular isomers of isophthalate based MOFs for CO2adsorption and transformation. *CrystEngComm* **19**, 4171–4174 (2017).

48. Chen, Y. *et al.* A Copper(II)-Paddlewheel Metal-Organic Framework with Exceptional Hydrolytic Stability and Selective Adsorption and Detection Ability of Aniline in Water. *ACS Appl. Mater. Interfaces* **9**, 27027–27035 (2017).

49. Matthews, J. R. *et al.* Metal coordination and aggregation properties of chiral polythiophenes and polythienylethynylenes. *Macromol. Rapid Commun.* **28**, 1809–1815 (2007).

50. Ming-Hua Xie, Miao Wang, C.-D. W. Catalytic Alkenylation of Phenylpyridines with Terminal Alkynes by a [12]Metallacrown-6 Ruthenium(II) Compound. *Inorg. Chem.* **48**, 10477–10479 (2009).

10. Acknowledgements

- Dr. Savannah Zacharias, for her patience, expertise and kindness. Thank you.
- Prof. Susan Bourne, for the constant encouragement and for correcting me with a smile whenever I strayed off course.
- Prof.ssa Alessia Bacchi, per il prezioso aiuto nella risoluzione di strutture cristallografiche e per la serenità che mi ha trasmesso durante questi mesi.
- I am grateful to the National Research Foundation of South Africa and the University of Parma for providing student funding in the form of the Overworld Program. Any conclusions expressed in this work are those of the author, and the NRF does not accept liability in this regard.
- To the administrative personnel at the University of Parma, the University of Cape Town and the South African Consulate in Milan, for the assistance in navigating the complex bureaucracy associated with this degree.
- Prof.ssa Francesca Terenziani, perché se non si inizia bene non si finisce affatto.
- Ad Andrea, il mio unico vero compagno di corso.
- All'Università di Parma, per avermi ospitato durante questi anni e per avermi dato l'opportunità di espandere i miei orizzonti sia accademici che personali.
- The University of Cape Town, for providing the structures and equipment essential to my work, for the opportunity of working in a well-respected institution and the pleasure of living in such a beautiful city.
- Boston College, for giving me a sense of what I was missing.
- Dr. Hong Su, for her invaluable contribution in collecting x-ray diffraction patterns.
- Prof. Mino Caira e Prof. Luigi Nassimbeni, grazie per aver reso Cape Town un po' più simile a casa, per le storie, le lezioni di storia e i consigli su come affrontare problemi in apparenza impossibili da risolvere.
- To all my colleagues at the Center for Supramolecular Chemistry Research at the University of Cape Town and all the other research groups: Nolwazi, Ana, Emma, Terence, Bernard, Alexios, Richard, Jacky, Nicole, Francoise, Adrian, Laurelle, Carine, Tido, Nolwazi, Ola, Emre and Marta. Thank you for making me feel part of your family.

- Ai miei genitori, Enrico e Raffaella, a mia sorella Alessia e a tutta la mia famiglia, grazie a quelli che ci sono stati dall'inizio e a quelli che si sono aggiunti lungo la via, non sarei qui senza di voi.
- Prof. Gianni Melegari, per avermi insegnato ad ascoltare, e perché arrivare a una risposta non sempre significa arrivarci nel modo giusto.
- Prof.ssa Elena Petrin, because talent needs to be able to breathe.
- To every single one of my friends, wherever they may be. They know why, each in their own way. Ai miei amici, dovunque si trovino. Sanno perché, ognuno a suo modo.
- To Steven Erikson, because somehow I need to apologize for not having watched Star Trek
- All'unica persona che non posso chiamare per nome. Grazie.